UCRL-ID-134479

# LLNL Heart Valve Condition Classification Project
# Anechoic Testing Results at the TRANSDEC Evaluation Facility
# Final Report
# to the
# Bowling-Pfizer Supervisory Panel

James V. Candy

**October 31, 1998**

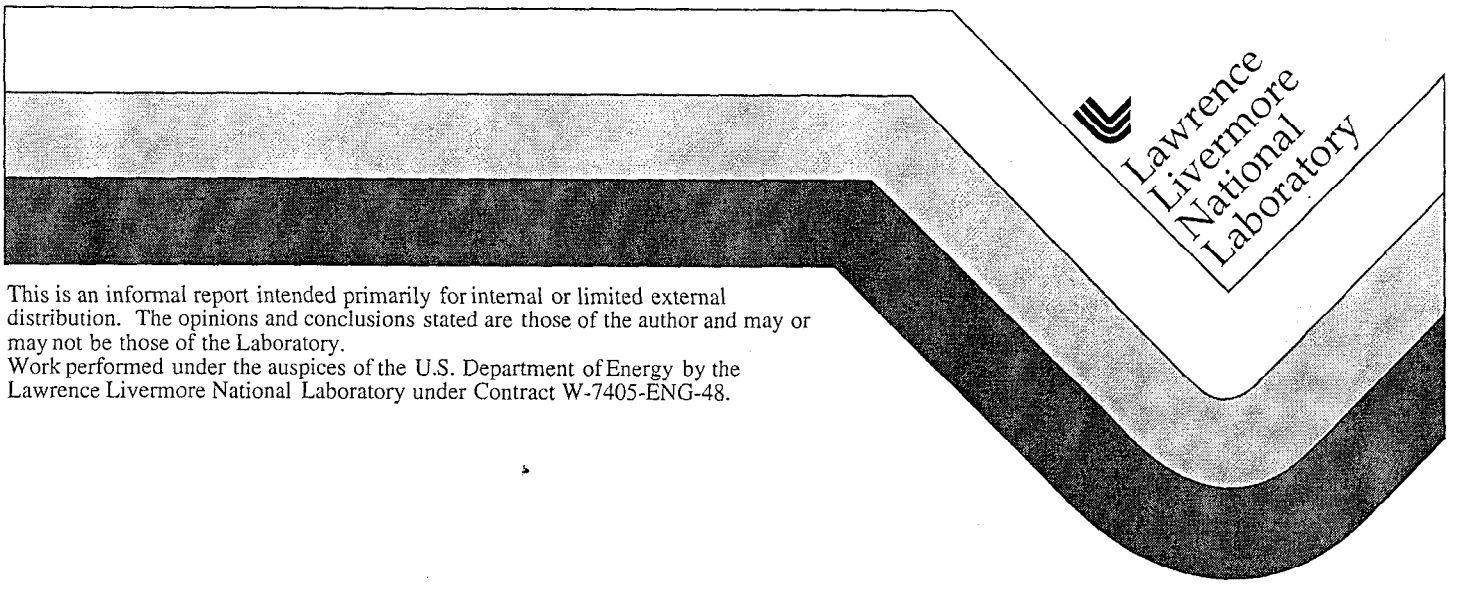

# *LLNL Heart Valve Condition Classification Project*

# Anechoic Testing Results at the TRANSDEC Evaluation Facility

**FINAL REPORT**
**to the**
**BOWLING-PFIZER SUPERVISORY PANEL**

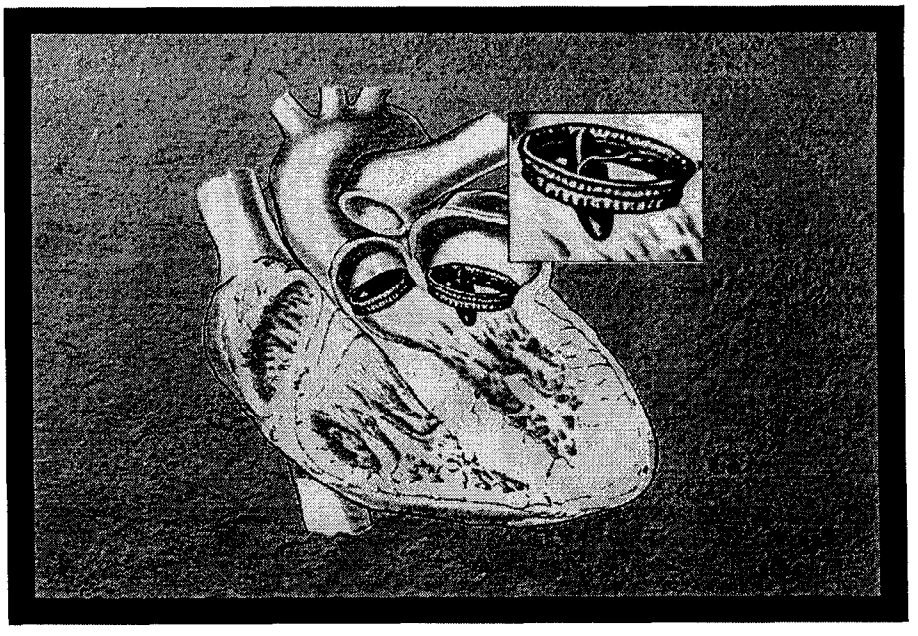

James V. Candy
Principal Investigator

October 31, 1998

# PREFACE

The results reported in this document are the culmination of the efforts of those members of the Lawrence Livermore National Laboratory (LLNL) Heart Valve Acoustics Classification Project team. Each person on the team contributed their expertise to develop the hardware, experiments and signal processing to produce these final results.

The members of the team (alphabetically) are:

| | |
|---|---|
| Michael Axelrod | (statistics) |
| Albert Brown | (acoustics) |
| James Candy | (signal processing) |
| Gregory Clark | (classification) |
| Robert Huber | (experiments, lasers) |
| Alan Meyer | (signal processing) |
| Dwight Perkins | (experiment, data acquisition) |
| Graham Thomas | (acoustics, classification) |

along with our colleagues:

| | |
|---|---|
| Howard Lynch | (TRANSDEC acoustics) |
| David Scott | (classification, signal processing) |
| John Skadberg | (TRANSDEC photography) |
| Arthur Weyman | (BP Panel) |

# ABSTRACT

This final report contains the Anechoic Test results for the Bowling-Pfizer Heart Valve Supervisory Panel (BPHVSP) in accordance with the Department of Energy Work for Others (WFO) Contract commencing on April 15, 1998. The report satisfies the requirements for Task I of said contract and describes the results of anechoic testing of a set of fifty (50) intact (INT) and explanted single-leg separated (SLS) Bjork-Shiley Convexo-Concave (BSCC) heart valves received from the Shiley Heart Valve Center. First we briefly outline the procedures and support/activation fixture developed at Lawrence Livermore National Laboratory (LLNL) to perform the heart valve tests in an anechoic-like tank at the U. S. Navy Transducer Evaluation Facility (TransDec) located in San Diego, CA. Next we discuss the basic experiments performed and the corresponding experimental plan employed to gather meaningful data systematically. The signal processing required to extract the desired information is briefly developed along with some of the data. Finally, we show the results of the individual runs for each valve, point out any of the meaningful features and summarize.

# EXECUTIVE SUMMARY

We report the results of anechoic acoustic measurements on 50 prosthetic BSCC values 21 of which have a specific mechanical defect known as *single leg separation* (SLS). The others are typical of non-defective valves known as *intact* (INT). We followed a measurement protocol (see Appendix A) designed to acquire acoustic signal data under controlled conditions and to be as free as possible from experimental artifacts. Refinements to our measurement protocol, instrumentation, fixtures and procedures incorporate the knowledge and experience we gained from prior experiments under different laboratory settings. We choose the US Navy Transducer Evaluation Center (TransDec) because it provides a low ambient noise environment free from acoustic boundary reflections. Our major refinements included the use wideband data acquisition equipment (1 kHz – 95 kHz) to enhance our signal frequency resolution, a custom fixture to hold and activate the valves, as well as custom instruments to identify and tag significant acoustic signal components.

Our major objectives (all satisfied) reported here were to:

- Record high-resolution signal data on both opening and closing sounds.
- Record instrument noise, environmental noise, and measurement noise.
- Measure the acoustic radiation pattern on a typical valve.
- Verify repeatability, stability and freedom from artifacts of our measurements.
- Extract opening and closing sound data from raw experimental records.
- Identify and eliminate aberrant signals.
- Compute estimates of the power spectral density for both opening and closing sounds.
- Summarize and display the salient characteristics of the power spectral density estimates for INT and SLS valves.
- Prepare processed opening and closing sound data for automatic classification.

The experiment produced a daunting quantity of digital measurement data. Fifty valves with 100 replications of both opening and closing sounds yielded 10,000 separate signals, each must be cut from the record and processed. Each transient sound or beat was captured in a 300 ms measurement window and sampled at a rate of 200k samples per second giving 1,200 MB of signal window data. This does not include noise measurements and other baseline data. We eliminated aberrant sound signals by the following strategy. For each sound signal we estimated its power spectral density (PSD) by the Minimum Variance Distortionless Response (MVDR) technique (Appendix C). This gives an ensemble of 100 spectra for each valve and for each sound type (opening, closing). We calculated a location statistic for an ensemble by computing the median at each frequency point, this produces a median spectrum for each ensemble. We cannot use this medium spectrum as typical of the ensemble because it does not belong to the

ensemble, so we selected the 25 members of the ensemble closest to the median using a robust statistical estimator known as MAD (Median Absolute Deviation). This procedure produces new ensembles each of size 25 pruned of aberrant signals. The first member of the ensemble is the signal closest to the median (CTM). The CTM for each ensemble belongs to the ensemble and is also a typical of the signals in that ensemble. Thus, we obtain 21 CTM spectra for each of the SLS class valves. We then repeat the procedure for a whole class giving us a single Universal CTM (UCTM) for each class. Thus the 10,000 signal spectra are reduced to only two. We summarize this approach in Figure X-1 below.

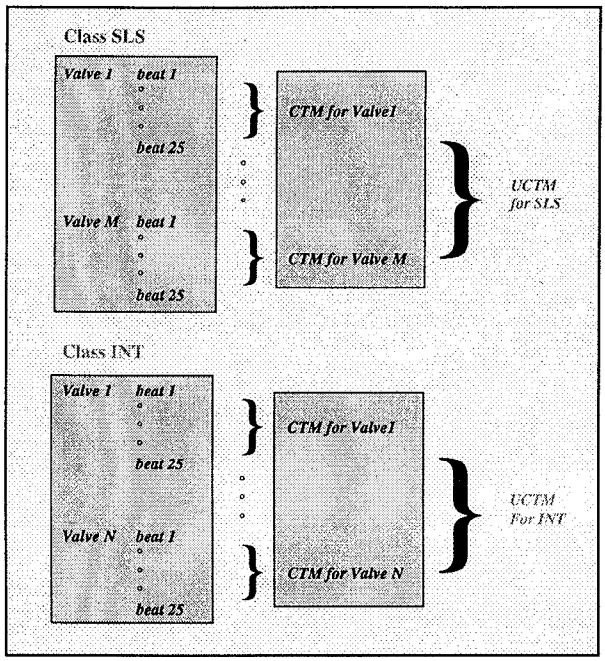


***Figure X-1.*** *Decomposition of Signals from Transient Sounds (beats) to closest-to-median (CTM) Signals and to Two Universal CTM Signals (UCTM).*

We found the 25 spectra for each valve (with one exception) to be tightly clustered demonstrating that the pruning process was effective. Visual inspection of the ensemble CTM spectra shows significant between-valve variation in the spectral fine structure, but general similarity in the peak locations. Visual comparison of the two UCTMs for INT and SLS reveal some differences. Note that UCTMs were calculated for the purposes of summary and display only and do not necessarily indicate that the spectra lack useful classification features. We include the UCTMs for the opening sounds INT and SLS valves and also for the closing sounds shown in Figure X-2 below. The arrows and bullets mark locations where the INT and SLS UCTMs differ offering some expectation that there is potential information available in these signatures to perform a

successful classification. Note that we used the criteria of placing a bullet on either UCTM spectra when a peak of one corresponds to a valley of the other.

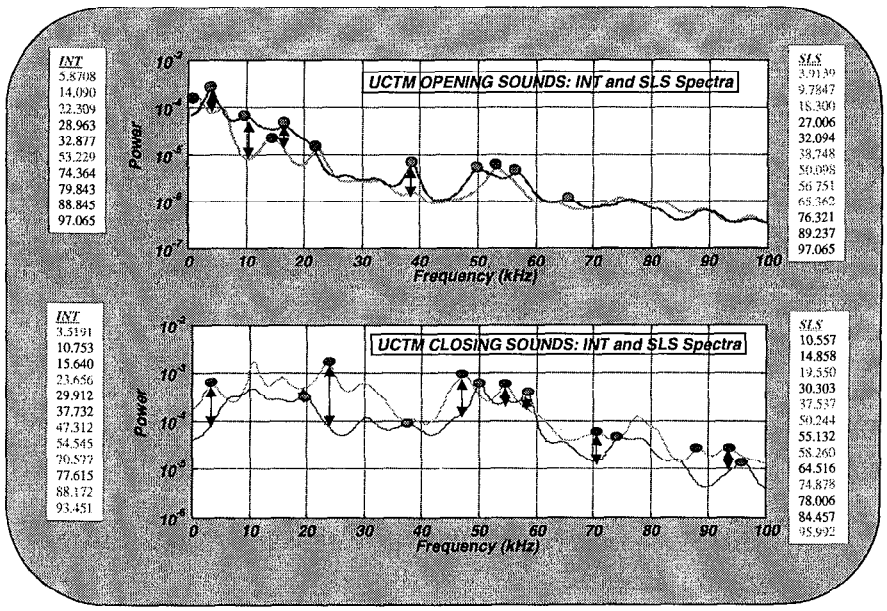


***Figure X-2.*** *Opening and Closing Sound UCTM Spectra Showing Similarity and Differences in Peaks and Valleys.*

# 1.0 BACKGROUND

The LLNL prosthetic heart valve tests were initiated by the need to understand the heart valve dynamics and sounds emitted sounds by the valves in a moderately quiet, reverberation free environment. The results of identifying the sound in the spectral domain could then be extrapolated to improve the overall processing of clinical data already available as well as indicate salient spectral features which could potentially be incorporated into a classification scheme to distinguish a fractured valve from one that is not. Thus, the Bjork-Shiley Convexo-Concave (BSCC) valves were to be tested in an anechoic test tank to eliminate the reverberations and other artifacts experienced in the human body.

The Bjork-Shiley prosthetic heart valve is shown below in Figure 1. Here we see the basic valve components: the flange, disk occluder, inlet strut and the outlet strut. Both the closing and opening valve positions are shown with the inlet strut excited strongly during the closing cycle and the outlet strut excited weakly directly during the opening cycle. The outlet strut is subject to fracturing during valve assembly because it must be bent to insert the disk and consists of a thin piece welded to the flange.

Chronologically, this effort follows a set of initial feasibility and design experiments to develop a heart valve support, activation and measurement system. The system developed at LLNL was feasibility tested in a set of shake down experiments at the SonaTech tank in Santa Barbara, CA during the fall of 1997. Further modifications and improvements to the apparatus were performed and then tested at the U. S. Navy TransDec facility in San Diego, CA during the winter of 1998. After the modified equipment was calibrated according to an experimental protocol (Appendix A), the actual valve tests were performed at TransDec during the summer of 1998. Dr. A. Weyman, the Acoustics Program leader for the panel, observed and participated in the testing in June, 1998. A video tape of the experiment was made available to the BP Panel (August, 1998). This report documents the anechoic testing phase (TASK I) of the LLNL program describing the results of the testing.

## 2.0 METHOD AND MATERIALS

The anechoic tests were performed at the US Navy Transducer Evaluation Center (TransDec) located at the Space and Naval Warfare Systems Center (SPAWARS) in San Diego, California as shown in Figure 2. This facility is used to perform research and development tests, pre-production and production evaluation, and acceptance testing of underwater electro-acoustic transducers. The TransDec facility consists of a 300' x 200' x 38' deep concrete pool spanned by a Bailey bridge supported only at its end points to minimize its interaction with the pool. The pool is contoured to a sector of a canted ellipse with an acoustic trap along the periphery thus simulating an infinite expanse of water nearly free from echoes, providing an anechoic environment. Coupled with the LLNL Heart Valve Support/Activation system (discussed below), the TransDec computer controlled data acquisition system offers an effective method of capturing the BSCC heart valve transient responses sampled at 200 kHz with a large 300 ms window enabling both opening and closing sounds to be captured in a single window for further analysis and eventual classification. We used TransDec's analog-to-digital converter and associated electronics to acquire all of the data during these tests. The LLNL data acquisition system was used in parallel and as backup system. It also enabled us to monitor the triggering system performance in real-time.

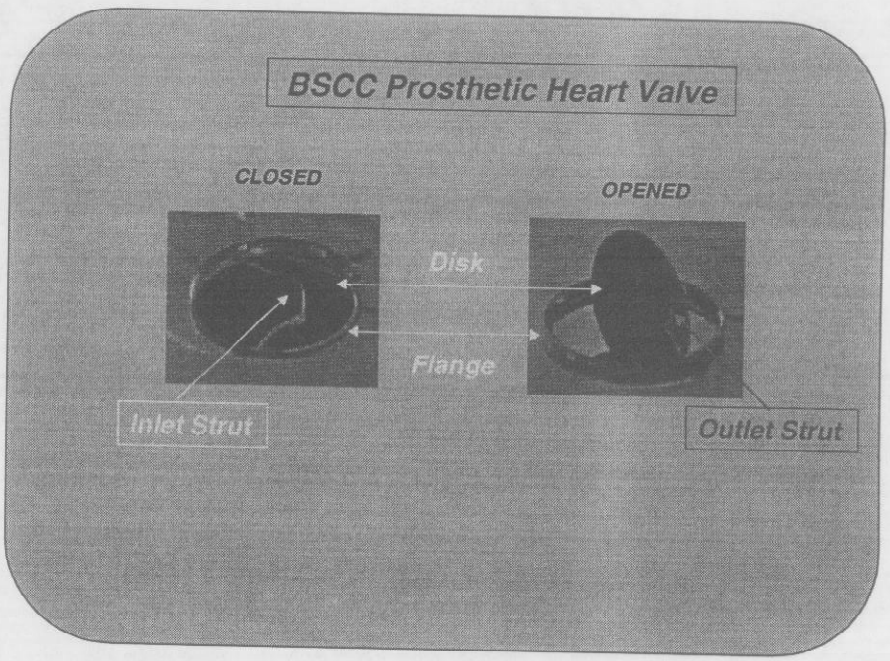


***Figure 1.*** *Bjork-Shiley Convexo-Concave Prosthetic Heart Valve Components with Closed Position Showing Inlet Strut and Opened Position Showing Outlet Strut.*

The structure of the LLNL Heart Valve Support Apparatus is shown in Figure 3 where the mechanism is composed of a sand-filled hoop structure anchored by thin microfilament cables and tied to a motor-driven cam enabling the system to raise and lower the support apparatus activating the valve in the tank. The "spider", which is constructed of silgard, is acoustically transparent in water and used to hold the valve by a friction fit in the valve's grooved ring. A cage-type, hemispherical, plastic structure is mounted on the hoop to hold the hydrophone which can be positioned anywhere along the 0.5 m radius relative to the valve position. After the apparatus is positioned in the tank with the sensitive hydrophone mounted below, the activation cycle begins with the apparatus raised approximately 1 inch by the lever arm. The lever is controlled by the motor-driven cam allowing a gravity free-fall resulting in the valve being opened in a consistent manner. The valve is activated with the disk initially in the closed position to yield an "opening sound." As in the body, the closing sounds are much louder analogous to a door slamming shut as compared to an opening sound which is more like the door hitting a stop (less surface area).

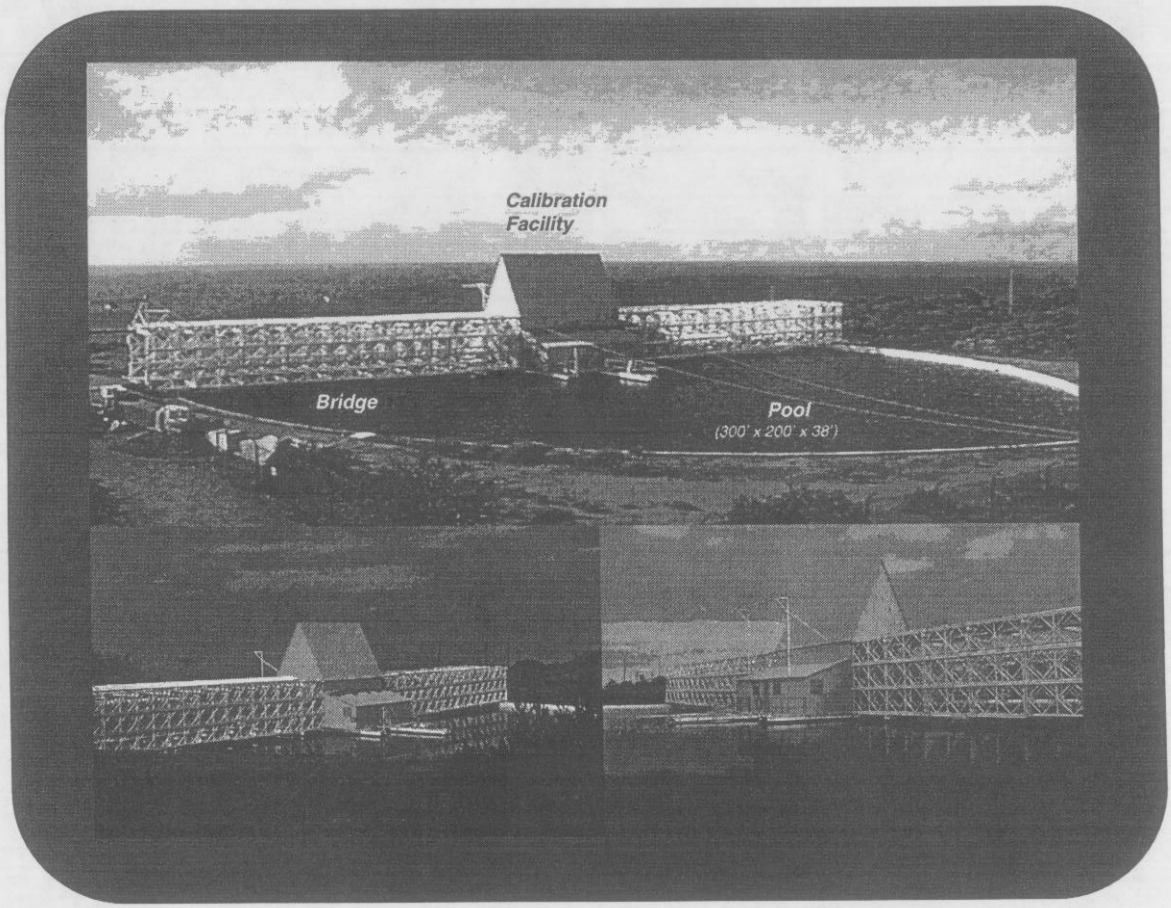


***Figure 2.*** *TransDec (Transducer Evaluation Center) in San Diego, CA is a U.S. Navy transducer calibration and underwater acoustic test facility featuring a 300' x 200' x 38' deep controlled acoustic environment.*

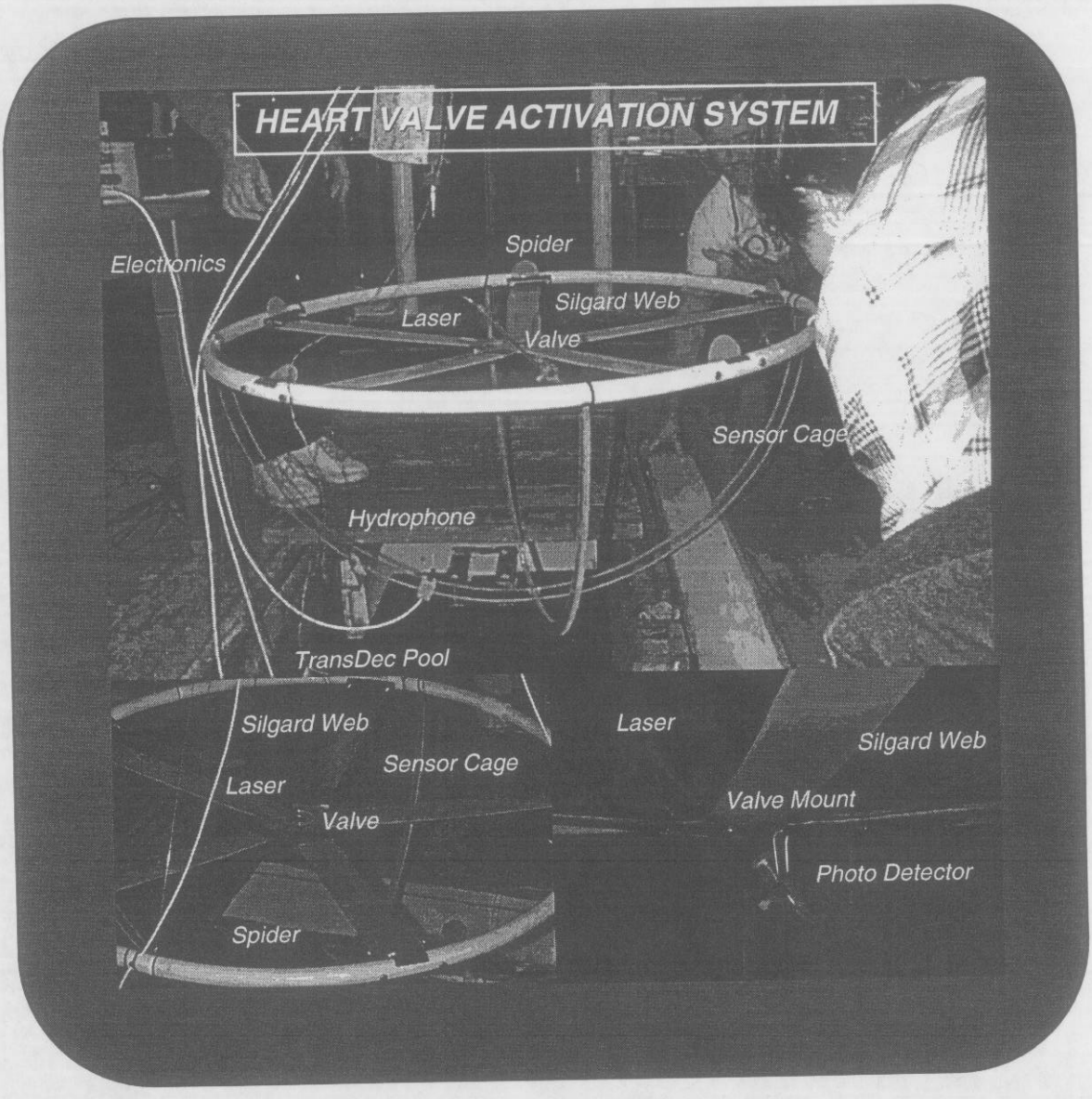


***Figure 3.*** *Heart Valve Activation Apparatus: Hoop with Silgard Valve Mount (spider), Laser Mount and Photo Detector, Valve, Sensor Cage, Hydrophone and associated Electronics.*

Besides these tests, the valve directivity or radiation patterns in the xyz-plane of the valve were obtained by positioning the hydrophone at various angles along the spherical cage shown above in Figure 3. The heart valve is activated as described above and its root-mean-squared response calculated from measurements at angular positions in the xz-plane for both opening and closing sounds.

A data acquisition system was designed and assembled to capture the sound radiated by the heart valve under test. The main objective of the tests was to acquire spectral features which will eventually be used to improve the acoustical signal processing of current and future patient acoustical data. Also this information can provide "input" signals to signal processing algorithms which will eventually be used to extract (deconvolve) the valve sounds from those measured and filtered by the body enabling direct comparisons (TASK III) with anechoic and eventual pulse duplicator spectra. The specifications of the system are shown in Table 1 below with its main design capability aimed at wide-band collection of heart valve sounds. The design frequency spectral band was 100 kHz thereby requiring a 200 kHz digitizer. The assembled system consists of (see block diagram in Figure 4 and system picture in Figure 5): (1) charge amplifier; (2) measurement amplifier; (3) conditioning filter (anti-alias); (4) digitizer; (5) computer; (6) disk storage and (7) associated laser trigger/tag system. This system enables the collection of the wide-band data which is synchronized by the laser trigger, tagged temporally, amplified, filtered, amplified again, supplied to the computer and archived on removable disk cartridges.

**Table 1.** ***LLNL Anechoic Study Digitization System Components***

| | | |
|---|---|---|
| Hydrophone | B&K | 0.1Hz-180 kHz |
| Digitizer | IOTech | 200 kHz (single channel) |
| Conditioning Filter | B&K | 100Hz-200kHz |
| Charge Amplifier | B&K | 0.2Hz-200kHz |
| Measurement Amplifier | B&K | 1.0Hz-200kHz |
| IBM-PC (Pentium Pro) | Dell Latitude | 160 MHz |
| Disk (Removable) | Iomega Jazz | 1GB cartridges |
| Helium Neon Laser | Melles Griot | 7 mw |
| Photodetector | Custom | |
| Trigger circuit | Custom | |

A portable, real-time data acquisition system was assembled to capture the acoustic sounds emanating from the heart valve when they are actuated. The main components of this system (outlined above) are an IOTech Wavebook 512 digitizer and a Dell Latitude laptop computer. LabView software was developed to control the data

acquisition and storage. The graphical user interface which appears on the computer screen allows various digitizer parameters to be set and displays the captured waveforms. These waveforms can be stored on the computer using the LabView program.

The acoustic signal detected by the hydrophone is amplified and filtered, and is then fed into one channel of the digitizer. The trigger signal is fed into the other channel. The desired parameters for the digitizer are chosen and it is then set to accept a trigger. When the digitizer receives a trigger signal, it captures the acoustic waveform as well as the trigger. These waveforms are immediately displayed on the screen as amplitude versus time plots. The signals can be stored to file on the computer for later processing and reduction. As mentioned previously, we used the TransDec digitizer to collect all of the data used in the analysis because of its larger data window. The portable system was used as a backup as well as an on-line monitor of the trigger during transient runs.

As mentioned above, the trigger signal for data acquisition is optics based. Light from the HeNe laser is transmitted by an optical fiber to the heart valve under test. The light is directed such that when the valve is open, light is transmitted through the opening left by the disk and is incident on the photodetector. The photodetector waveform is affected by the duration of the opening and also by the amount (distance opened) of disk opening. If the valve only opens partially, the photodetector signal will not be at maximum amplitude. The optical trigger signal is amplified, debounced and delayed by a user selectable amount before being used to trigger the data acquisition. This is accomplished in the custom trigger circuit.

System operation commences when the motor-driven cam raises the lever and therefore the hoop and then drops it into a gravity free fall. During ascension the valve is closed (disk shut) and the trigger signal is high, no light on the photodetector. Once in free fall, the valve opens suddenly when the pressure is increased sufficiently. The laser beam is detected giving a low amplitude during opening. This cycle is depicted in Figure 6 below, where a typical opening-closing sequence is captured in the time domain. In this way the acquisition system is initiated and the data captured during operation. This laser-driven trigger system was used to trigger the LLNL portable system as well as the TransDec system.

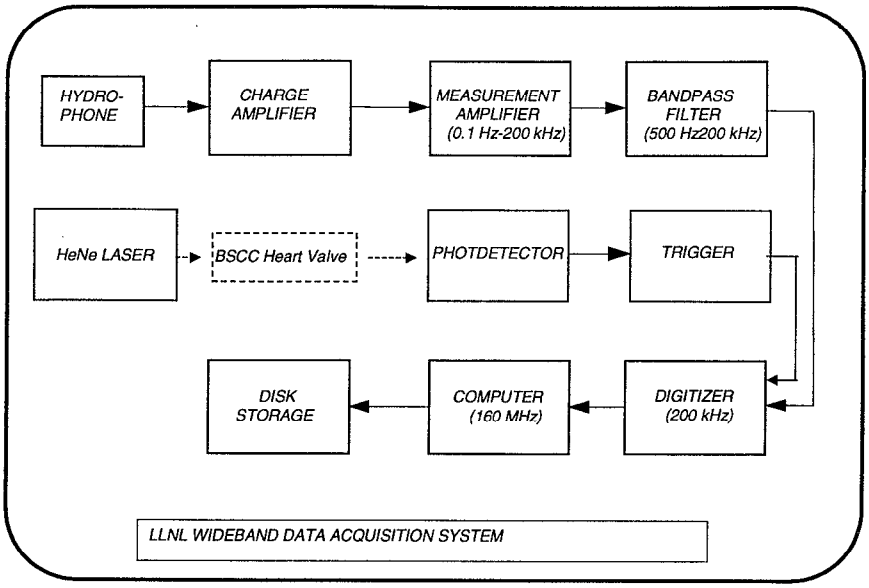


***Figure 4.*** *Block Diagram of Heart Valve Activation System Including Laser Tagging/Trigger System.*

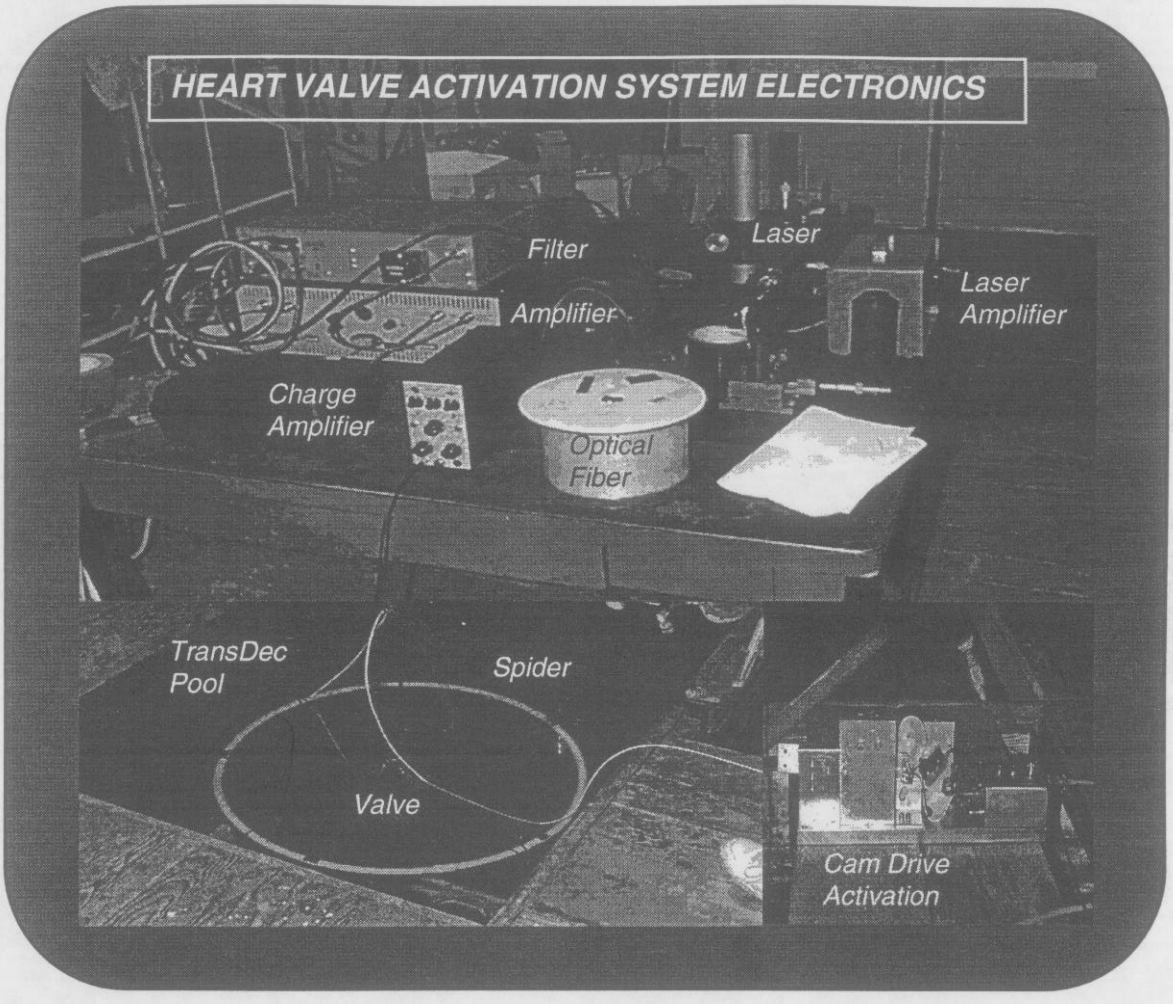


***Figure 5.*** *Heart Valve Activation System Electronics: (a) Laser, Amplifier, Fiber Optics. (b) Sensor Amplifier, Bandpass Filter and Charge Amplifier. (c) Motor Driven Cam with associated Electronics for Filtering and Triggering.*

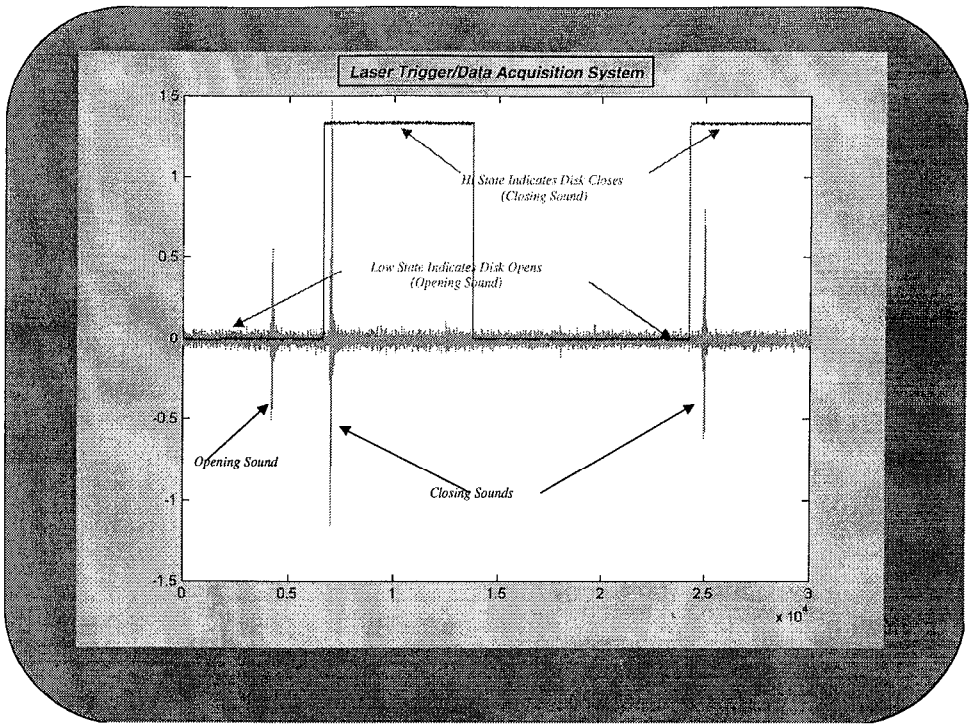


***Figure 6.*** *Typical Laser Trigger/Tagging of Heart Valve Sounds.*

# 3.0 EXPERIMENT

In this section we describe the experimental procedure or protocol followed to gather the anechoic heart valve acoustic data systematically. We include the full protocol in Appendix A for the interested reader. The testing proceeded in a systematic manner consisting of the following basic measurements:

1. Data Acquisition System Calibration and Baseline Measurements
2. Background Noise Measurements
3. Sensor Noise Measurements
4. Instrumentation Noise Measurements
5. Transient Response Measurements (50 Valves):
   - 1 Background Noise Run
   - 100 Closing Sounds
   - 2 Background Noise Runs
   - 100 Opening Sounds
   - 1 Background Noise Run
6. Noise Measurements
   - 1 Background Noise
   - 50 Drop Cycles (valve held opened)
   - 1 Background Noise
   - 50 Drop Cycles (valve held closed)
7. Heart Valve Directivity Pattern Measurements
   - Position the hydrophone at the prescribed position and secure
   - Activate the heart valve as in Step 6 above (w/o valve held closed)
   - 5 runs per angle
   - Calculate the root-mean-squared (RMS) power at the specified angle
8. Environmental Noise Measurements

The data acquisition system calibration and baseline measurements essentially check the electronics and validate overall system integrity and performance to assure reliable measurements. Since we used both the real-time and TransDec systems, the performance of both systems was validated simultaneously. Once completed, background noise measurements were performed to establish the environmental conditions and localize potential noise sources in the tank. Here, various sources of noise were determined and eliminated where possible (e.g. recirculating pumps, extraneous electronics, etc.). The spectral response of the tank background noise was established as correlated with the instrumentation. The results are shown in Figure 7. The spectrum

rolls off exponentially, which is the characteristic of a simple one-pole system and then flattens after approximately 10 kHz with minimal noise which is approximately two orders of magnitude lower in amplitude with slight gains in the 20 kHz and 35-60 kHz bands. These results imply that we need not worry about any tank resonances generating false peaks in the measured valve spectrum.

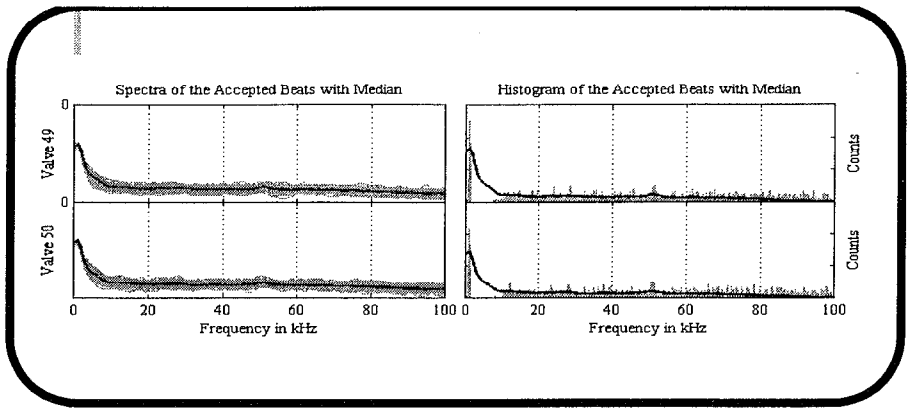


***Figure 7.*** *Typical Background Noise Spectrum with Exponential (1 pole) Roll-Off and Flat Broadband Response.*

A heart valve, identified only by a randomly assigned number (see Appendix B for list), was cleaned in an ultrasonic cleaner, rinsed in tap water, placed in the "spider" and aligned with fiduciary marks. The "spider", heart valve, and hydrophone were then sprayed with a soap solution to limit the formation of bubbles on these parts. The entire apparatus was then lowered into the water to a depth of a few inches. Remaining bubbles were removed from the "spider" by gently running a hand along it. The apparatus was positioned below the cam actuator and lowered to the test depth and the cam actuator was switched on. The hydrophone signals were monitored for consistency and level to determine the gain setting for the digitizer. The opening and closing of the heart valve was observed from the surface to ensure that it was opening and closing correctly. Also, the correct operation of the fiber optic-photodetector trigger circuit was verified. Adjustments were made to the system as necessary until operation was satisfactory.

The header information for the data file was changed to reflect the current conditions and appropriate log entries were noted. The cam actuator was then switched off, and a background noise waveform was captured with the gain of the digitizer set for closings. The cam actuator was then switched on, and 100 signals were captured with the gain level at this level. After capturing 100 waveforms, the cam actuator was switched off and another noise trace was captured at the same gain setting. The digitizer gain was then adjusted for openings and a background noise trace was captured. The cam actuator was then switched on and 100 waveforms were captured with the digitizer at this gain setting. The cam actuator was then switched off and a final background noise trace was captured. This completed the testing of the heart valve, and the hoop was raised out of the water and the heart valve removed.

As noted above, different amplifier gain settings were used for the opening and closing sounds. This was to facilitate the goal of using as much of the dynamic range of the digitizers as possible for the signals of interest. As a consequence, when the gain setting was adjusted for the quieter opening signals the closing signals would often saturate the digitizer because of their larger amplitude.

# 4.0 SIGNAL PROCESSING

In this section we discuss the basic signal processing performed on the raw heart valve transient response measurements after they had been acquired at the TransDec facility during the suite of tests performed in mid-May and early June 1998. The extraction of data from the 1 gigabyte (GB) Jazz cartridges consisted of the following steps:

1. Raw *Data Conversion* from TransDec ASCII to MATLAB binary format;
2. *Coarse Cutting* of Data into:
   - Opening Sounds (3000 samples)
   - Closing Sounds (3000 samples)
   - Noise (just prior to valve initiation)
3. *Fine Cutting* of Data for:
   - Opening Sounds (512 samples)
   - Closing Sounds (1024 samples)
   - Pre-Activation Noise
4. *Preprocessing* of Cut Data for each sound and noise consisting of:
   - Trend Removal
   - Piecewise tapered windowing
5. *Spectral Estimation/Screening*
6. *Peak Frequency* Response Histogram Estimation
7. *Median* Signal Estimation
8. *CTM Estimation*
9. *Spectrogram* Estimation

Initially the data gathered at the TransDec facility was written to the 1 (GB) Jazz disks in ASCII format for archiving purposes enabling BPHVP the flexibility to distribute the data in the future. This data was read into MATLAB, our basic processing package, and converted to its internal binary format reducing the size and facilitating further processing. Next, a coarse cut of the large 300 ms data files was automatically executed by locating the maximum peak fiducial (closing sound) and extracting a 15 ms window (3000 samples) centered on the peak of the data assuring the capture of both opening and closing sounds. Once the coarse cuts were accomplished, the fine cutting of the data commenced. Here the procedure was minimally interactive, since the capture and cutting does not guarantee that all of the transient maxima align. After overlaying all of the coarse cut transients, a cursor was positioned over the appropriate location and all transients was cut to that location. It was found that most opening sounds could be captured in a 2.5 ms window (512 samples), while it required a 5 ms window (1024 samples) to capture the complete closing transients due to the long pre-cursor and bounce transients that followed. A typical set of 24 INT valve opening sounds produced by the fine cut procedure is shown in Figure 8 below.

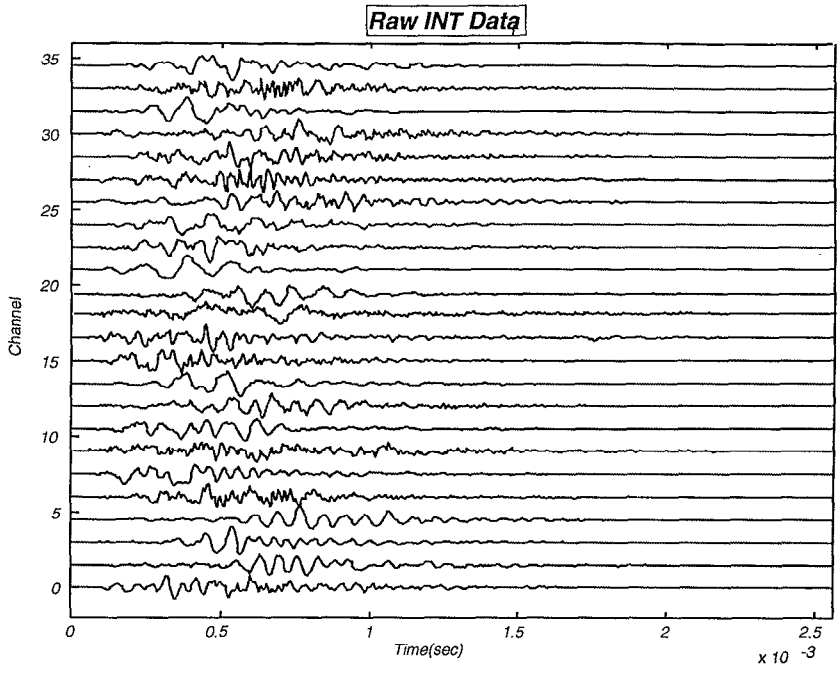


***Figure 8.*** *Tank Transient Response Tests: Typical Set of INT Valve Opening Sounds.*

The preprocessing of the fine cut transients is necessary to reduce the measurement noise and potential artifacts for performing the subsequent spectral estimation. Trends (linear) are removed from the data and they are piecewise windowed, that is, they are tapered on each end using a 2% tapering window (Blackman) to assure no end effect artifacts (Gibb's phenomena) in the spectra. Following the tapering, the data are half-windowed, which means that a typical window (Blackman here) is cut in half with its maximum at the origin. This type of window assures the energy in the transient is preserved approximately. Once this is accomplished the data are ready for spectral estimation and screening.

Of the 100 transient responses gathered, we chose to use the "best" set of 25 spectra to represent the ensemble statistically. The approach was to estimate the spectra and use the median absolute deviation (MAD) statistic to select the best spectra (see Appendix C for more details). We used various spectral estimators to accomplish this task with varying results. Our usual approach was to use the parametric maximum entropy method (MEM) consisting of estimating an all-pole or equivalently autoregressive model from the noisy measurement data [1]. We found that it was not possible to estimate a consistent model order using the Minimum Akaike Information Criterion (MAICE). We used a nonparametric approach and applied the minimum variance distortionless response (MVDR) method known to produce reliable spectra along with its inherent smoothing. The MVDR is a data adaptive technique which

essentially provides unity gain in the center of each Fourier bin and minimizes the noise by producing a data adaptive taper [1,2] rather than the default rectangular taper inherent in the bin structure. It is particularly effective when SNR are low and smoothing is necessary. Details of the MVDR approach to spectral estimation are reported briefly in Appendix C. We discuss the results of applying the MVDR spectral estimator subsequently, but we first describe the entire suite of processing used to perform the analysis.

The *Peak Frequency Histogram* estimate is performed by simply detecting the spectral peaks of each of the 25 best transient spectra and estimating their distribution using a histogram. This display is quite helpful in finding the predominance of valve spectral peaks and can be very useful for analysis and comparisons.

The *CTM signal*, which can be assumed to represent the response of the particular valve under test, is determined by a robust statistical approach. After the best 25 spectra have been selected using the MAD approach, the sample median spectrum is determined by simply estimating the median amplitude in *each* bin. The resulting median spectra estimate is then used as the reference to determine which of the individual spectra is closest to it, which is precisely what the MAD algorithm provides. The number of this transient signal (beat) is identified and taken as the best representative of the particular valve's transient response. The CTM signal is used in subsequent analysis to study the valve performance. For instance, we compare the ensemble of CTM spectra (overlay plot) to demonstrate the similarity of each spectrum of the INT and SLS class and perform peak comparisons. Performing this same procedure on the CTM ensemble of the INT and SLS class we can obtain the universal or UCTM for each resulting in two signals to perform analysis. Thus, the UCTMs are taken in this analysis to be representative of the INT and SLS classes. The UCTM is used in the final step to perform comparative analyses as well as time-frequency estimation using a parametric processor. By observing the time-frequency spectrum, we can see how the valve frequency response changes as a function of time. This phenomena was observed and utilized in classification by both TRACOR [3] and the SAI [4] teams for closing sounds.

This completes the discussion of the signal processing of the heart valve sounds for eventual classification and comparison. Next we discuss the results of this effort.

# 5.0 ANALYSIS

In this section we discuss the results of spectral estimation applied to the INT and SLS valves. The preprocessed data (discussed above) are processed beat-by-beat using the nonparametric MVDR spectral estimator. Initially, in the first subsection, we investigate the *opening* sounds and analyze them independently, then we examined the *closing* sounds. Finally, we compare our results for both.

The goal of this effort is to uncover differences between the INT and SLS spectra by visual inspection because we are looking for discriminants between these two classes. However, recall that in the LLNL classifier this task is performed automatically by the feature extraction. The detailed classification results will be reported on independently when that effort is completed.

## *5.1 ANALYSIS: HEART VALVE OPENING SOUNDS*

We discussed the experiments performed in the TransDec anechoic tank in previous sections. In this section we concentrate on analyzing the opening sounds of the INT and SLS valves tested in the tank. Typical results for intact valve opening sounds are shown in Figure 9 below. Recall that we use the MAD statistic to select the "best" 25 transient spectra for the valve. A typical ensemble (green) is shown in the Figure 9a along with its corresponding median spectral estimate (red). The associated Peak Frequency Histogram is shown in Figure 9b indicating dominant resonant peaks at approximately 12, 18, 22, 32, and 55 kHz, that is, over more than 10 counts in the histogram. The valve transient CTM signal is shown in Figure 9d along with its corresponding spectra in Figure 9c. The results appear quite good for this valve in the sense that the ensemble bounds are small with the variance significantly smaller below 60 kHz. The CTM signal (time series) is used in the spectrogram analysis to follow. These results indicate that our mechanism appears to excite the valve sufficiently to make these measurements in a reasonable manner. We catalog all of the tested valves in this manner for both opening and closing sounds shown in Appendices C and D.

To compare the spectral response of the valves of either the INT or SLS class, we create a CTM ensemble for each class. These results are shown in Figure 10 below. In Figure 10a we see the ensemble of CTM spectra for both the INT valves along with their corresponding Peak Frequency Histogram estimates below in Figure 10b. The results for the SLS opening sounds are shown in Figure 10c and Figure 10d. The peak-valley differences are shown in the color coded lists of these figures. It is interesting to note from this figure that if we first mentally "smooth" the spectra ignoring resonant peaks that the resulting overall spectra have similar shapes which is not unexpected because other non-fractured parts of the valve still vibrate under both INT and SLS conditions. We

notice an initial peaking of both spectra around *10* to *15 kHz,* peaking in the *20 kHz* band with a linear decay up until *40 kHz*, a broad response follows with peaking between *40* and *60 kHz* and from *60 kHz* on the spectra flattens out (high frequency noise). A more detailed observation of the figure indicates that the INT spectra are similar with dominant resonant peaks (histogram) at 4, 6, 8, 17, 29, 30, 40, 50 kHz (above 3 counts), while those for the SLS spectra (above 3 counts) are 4, 7.4, 12.4, 21.6, 53 kHz.

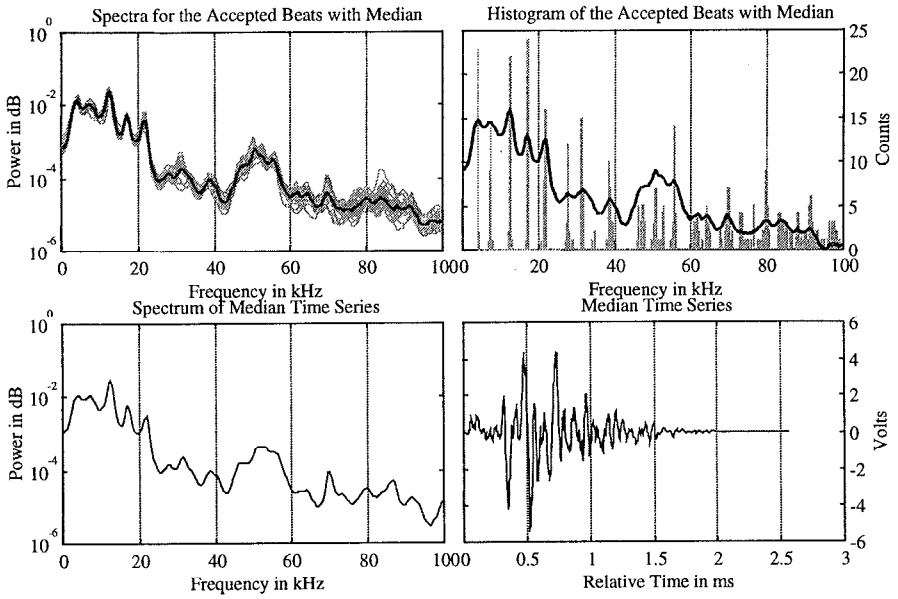


***Figure 9.*** *Typical MVDR Spectral Estimation for INTACT Valve No. 1 Opening Sounds: (a) Ensemble (green) and Median (red) Spectra. (b) Peak Frequency Histogram Estimates (green) with Median (blue) Spectra. (c) CTM Transient Spectra . (d) CTM Signal.*

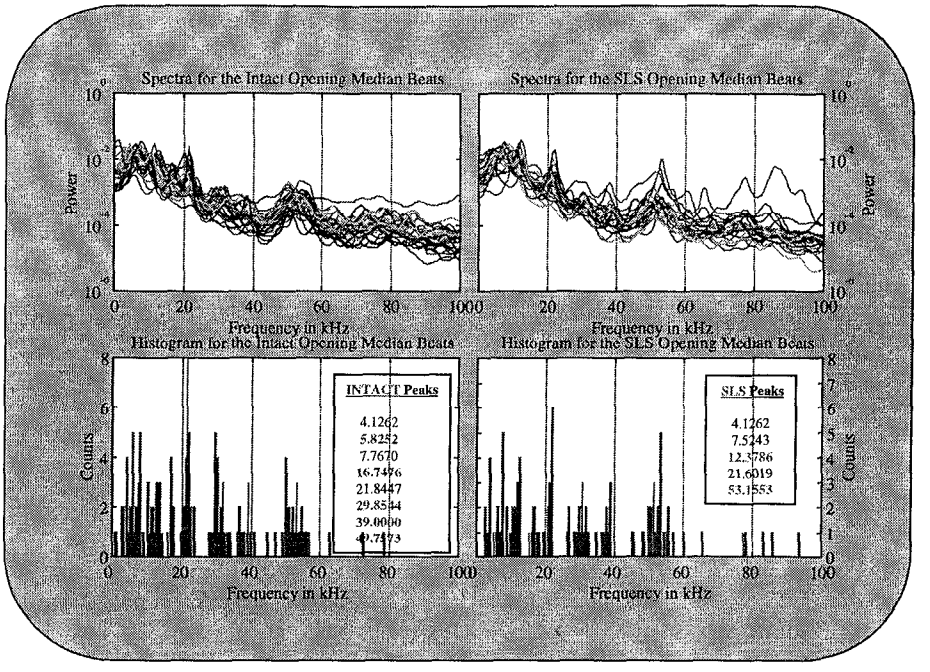


***Figure 10.*** *Ensemble CTM Opening Sound Spectra for Tested INTACT and SLS Valves: (a) INT Valves Ensemble CTM Spectra. (b) INT Valves Peak Frequency Histogram Estimates. (c) SLS Valves Ensemble CTM Spectra. (d) SLS Valves Peak Frequency Histogram Estimates.*

The spectral response of each valve is depicted as an image in Figure 11. Here we apply the MUSIC algorithm (see Appendix C) to enhance the peaks of the responses and make it easier to identify patterns in the data. This figure shows the similarity and differences of spectral responses in both the SLS and INT valves across the ensemble. There is a lot of power in the lower frequency bands (<25 kHz) as indicated in the figure. However, from these spectra there appear to be differences in the bands above 25 kHz. The SLS (red) and INT (green) boxes are shown to identify some of these bands centered at approximately, SLS:***12, 21, 30, 38, 53*** kHz; and for INT: ***6*** kHz. We use the histograms as well to help identify some of these bands as shown in Figure 12 where we observe the Peak Frequency Histogram estimates (threshold) displayed with the dominant bands for both SLS and INT. From this figure we can observe the location of peak frequencies present in marked bands. Note that some peaks have been eliminated for ease of viewing by the threshold technique. This figure again shows the similarity and differences of spectral responses in both the SLS and INT valves across the ensemble. The SLS (red) and INT (green) boxes are shown to identify some of these bands centered

at approximately, SLS: ***12, 53 kHz; INT: 6, 17, 30, 50 kHz.*** Just how this property affects the performance of the classifier will be investigated when the actual classification is performed in TASK II.

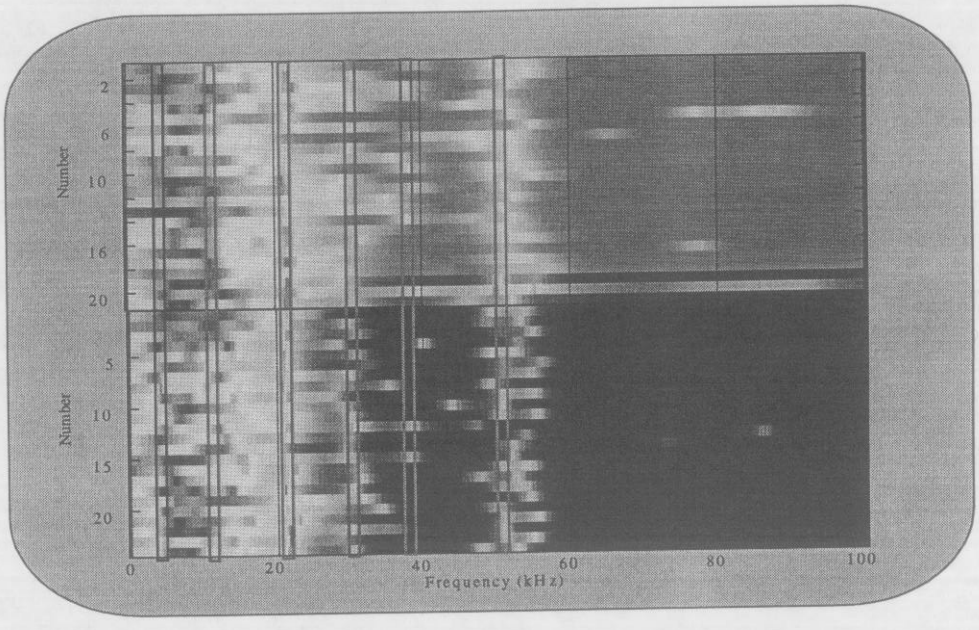


***Figure 11.*** *Spectral (MUSIC) Images of SLS (upper) and INTACT (lower) Opening Sounds in Frequency Bands (SLS: **12, 21, 30, 38, 53** kHz; INT: **6** kHz).*

Another approach to observing any differences between the SLS and INT valve responses is to estimate the UCTM of the SLS and INT spectra and then use it for comparison purposes. The idea here is to say that these signals can be considered representative of the particular valve class as measured in the anechoic tank. The estimation was performed using the MAD statistic (Appendix C) for selection as before and the results are shown in Figure 13 below. Here we see the selected (Valve No. 6) INT sound time series and its corresponding power spectrum in Figure 13a and 13b with the SLS time series (Valve No. 10) and its spectrum shown in Figure13c and 13d. The

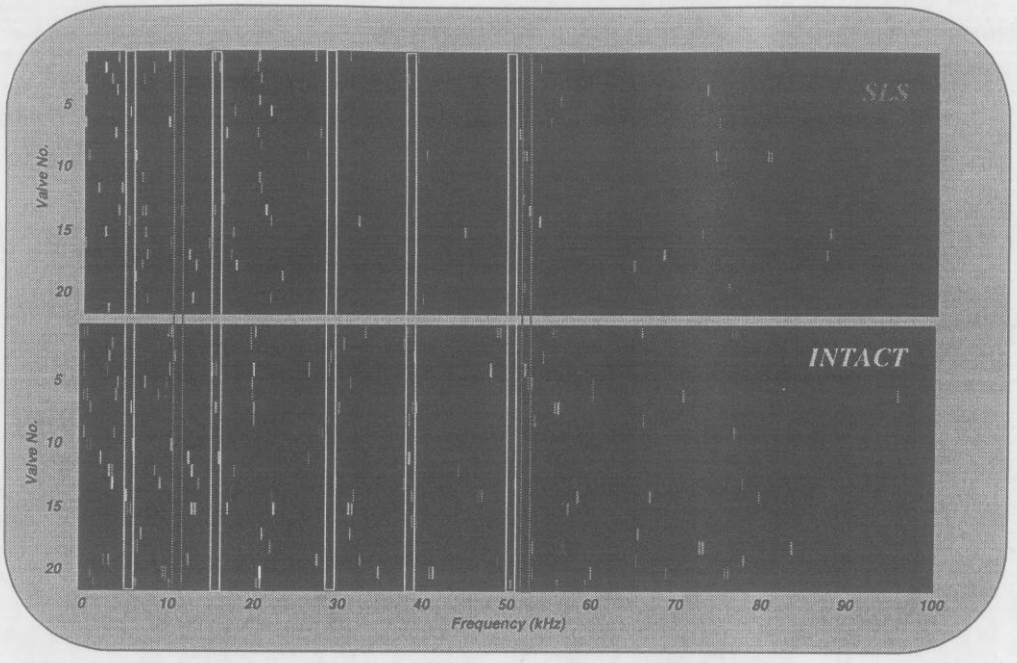


***Figure 12.*** *Thresholded Peak Frequency Histogram Images of SLS and INTACT Opening Sounds in Frequency Bands (SLS: **12, 53** kHz; INT: **6, 17, 30, 50** kHz).*

differences between these spectra are noted in the figure with *SLS: **3.9, 9.8, 18.3, 38.8, 50.1, 56.8, 65.4** kHz; INT: **5.9, 14.3, 22.3, 53.2** kHz).* By differences, for example, we mean the appearances of a peak in one spectrum and a valley in the other class. Spectral classifiers are based on difference features, which are sometimes readily observed by visual inspection or are more subtle and must be found by sensitive spectral feature selectors [5]. Even though the opening sounds contain more direct information about the outlet strut fracture [6], they are plagued by noise because their intensity is low yielding a much lower SNR than the closing sounds. Therefore, we develop a noise cancelling algorithm which uses on input each of the measured time series shown in Figure 13 as well as a reference noise time series characterizing the noise contaminating these measurements. We choose to use the noise just prior to the onset of the opening sound transient for our reference, since it should contain the contaminating noise without signal --- an ideal condition for canceller design. We show both the INT and SLS signals with their corresponding "pre-noise" time series used in the cancellation scheme in Figure 14. Since the data are assumed non-stationary, we use an adaptive cancellation scheme based on the LMS algorithm discussed briefly in Appendix E [7]. The results of preprocessing the data (trend removal, tapering, and windowing) and applying the noise canceller to the

valve class CTM spectra are shown in Figure 15 below. Here we see the cancelled INT (solid green) and SLS (solid red) spectra with the original INT (blue dots) and SLS (magenta dots) shown in the background for comparison. We again show the difference in the spectra. These peaks (shown in the Figure) are *SLS: 27.8, 38.8, 63.4, 76.3, 93.5 kHz; and INT: 6.7, 22.3, 70.1 kHz.* Next we utilize the same algorithm for analysis purposes, but again the aim is to extract any of the differences between INT and SLS opening sounds.

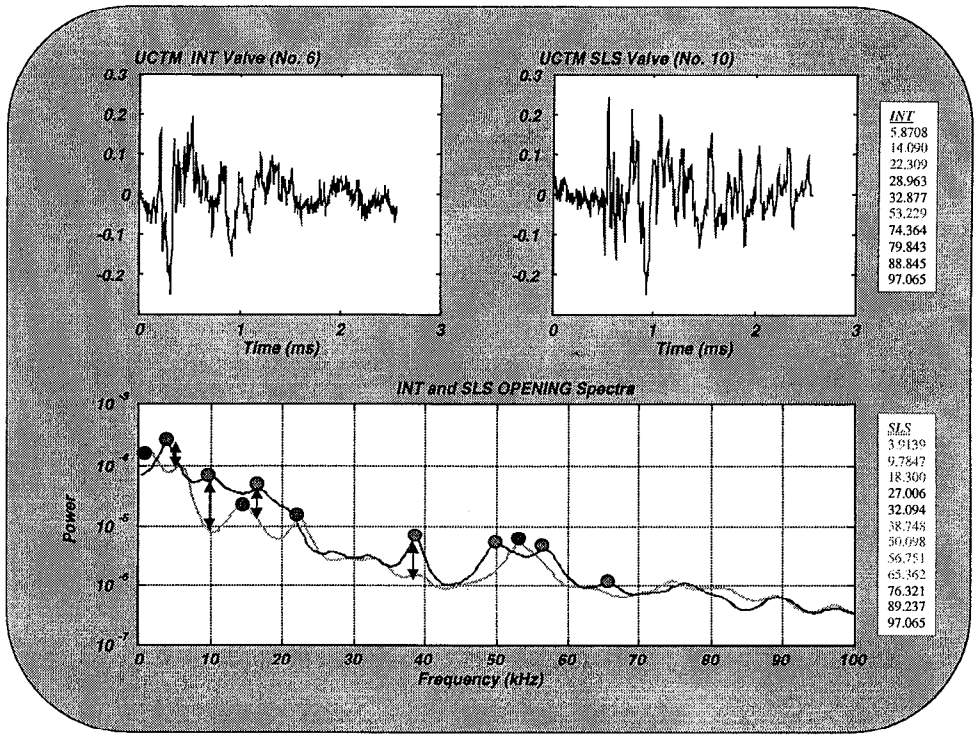


***Figure 13.*** *UCTMs of SLS and INTACT Opening Sounds and Spectra and Differences (SLS: **3.9, 9.8, 18.3, 38.8, 50.1, 56.8, 65.4** kHz; INT: **5.9, 14.3, 22.3, 53.2** kHz).*

Next we applied the adaptive correlation (noise) cancelling algorithm (see Appendix E) to observe the differences more readily. With the INT UCTM used as the data channel and the SLS sound (see Figure 13) used as the reference channel respectively, the correlation canceller was designed (64 weights, step-size of 0.1). It essentially produces two outputs: the portion of the two signals (SLS/INT) that is correlated (COR) with corresponding spectra (green) and the portion of the two signals that is uncorrelated (UNCOR) with the spectra (red). The resulting spectra are shown in Figure 16 including the UCTM spectra for both original SLS (magenta dots) and INT

(blue dots) spectra for comparison. Again we observe the spectral "differences" that a classifier might utilize with the peaks corresponding to nulls annotated with circles and

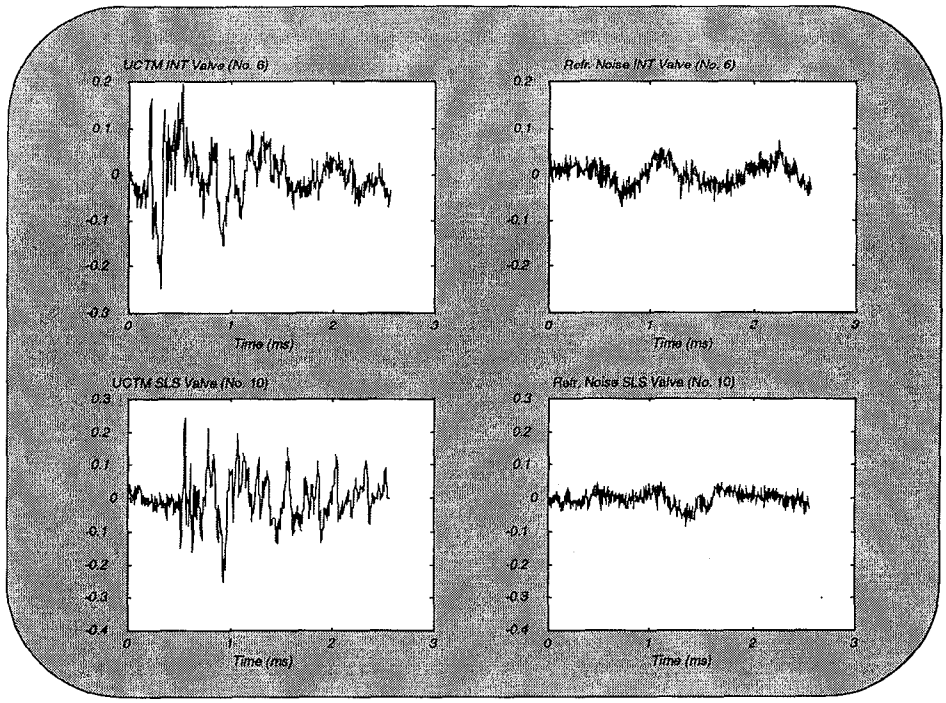


***Figure 14.*** *UCTMs SLS and INTACT Opening Sounds and Corresponding Pre-Noise Sections for Noise Cancelling.*

labeled. The uncorrelated spectrum shows peak differences at: *3.7, 9.9, 38.5, 75.5 kHz;* and the correlated at*: 29.5, 53.7, 62, 73, 79 kHz.* Comparing these peaks with the original SLS/INT spectra data validates the observation.

We compile the results of all of this analysis of the opening sound in Table 2 below where we incorporate all of the information from each individual technique and highlight the peak/valley differences for both SLS (red) and INT (green). This completes the analysis of opening sounds.

For completeness we include the spectograms (instantaneous spectrum) of the UCTM valve sounds. The recursive-in-time spectogram estimator is discussed in detail in Appendix G. The main purpose of this analysis is to observe the time-frequency response of the UCTM INT and SLS class signals. We are looking for changes in the resonances at particular times to view the non-stationary nature of the valve response function. Once the spectogram estimator converges to steady state the underlying pole-zero parameters yield a fixed spectrum equivalent to the MVDR estimator (Appendix C).

Recall that most of the closing sound classifiers use the time-frequency approach to select features [3,4]. We found that the UCTM closing sounds did exhibit more non-stationary characteristics when compared to the UCTM opening spectograms (see Appendix G for details).

which shows the non-stationary nature of the sounds and led us to incorporate adaptive schemes for processing. Next we analyze the closing sounds in a similar fashion.

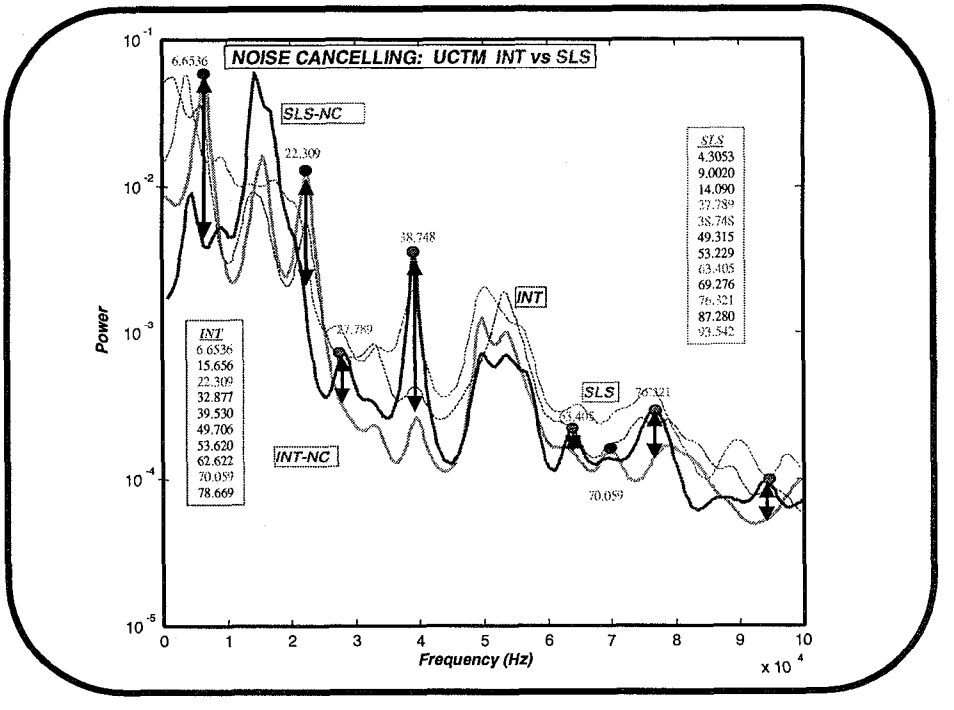


***Figure 15.*** *Comparison of "Noise-Cancelled" OPENING Sound Spectra for UCTM SLS and INT Valve Responses. Frequencies are annotated for spectral peaks as SLS: 27.8, 38.8, 63.4, 76.3, 93.5 kHz; and INT: 6.7, 22.3, 70.1 kHz.*

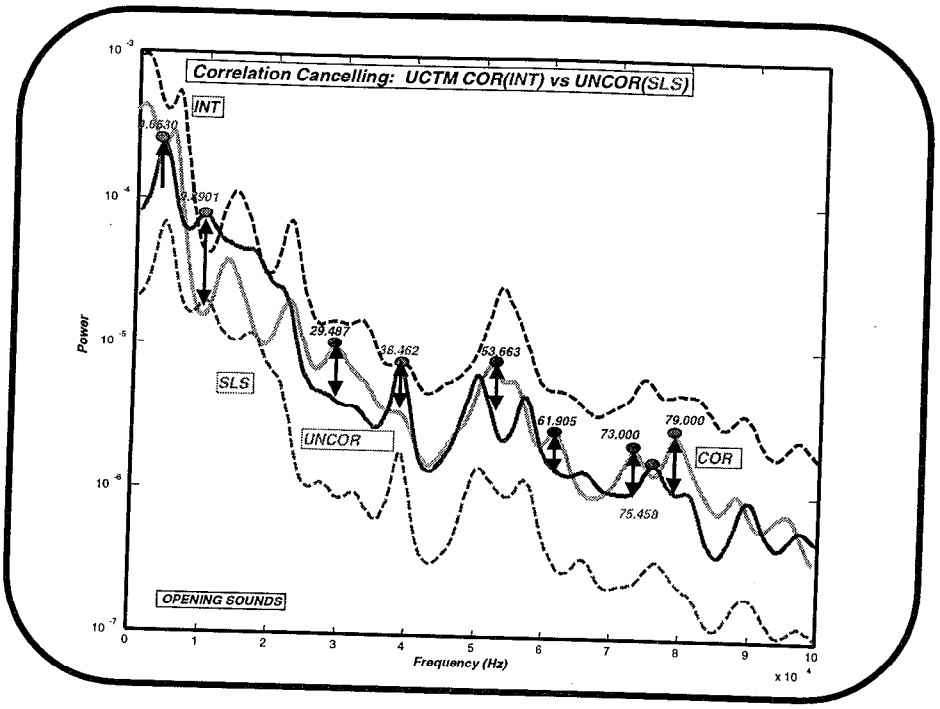


***Figure 16.*** *Comparison of OPENING Sound Spectra for UCTM SLS and INT Valve Responses. Frequencies are annotated for spectral peaks as SLS: 3.7, 9.9, 38.5, 75.5 kHz; and INT: 29.5, 53.7, 62, 73, 79 kHz.*

**Table 2. COMPOSITE ANALYSIS of HEART VALVE OPENING SOUNDS with Peak/Valley Differences**

| Ccanl | CTM Spectra | | CTM Image | | CTM Histogram | | CTM-CTM Spec | | CTM-CTM Ncanl | | CTM-CTM | |
|---|---|---|---|---|---|---|---|---|---|---|---|---|
| Freq | SLS | INT | SLS | INT | SLS | INT | SLS | INT | SLS | INT | UNC | COR |
| 0 | 4.1<br>7.5 | 4.1<br>5.8<br>7.8 | | 6 | | 6 | 3.9<br>9.8 | 5.9 | 4.3<br>9 | 6.6 | 3.7<br>9.9 | |
| 10 | 12.4 | 16.8 | 12 | | 12 | 17 | 18.3 | 14.3 | 14.1 | 15 | | |
| 20 | 21.6 | 21.8<br>29.9 | 21 | | | | 27 | 22.3<br>28.9 | 27.8 | 22.3 | | 29.5 |
| 30 | | 39 | 30<br>38 | | | 30 | 32<br>38.8 | 32.9 | 38.8 | 32.9<br>39.5 | | |
| 40 | | 49.8 | | | | | 40 | | 49.3 | 49.7 | | |
| 50 | 53.2 | | 53 | | 53 | 50 | 50.1<br>56.8 | 53.2 | 53.2 | 53.2 | | 53.7 |
| 60 | | | | | | | 65.4 | 60 | 63.4<br>69.3 | 62.6 | | 61.9 |
| 70 | | | | | | | 76.3 | 70 | 76.3 | 70.1<br>78.7 | 75.5 | 73<br>79 |
| 80 | | | | | | | 89.2 | 80 | 87.3 | 80 | | |
| 90 | | | | | | | 97.1 | 90 | 93.5 | 90 | | |
| 100 | | | | | | | | | | | | |

## 5.2 *ANALYSIS: HEART VALVE CLOSING SOUNDS*

In this subsection we perform an analysis of the closing sounds produced by the valve during anechoic testing similar to the previous subsection. Since the closing sounds offer a much better SNR than the openings, we did not apply the noise cancelling processor to this data. The analysis proceeds identically as for the openings. We selected the "best"25 spectra for each valve using the MAD statistic (see Appendix D for detailed spectra), and estimated the CTM signal representing the valve response (in a mean-squared error sense). Next we collected all of the CTM sounds representing the particular class, INT or SLS and estimated the UCTM. From this ensemble we estimated the power spectrum using the nonparametric MVDR estimator along with the corresponding Peak Frequency Histograms. From this data we performed the basic analysis to follow.

The ensemble of CTM spectra is shown below in Figure 17 where we see the results of the selection process. From the histogram results the differences in spectral peaks are for SLS: *10.2, 11.9, 30.3, 33.3 kHz;* and for INT: *2.7, 11.2, 27.9, 39.6, 47.1, 48.3, 77, 78, 80.6 kHz.* From these spectral differences a classifier using these features should be able to differentiate between the two classes. It is interesting to note from this figure that if we mentally "smooth" the spectra ignoring resonant peaks (as before in the opening sounds) then the resulting overall spectra have a similar shape. This is not unexpected because other non-fractured parts of the valve still vibrate under both INT and SLS conditions. Notice the broad response in both between *0* and *40 kHz*, with peaking between *40* and *60 kHz* and some peaking in the *70* to *90 kHz* region of the INT valves. The high frequency peaking of the INT also makes sense because intuitively it should possess higher frequency response, since it is not fractured.

We estimated the spectra for each of the CTM signals representing the INT and SLS classes and stacked them for analysis. The images are shown in Figure 18. By carefully sliding a window through the images and searching for peak/valley differences, we located the following spectral bands for *(SLS: **4.5, 10, 22, 54, 58** kHz;* and *INT: **3, 24, 26, 28, 48** kHz).*

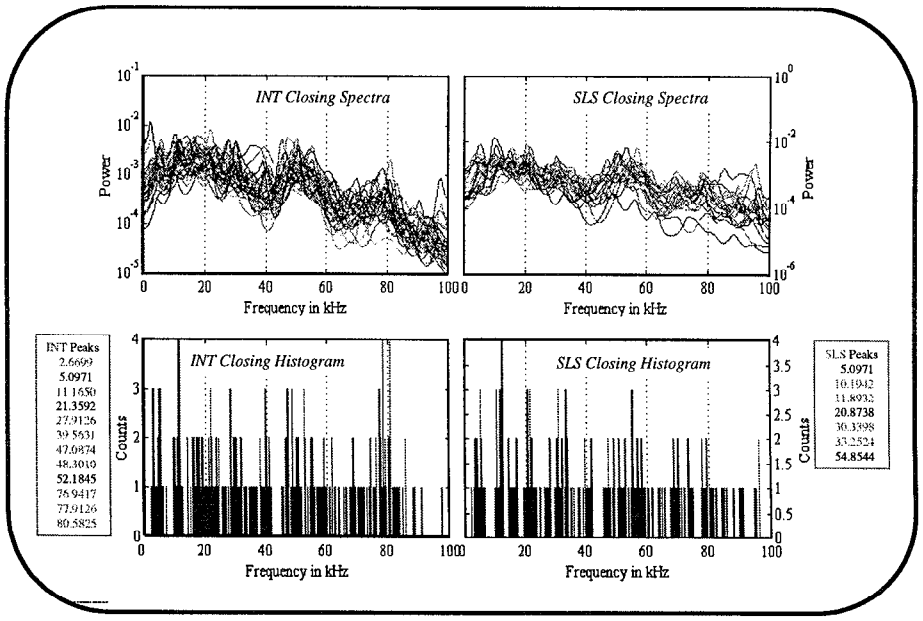


***Figure 17.*** *Ensemble CTM Closing Sound Spectra for Tested INTACT and SLS Valves: (a) INT Valves Ensemble CTM Spectra. (b) INT Valves Peak Frequency Histogram Estimates. (c) SLS Valves Ensemble CTM Spectra. (d) SLS Valves Peak Frequency Histogram Estimates.*

Next we estimated the UCTM spectrum for analysis (as before). The raw time series are shown in Figure 19 along with the INT and SLS spectra. Here we clearly observe the spectral peak/valley differences that a classifier might capitalize on for classification. The peaks in the spectra corresponding to valleys in the other are *SLS: **19.6, 37.5, 50.2, 58.3, 74.9, 96** kHz; INT: **3.5, 23.7, 47.3, 54.6, 70.6, 88.2, 93.5*** (as shown in Figure 19 below).

Finally we performed the correlation cancellation operation using the INT UCTM transient as the data channel and the SLS UCTM signal as the reference channel with the results shown in Figure 20. Here we again note the peak/valley difference between the correlated and uncorrelated parts of the INT and SLS CTM signals. These difference can be located under the following peaks shown in the figure: *as <u>SLS</u>: **5.9, 41.6, 50.2, 58.3, 67.1, 96.6** kHz; and <u>INT</u>: **10.8, 68.4** kHz.* This completes the analysis of the closing sounds.

We summarize the composite results of the analysis of closing sounds in Table 3. Next we compare both openings and closings.

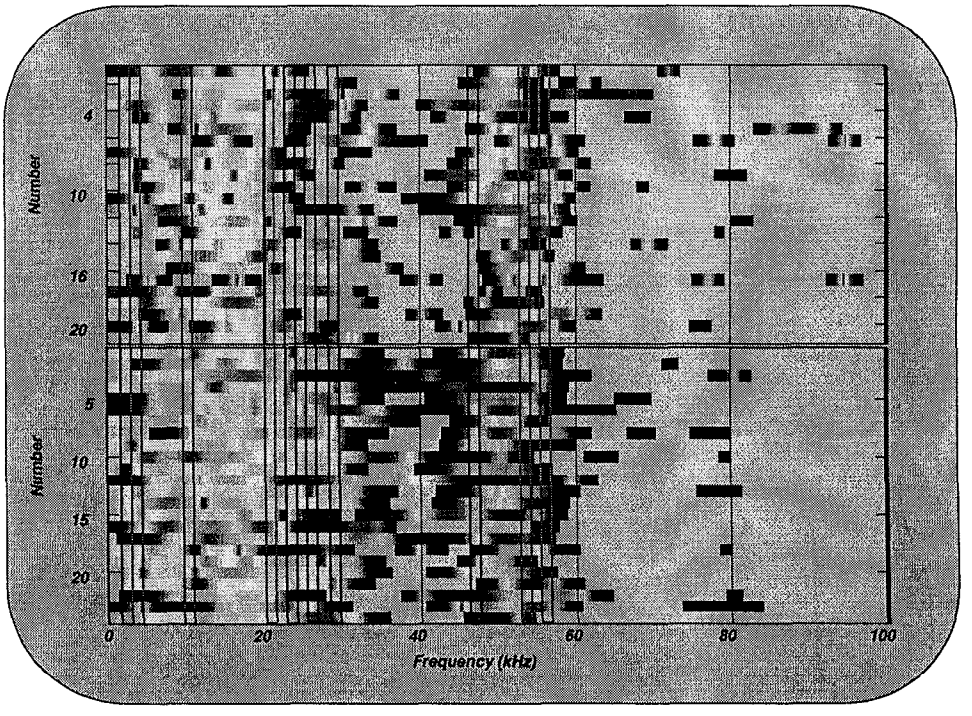


***Figure 18.*** *Spectral (MUSIC) Images of Ensemble CTM, SLS (upper) and INTACT (lower) Closing Sounds in Frequency Bands (SLS: **4.5, 10, 22, 54, 58** kHz; INT: **3, 24, 26, 28, 48** kHz).*

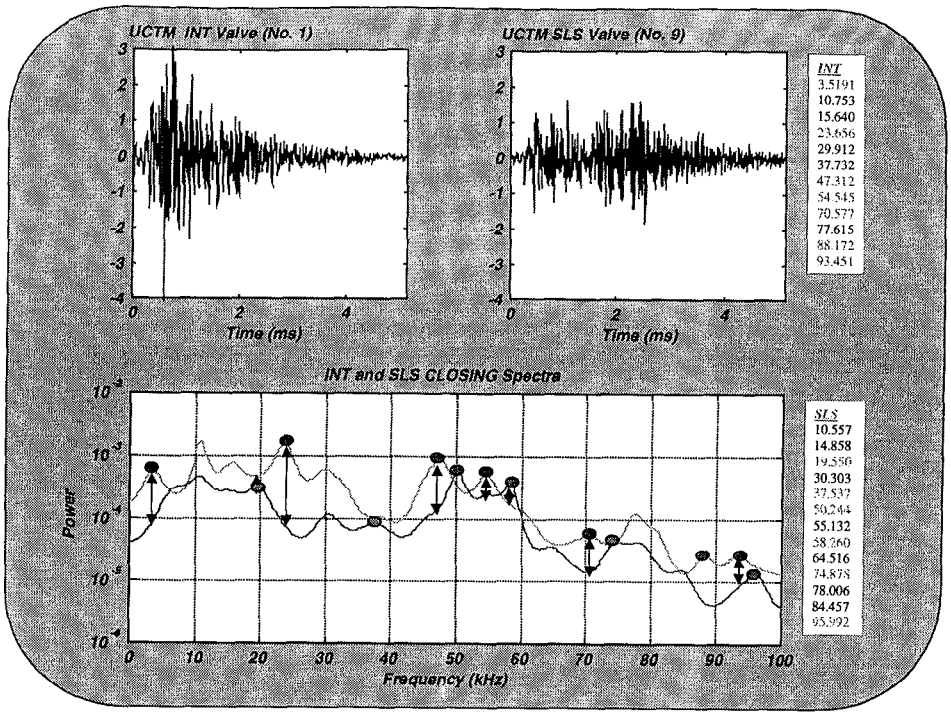


***Figure 19.*** *UCTMs SLS and INTACT Closing Sounds, Spectra and Spectral Differences (SLS:* ***19.6, 37.5, 50.2, 58.3, 74.9, 96*** *kHz; INT:* ***3.5, 23.7, 47.3, 54.6, 70.6, 88.2, 93.5*** *kHz).*

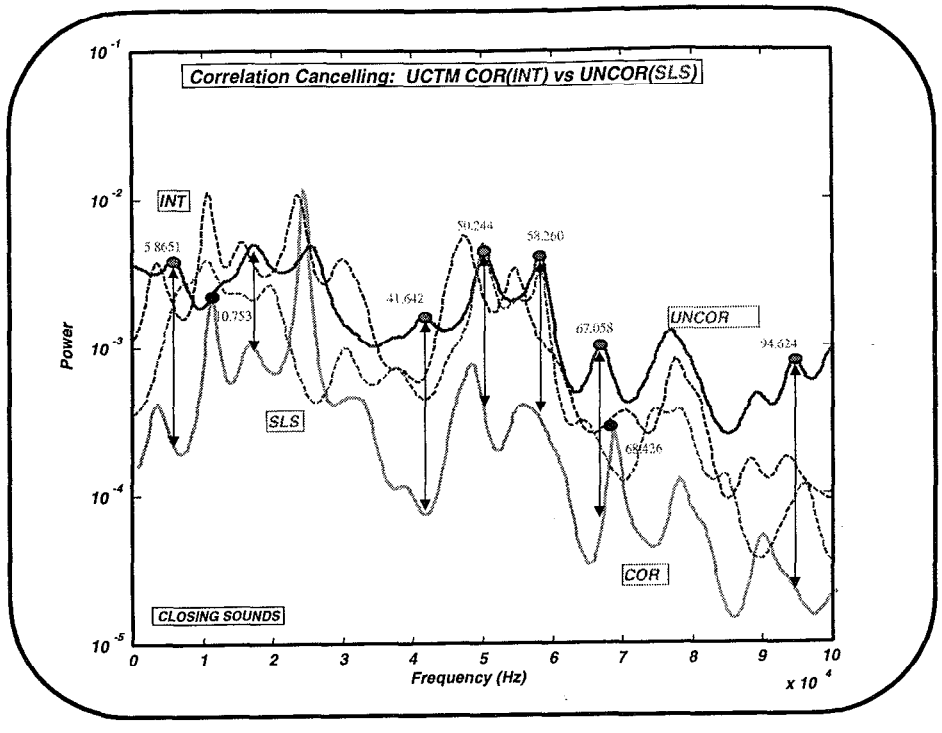


***Figure 20.*** *Comparison of CLOSING Sound Spectra for UCTM SLS and INT Valve Responses. Frequencies are annotated for spectral peaks as SLS: 5.9, 41.6, 50.2, 58.3, 67.1, 96.6 kHz; and INT: 10.8, 68.4 kHz.*

## Table 3. COMPOSITE ANALYSIS of HEART VALVE CLOSING SOUNDS with Peak/Valley Differences

| Ccanl | CTM Spectra | | CTM Image | | CTM Histogram | | CTM-CTM Spec | | CTM-CTM Ncanl | | CTM-CTM | |
|---|---|---|---|---|---|---|---|---|---|---|---|---|
| Freq | SLS | INT | SLS | INT | SLS | INT | SLS | INT | SLS | INT | UNC | COR |
| 0 | 5.1 | 2.7<br>5.1 | 4.5 | 3 | | | | 3.5 | | | 5.9 | |
| 10 | 10.2<br>11.9 | 11.2 | 10 | | | | 10.6<br>19.3 | 10.7<br>14.3<br>15.9 | | | | 10.8 |
| 20 | 20.9 | 21.3<br>27.9 | 22 | 24<br>26<br>28 | | | 27 | 23.7<br>29.9 | | | | |
| 30 | 30.3<br>33.3 | 39.6 | | | | | 30.3<br>37.5 | 37.7 | | | | |
| 40 | | 47.1 | | 48 | | | 40 | 47.3 | | | 41.6 | |
| 50 | 54.9 | 52.6 | 54<br>58 | | | | 50.2<br>55.1<br>58.3 | 54.6 | | | 50.2<br>58.3 | |
| 60 | | | | | | | 64.5 | 60 | | | 67.1 | 68.4 |
| 70 | | 77<br>78 | | | | | 74.9<br>78 | 70.6<br>77.6 | | | | |
| 80 | | 80.6 | | | | | 84.5 | 88.2 | | | | |
| 90 | | | | | | | 96 | 93.5 | | | 96.6 | |
| 100 | | | | | | | | | | | | |

## *5.3 ANALYSIS: COMPARISON OF OPENING /CLOSING SOUNDS*

In this subsection we examine the analysis of the previous individual analysis on both opening and closing sounds and investigate the similarities of resonances owing to component parts that are common to both valve sounds. For instance, the disk is excited in both cases, perhaps not as strongly for the opening relative to the closing sounds, but its resonances should remain consistent throughout. Here will we first observe the CTM spectra of each in Figure 21 and search for these similarities and differences and then compile the results of the previous two subsections in a summarizing table (see Table 4).

Perhaps the most obvious spectral features comparing the opening to the closing sounds is that the closings appear to have more structure in the higher frequency bands (> *60 kHz)* for both INT and SLS bands. This is especially noticeable in Figure 21c where we observe a spectral "hill" between *70* to *90 kHz* and more peaking in the SLS closing spectra in the same band (Figure 21d). This makes sense from a physical viewpoint because the closing sound is much stronger (door slamming) than the openings and the higher valve frequencies are no longer lost in the noise. However, more than likely these features are common to both in the sense that that are higher order harmonics of functions parts (disk, ring, etc.) and not necessarily associated with the potential fracture. A more thorough analysis of this information will probably lead to more insight, but it is beyond the scope of this effort at this time; therefore, we will conclude this sub-section due to time and resource constraints.

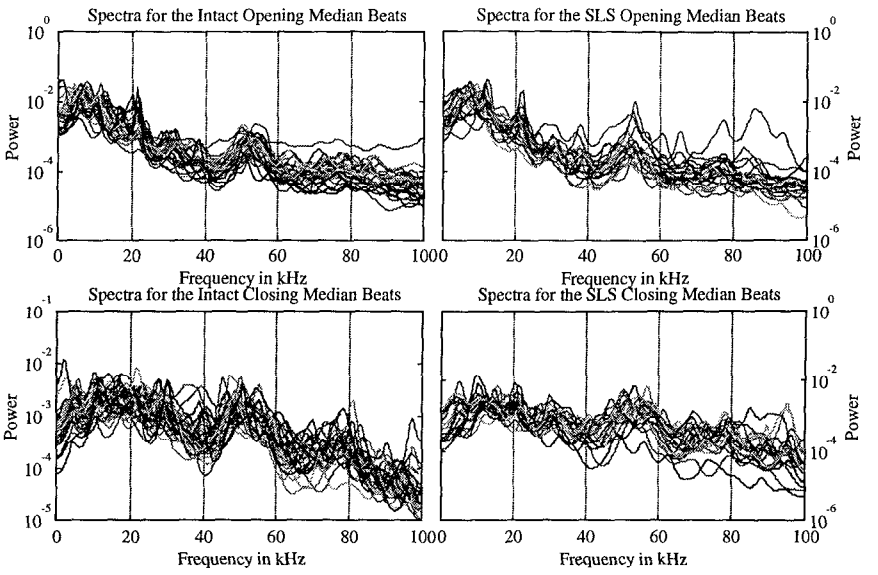


***Figure 21.*** *Comparison of OPENING and CLOSING Sound CTM Spectra for SLS* and INT valves.

## Table 4. COMPOSITE ANALYSIS of HEART VALVE OPENING and CLOSING SOUNDS with Peak/Valley Differences

| Ccanl | CTM Spectra | | CTM Image | | CTM Histogram | | CTM-CTM Spec | | CTM-CTM Ncanl | | CTM-CTM | |
|---|---|---|---|---|---|---|---|---|---|---|---|---|
| Freq | SLS | INT | SLS | INT | SLS | INT | SLS | INT | SLS | INT | UNC | COR |
| 0 | 4.1<br>7.5 | 4.1<br>5.8<br>7.8 | | 6 | | 6 | 3.9<br>9.8 | 5.9 | 4.3<br>9 | 6.6 | 3.7<br>9.9 | |
| 10 | 12.4 | 16.8 | 12 | | 12 | 17 | 18.3 | 14.3 | 14.1 | 15 | | |
| 20 | 21.6 | 21.8<br>29.9 | 21 | | | | 27 | 22.3<br>28.9 | 27.8 | 22.3 | | 29.5 |
| 30 | | 39 | 30<br>38 | | | 30 | 32<br>38.8 | 32.9 | 38.8 | 32.9<br>39.5 | | |
| 40 | | 49.8 | | | | | 40 | | 49.3 | 49.7 | | |
| 50 | 53.2 | | 53 | | 53 | 50 | 50.1<br>56.8 | 53.2 | 53.2 | 53.2 | | 53.7 |
| 60 | | | | | | | 65.4 | 60 | 63.4<br>69.3 | 62.6 | | 61.9 |
| 70 | | | | | | | 76.3 | 70 | 76.3 | 70.1<br>78.7 | 75.5 | 73<br>79 |
| 80 | | | | | | | 89.2 | 80 | 87.3 | 80 | | |
| 90 | | | | | | | 97.1 | 90 | 93.5 | 90 | | |
| 100 | | | | | | | | | | | | |

| Ccanl | CTM Spectra | | CTM Image | | CTM Histogram | | CTM-CTM Spec | | CTM-CTM Ncanl | | CTM-CTM | |
|---|---|---|---|---|---|---|---|---|---|---|---|---|
| Freq | SLS | INT | SLS | INT | SLS | INT | SLS | INT | SLS | INT | UNC | COR |
| 0 | 5.1 | 2.7<br>5.1 | 4.5 | 3 | | | | 3.5 | | | 5.9 | |
| 10 | 10.2<br>11.9 | 11.2 | 10 | | | | 10.6<br>19.3 | 10.7<br>14.3<br>15.9 | | | | 10.8 |
| 20 | 20.9 | 21.3<br>27.9 | 22 | 24<br>26<br>28 | | | 27 | 23.7<br>29.9 | | | | |
| 30 | 30.3<br>33.3 | 39.6 | | | | | 30.3<br>37.5 | 37.7 | | | | |
| 40 | | 47.1 | | 48 | | | 40 | 47.3 | | | 41.6 | |
| 50 | 54.9 | 52.6 | 54<br>58 | | | | 50.2<br>55.1<br>58.3 | 54.6 | | | 50.2<br>58.3 | |
| 60 | | | | | | | 64.5 | 60 | | | 67.1 | 68.4 |
| 70 | | 77<br>78 | | | | | 74.9<br>78 | 70.6<br>77.6 | | | | |
| 80 | | 80.6 | | | | | 84.5 | 88.2 | | | | |
| 90 | | | | | | | 96 | 93.5 | | | 96.6 | |
| 100 | | | | | | | | | | | | |

## 5.4 *ANALYSIS: VALVE DIRECTIVITY MEASUREMENTS*

In this subsection we show the results of the valve directivity pattern measurements. There has been speculation that the directivity of sound radiation from the heart valve is significant and could be the cause of weak measurements from various patients thereby requiring a more sophisticated measurement system capable of localizing the sound. The directivity or radiation patterns in the xy-plane of the valve were obtained using the set up discussed in the previous report [8] and shown to be omnidirectional.

Here the valve is activated as described above and its root-mean-squared (RMS) response calculated at carefully measured angular positions in the z-plane. We used the hemispherical cage shown in Figure 3 along the xz and yz axes with the origin (zero degrees) defined at the south pole. We then performed 10 measurements at each position, calculated the RMS valve of each transient sound (openings and closings) to obtain the

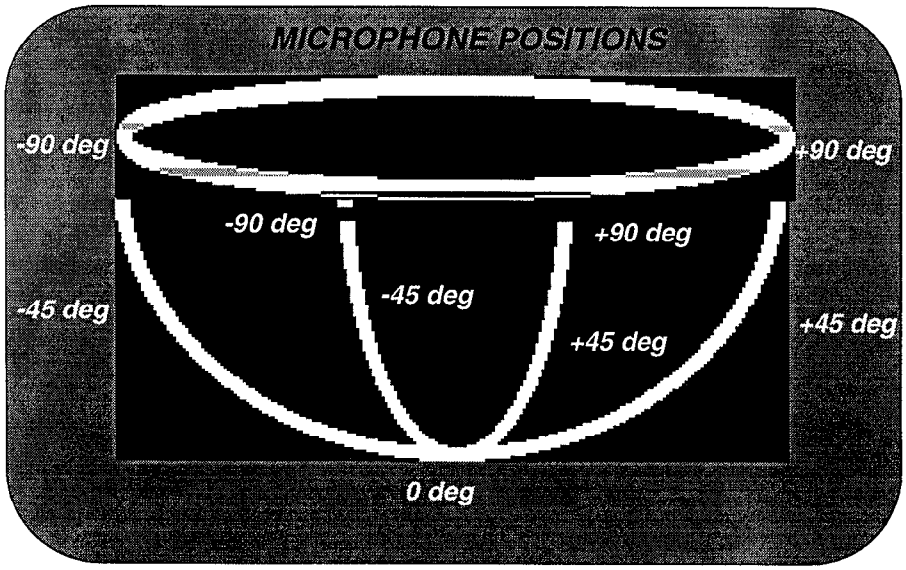


valve directivity pattern. The set-up is shown below in Figure 22.

***Figure 22.*** *Test-Set Up for Valve Directivity Pattern Tests.*

The directivity tests were run on the a valve which was deemed "canonical" (uniquely representing the SLS class) [8,9]. This valve is an SLS valve No. 33MBRC40066 which was explanted and obtained from Shiley, Inc. It had previously been patient recorded (acoustically). The valve was tested with the disc initially open (closing sound) and closed (opening sound).

The directivity patterns are shown below in Figure 23. The test, was accomplished in the vertical xz (labeled A in the figure) and xy-planes (labeled B) using the canonical valve [8,9] of the previous experiment at SonaTech. The results, shown in Figure 23, indicate that the pattern in the xz-plane had a lobed structure with dominant lobes at an angle of 45 degrees from the south pole (0 degrees) of the support cage hemisphere. We used this information to position our hydrophone sensor for the testing of each valve.

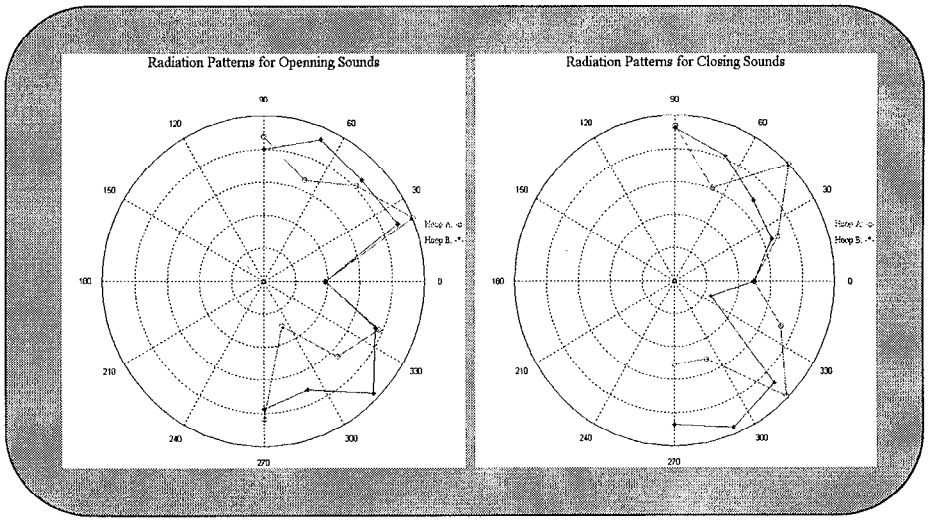


***Figure* 23.** *Heart Valve Directivity Tests: Canonical Valve SLS 33MBRC40066. BSCC Heart Valve. (a) Opening Sound. (b) Closing Sound.*

# 6.0 SUMMARY

We have performed a set of anechoic tests on 50 valves borrowed from the Shiley Heart Valve Research Center. These tests reveal differences between the INT and SLS spectral response which will be used to design the classifier (TASK II). The thinking here is that if the classifier cannot perform on the "clean" anechoic data, then its performance on clinical data obscured by reverberations is limited. This question can only be answered by designing and applying the classifier to the processed data on which we report herein.

The results of the transient tests are best summarized in Table 4. The composite analysis of both opening and closing sounds showing the various spectral peaks obtained by visual inspection of the ensemble closest-to-median (CTM) spectra. The variety of methods used were displayed in varying manners: overlay spectral plots, spectral images, and Peak Frequency Histogram images as well as a detailed analysis of the ensemble CTM spectral and the universal CTM (UCTM) signals. The result if this analysis show visible differences between the INT and SLS valves which could potentially be used by a classifier based on spectral features such as peak, energy bands, band ratios, etc. However classifiers are not limited to just spectral features even though those features are more appealing because of their physical relationship to the valve acoustic response.

Finally, it should be noted that these results are for the system chosen to excite the valve and are no means offered as the best possible set-up to test prosthetic heart valves. Clearly many different experimental designs could be formulated that may offer an improved SNR when gathering heart valve sounds. It appears from the results reported on above that these experiments show sufficient repeatability. The individual valve spectra are included for completeness and shown in the Appendices C and D. This completes the body of the report.

## 7.0 REFERENCES


[1] S. Kay. *Modern Spectrum Estimation: Theory and Applications.* Prentice-Hall, Engelwood Cliffs, N. J., 1988.

[2] J. V. Candy. *Signal Processing: The Modern Approach.* McGraw-Hill, New York, N.Y., 1988.

[3] T. D. Plemons, S. Shreck, R. S. Interbitzen. "Stability of the BSCC Heart Valve Outlet Strut Resonance Frequency Under Changing Physiological Conditions and Observation Times," *Proc. IEEE 7th Symposium of Computer-Based Medical Systems*, NC, 1994.

[4] A. C. Eberhardt, and C. E. Chassaing, R. S. Interbitzen, and D. W. Wieting. "Acoustic Evaluation of Progressive Failure of BSCC Heart Valves," *Proc. IEEE 7th Symposium of Computer-Based Medical Systems*, NC, 1994.

[5] R. O. Duda and P. E. Hart. *Pattern Classification and Scene Analysis.* John Wiley, New York, N. Y., 1973.

[6] J. V. Candy and H. E. Jones. "Classification of Prosthetic Heart Valve Sounds: A Parametric Approach," *J. Acoustic. Soc. Amer.*, **97** (6), pp 3675-3687, 1995.

[7] M. Hayes. *Statistical Digital Signal Processing and Modeling.* John Wiley, New York, N. Y., 1996.

[8] J. V. Candy, Ed. "Final Report for BP Panel on Anechoic Study Results," **LLNL-Report**, UCRL-ID-126508, 1996.

[9] A. L. Warrick, J. V. Candy and A. E. Brown. "Parametric Signal Processing of Anechoic Data From Prosthetic Heart Valve Testing," *Circuits, Systems Signal Proc.* **17**, pp 123-136, 1998.

[10] *Statistical Toolbox.* MathWorks Inc., Boston, MA., 1995.

[11] J. Capon. "High Resolution Frequency Wavenumber Spectral Analysis," *Proc. IEEE,* **57**, pp 1408-1418, 1975.

[12] B. Widrow and S. Stearns. *Adaptive Signal Processing.* Prentice-Hall, Engelwood Cliffs, N. J., 1985.

[13] L. Ljung. *System Identification: Theory For the User.* Prentice-Hall, Engelwood Cliffs, N. J., 1987.

[14] L. Cohen. *Time-Frequency Analysis.* Prentice-Hall, Engelwood Cliffs, N. J., 1994.

[15] G. Kaiser. *A Friendly Guide to Wavelets.* Birkhauser, Boston, MA., 1994.

# *APPENDICES*

# *LIST OF APPENDICES*

# *APPENDIX A: TransDec Test Protocol*

## *EXPERIMENTAL SETUP PROTOCOL:*

| |
|---|
| Verify equipment inventory |
| Make sure hydrophone cable is at least 13 feet |
| Clean and inspect valves |
| Verify valve serial numbers with box id |
| Visually inspect a sample of tank water |
| Measure and record tank water temperature at 3 depths |
| Setup all equipment |
| Eliminate cable clutter |
| Inspect for hazards |
| Photograph all equipment- front and back panels |
| Perform Far-Field verification Tests |

## *HEART VALVE TESING PROTOCOL:*

| | | File Name |
|---|---|---|
| Sampling Rate | 200,000 | |
| Lower cutoff | 1,000 | |
| Upper cutoff | 100,000 | |
| Data window | 8,192 | |
| | | |
| Consult randomized list | | |
| Lower spider to depth | 13 feet | |
| Amplifier gain | FS for opening signal | |
| Background noise capture | | |
| 50 drop cycles | | |
| Background noise capture | | |
| Amplifier gain | FS for closing sound | |
| Background noise capture | | |
| 50 drop cycles | | |
| Background noise capture | | |

## *SYSTEM NOISE PROTOCOL:*

| | | | |
|---|---|---|---|
| Sampling Rate | 200,000 | | |
| Lower cutoff | 1,000 | | |
| Upper cutoff | 100,000 | | |
| Data window | 6 blocks of 8,192 | | |
| Amplifier gain | 3 SD is full scale | See Notes | |
| No equipment in tank | | | |
| | | | |
| | | | |
| Hydrophone electrically disconnected from Q-Amp | | | |
| Compute mean to check for offset | | | |
| Examine Power Spectrum | | | |
| | | | |
| Hydrophone out of water and connected to Q-Amp | | | |
| Compute mean to check for offset | | | |
| Examine Power Spectrum | | | |
| | | | |
| | | | |
| Notes | | | |
| System noise check should be done every time the system is powered down and restarted or initially every day. | | | |
| To compute SD (standard deviation) first use nominal gain then recompute, several iterations might be necessary the first time. | | | |
| Debug if offset > 3% of 2 standard deviations. | | | |
| Power spectrum should be consistent with white noise, if not debug. | | | |

## *INITIAL TransDec TANK NOISE PROTOCOL:*

| | | | File Name | |
|---|---|---|---|---|
| Sampling Rate | 200,000 | | | |
| Lower cutoff | 1,000 | | | |
| Upper cutoff | 100,000 | | | |
| Data window | 6 blocks of 8,192 | | | |
| Amplifier gain | 3 SD is full scale | See notes | | |
| | | | | |
| Check for depth variation | | | | |
| Only hydrophone in tank | | | | |
| Measure at 3 depths | 3, 10, 13 feet | | | |
| Compute mean to check for offset | | | | |
| Examine Power Spectrum | | | | |
| | | | | |
| Check for time variation | | | | |
| Only hydrophone in tank | | | | |
| Measure at depth | 13 feet | | | |
| Repeat measurement 3 times, each 10 minutes apart | | | | |
| Compute mean to check for offset | | | | |
| Examine Power Spectrum | | | | |
| | | | | |
| Check with Spider | | | | |
| Spider in tank with mounted intact valve | | | | |
| Hydrophone mounted on cage | | | | |
| Measure at 13 feet | | | | |
| Compute mean to check for offset | | | | |
| Examine Power Spectrum | | | | |
| | | | | |
| Notes | | | | |
| If significant variation of noise level with depth take at additional depths, discuss debug. | | | | |
| To compute SD (standard deviation) first use nominal gain then recompute, several iterations might be necessary the first time. | | | | |
| Debug if offset > 3% of 2 standard deviation. | | | | |

## *MEASUREMENT NOISE PROTOCOL:*

| | | File Name |
|---|---|---|
| Sampling Rate | 200,000 | |
| Lower cutoff | 1,000 | |
| Upper cutoff | 100,000 | |
| Data window | 8,192 | |
| Spider at depth | 13 feet | |
| Amplifier gain | as in init tank noise | |
| Intact valve 29EMBRC10154 | | |
| | | |
| | | |
| No valve in spider | | |
| Background noise capture | 1 window | |
| 50 drop cycles | 1 window per cycle | |
| Background noise capture | 1 window | |
| | | |
| Valve w/ plate glued open | | |
| Background noise capture | 1 window | |
| 50 drop cycles | 1 window per cycle | |
| Background noise capture | 1 window | |
| | | |
| Valve w/ plate glued closed | | |
| Background noise capture | 1 window | |
| 50 drop cycles | 1 window per cycle | |
| Background noise capture | 1 window | |
| | | |

## *INTACT OPENING SOUND PROTOCOL:*

| | | File Name |
|---|---|---|
| Sampling Rate | 200,000 | |
| Lower cutoff | 1,000 | |
| Upper cutoff | 100,000 | |
| Data window | 8,192 | |
| Spider at depth | 13 feet | |
| Amplifier gain | FS for Opening Signal | |
| Intact valve 29EMBRC10154 | | |
| | | |
| Skip mounts valve with spider out of water | | |
| Lower spider with valve to depth | 13 feet | |
| Background noise capture | 1 window | |
| 50 drop cycles | 1 window per cycle | |
| Background noise capture | 1 window | |
| Spider remains at depth | 13 feet | |
| wait 5 minutes | | |
| Background noise capture | 1 window | |
| 50 drop cycles | 1 window per cycle | |
| Background noise capture | 1 window | |
| Raise spider with valve to depth | 10 feet | |
| wait 5 minutes | | |
| Background noise capture | 1 window | |
| 50 drop cycles | 1 window per cycle | |
| Background noise capture | 1 window | |
| Raise spider with valve to depth | 3 feet | |
| wait 5 minutes | | |
| Background noise capture | | |
| 50 drop cycles | | |
| Background noise capture | | |
| | | |
| Raise spider from tank into air | | |
| Do not touch valve | | |
| wait 5 minutes | | |
| lower spider to depth | 13 feet | |
| Background noise capture | 1 window | |
| 50 drop cycles | 1 window per cycle | |
| Background noise capture | 1 window | |
| | | |
| Raise spider from tank into air | | |
| Skip removes valve | | |
| Skip remounts same valve | | |

| | | |
|---|---|---|
| Lower spider to depth | 13 feet | |
| Background noise capture | 1 window | |
| 50 drop cycles | 1 window per cycle | |
| Background noise capture | 1 window | |
| | | |

## *INTACT CLOSING SOUND PROTOCOL:*

| | | File Name |
|---|---|---|
| Sampling Rate | 200,000 | |
| Lower cutoff | 1,000 | |
| Upper cutoff | 100,000 | |
| Data window | 8,192 | |
| Spider at depth | 13 feet | |
| Amplifier gain | FS for Closing Signal | |
| Depth | 13 feet | |
| Intact valve 29EMBRC10154 | | |
| | | |
| Skip mounts valve with spider out of water | | |
| Lower spider with valve to depth | 13 feet | |
| Background noise capture | 1 window | |
| 50 drop cycles | 1 window per cycle | |
| Background noise capture | 1 window | |
| wait 5 minutes | | |
| Background noise capture | 1 window | |
| 50 drop cycles | 1 window per cycle | |
| Background noise capture | 1 window | |
| | | |
| Raise spider from tank into air | | |
| Do not touch valve | | |
| wait 5 minutes | | |
| lower spider to depth | 13 feet | |
| Background noise capture | 1 window | |
| 50 drop cycles | 1 window per cycle | |
| Background noise capture | 1 window | |
| | | |
| Raise spider from tank into air | | |
| Skip removes valve | | |
| Skip remounts same valve | | |
| lower spider to depth | 13 feet | |
| Background noise capture | 1 window | |
| 50 drop cycles | 1 window per cycle | |
| Background noise capture | 1 window | |
| | | |

## *SLS OPENING SOUND PROTOCOL:*

| | | File Name |
|---|---|---|
| Sampling Rate | 200,000 | |
| Lower cutoff | 1,000 | |
| Upper cutoff | 100,000 | |
| Data window | 8,192 | |
| Spider at depth | 13 feet | |
| Amplifier gain | FS for Opening Signal | |
| Depth | 13 feet | |
| SLS Valve | | |
| | | |
| | | |
| Skip mounts valve with spider out of water | | |
| Lower spider with valve to depth | 13 feet | |
| Background noise capture | 1 window | |
| 50 drop cycles | 1 window per cycle | |
| Background noise capture | 1 window | |
| wait 5 minutes | | |
| Background noise capture | 1 window | |
| 50 drop cycles | 1 window per cycle | |
| Background noise capture | 1 window | |
| | | |
| Raise spider from tank into air | | |
| Do not touch valve | | |
| wait 5 minutes | | |
| lower spider to depth | 13 feet | |
| Background noise capture | 1 window | |
| 50 drop cycles | 1 window per cycle | |
| Background noise capture | 1 window | |
| | | |
| Raise spider from tank into air | | |
| Skip removes valve | | |
| Skip remounts same valve | | |
| lower spider to depth | 13 feet | |
| Background noise capture | 1 window | |
| 50 drop cycles | 1 window per cycle | |
| Background noise capture | 1 window | |

## *SLS CLOSING SOUND PROTOCOL:*

| | |
|---|---|
| Sampling Rate | 200,000 |
| Lower cutoff | 1,000 |
| Upper cutoff | 100,000 |
| Data window | 8,192 |
| Spider at depth | 13 feet |
| Amplifier gain | FS for Closing Signal |
| Depth | 13 feet |
| SLS Valve | |
| | |
| Skip mounts valve with spider out of water | |
| Lower spider with valve to depth | 13 feet |
| Background noise capture | 1 window |
| 50 drop cycles | 1 window per cycle |
| Background noise capture | 1 window |
| wait 5 minutes | |
| Background noise capture | 1 window |
| 50 drop cycles | 1 window per cycle |
| Background noise capture | 1 window |
| | |
| Raise spider from tank into air | |
| Do not touch valve | |
| wait 5 minutes | |
| lower spider to depth | 13 feet |
| Background noise capture | 1 window |
| 50 drop cycles | 1 window per cycle |
| Background noise capture | 1 window |
| | |
| Raise spider from tank into air | |
| Skip removes valve | |
| Skip remounts same valve | |
| lower spider to depth | 13 feet |
| Background noise capture | 1 window |
| 50 drop cycles | 1 window per cycle |
| Background noise capture | 1 window |
| | |

# *APPENDIX B: Randomized Valve List*

| *No.* | *Class(I/S)* | *Valve SN* | *actual frame* |
|---|---|---|---|
| 11 | I | 31ABCA10001 | 65873 |
| 40 | I | 29ABCA10003 | 65885 |
| 31 | I | 29EMUC10005 | 72558 |
| 36 | S | 31MBRCB10006 | 84093 |
| 1 | I | 31MBRCA10014 | 89413 |
| 16 | I | 31EMBUC10016 | 90710 |
| 38 | I | 31EMBRC10025 | 75389 |
| 49 | S | 31MBRC10032 | 115573 |
| 46 | I | 29MBC10100 | 63333 |
| 45 | I | 31ABC10114 | 60248 |
| 48 | I | 33MBRC10146 | 68426 |
| 26 | I | 33MBRC10151 | 68445 |
| 29 | I | 31MBC10162 | 67424 |
| 19 | I | 29MBRCB10288 | 99618 |
| 4 | S | 33MBRC10383 | 74260 |
| 20 | I | 33MBRC10438 | A6750 |
| 28 | I | 31MBRC10451 | 59841 |
| 12 | S | 31ABC10467 | 73021 |
| 7 | I | 31ABC10470 | 73177 |
| 43 | S | 31ABC10475 | 73184 |
| 42 | I | 29MBRC10525 | 60159 |
| 24 | I | 33MBRC10700 | 85591 |
| 41 | I | 33MBRC10721 | 87134 |
| 25 | I | 29MBRC10762 | 61397 |
| 23 | S | 29MBRC10776 | 61046 |
| 13 | I | 33MBRC10808 | 90709 |
| 10 | S | 29ABC10925 | 73159 |
| 18 | I | 29ABC11093 | 74873 |
| 34 | I | 29ABC11842 | 92569 |
| 32 | I | 29ABC11940 | 95282 |
| 9 | S | 31MBRC12282 | |
| 27 | I | 29ABC12300 | 99901 |
| 33 | I | 29MBRC12674 | 73539 |
| 50 | S | 31MBRC12926 | 76225 |
| 8 | S | 29MBRC13469 | 77335 |
| 35 | I | 31MBRC14531 | 92007 |
| 5 | S | 29MBRC15994 | 90063 |
| 47 | S | 29MBRC16078 | 95056 |
| 37 | S | 29MBRC16797 | 102268 |
| 30 | S | 33MBRC40040 | 72016 |
| 44 | S | 33MBRC40066 | 78532 |
| 22 | S | 33MBRC40098 | 88691 |
| 15 | S | 31MBRC40630 | 97866 |
| 39 | S | 29ABC60169 | A4312 |
| 2 | S | 31MBRC60939 | A4567 |
| 14 | I | 29MBRC61070 | A2404 |
| 17 | S | 31MBRC61089 | A5023 |
| 21 | S | 31MBRC61213 | A6333 |
| 3 | I | 29MBRC61622 | A4815 |
| 6 | I | 29MBRC62298 | 76060 |

# *APPENDIX C:*

# *MAD Statistic, MVDR & MUSIC Spectral Estimation*

In this appendix we show the results of minimum variance distortionless response (MVDR) spectral estimator applied to the opening sounds measured in both SLS and INT valves during anechoic testing. The following figures show the ensemble (green) spectra indicating the reliability of the measurement system and valve to reproduce the sound (standard deviation listed in Table D-1 and E-1). The red plots show the corresponding closest-to_median (CTM) spectra for each valve. The accompanying plots (in Appendices D and E) also display the individual valve peak frequency histogram estimates along with CTM spectra (blue) superimposed to indicate how to weight the histogram amplitudes, that is, high count and high amplitude indicate a strong and repeatible resonance. Observing each of these plots show the correlation between the valve and it peak response. Valve similarity can be deduced by carefully sorting similar responses; however, we choose to use the CTM signal to represent the individual valves and the *universal* CTM (UCTM) to represent the class for analysis purposes as discussed in the body of this report. Here we offer the detailed spectral plots for further analysis and completeness.

First, we briefly discuss the Median Absolute Deviation (MAD) statistic that we used to prune outliers from the spectral ensembles [10]. MAD is a robust/resistant estimate of the population standard deviation. When the data arise from non-normal distributions characterized by long tails, the MAD estimator will more efficiently estimate population standard deviation than the sample standard deviation (SD). The gain in efficiency depends is particularly great in the case of outliers, a common form of non-normality.

The formulas for SD and MAD are:

$$s = \sqrt{\frac{1}{n-1}\sum_{i=1}^{n} x_i - \bar{x}^{-2}} \qquad \text{(C-1)}$$

and

$$m \equiv \text{Median } x_i\Big|_1^n; \quad M \equiv K \times \text{Median}\left|x_i - m\right|_1^n \quad .$$

The constant $K$ is adjusted so that MAD gives nearly the same result as SD when the data are exactly normal. Both SD and MAD are estimating the same thing, the population standard deviation $\sigma$. If the data are normal, then the SD (n>10) estimates $\sigma$ with optimal efficiency as show by its variance.

$$\mathrm{Var}(\mathrm{SD}) = \frac{\sigma^2}{2n} \tag{C-2}$$

On the other hand when the data come from a non-normal and long-tailed distribution the efficiency of the SD degrades significantly. The usual measure of the non-normality of long-tailed distributions is the *kurtosis*. Distributions with excess kurtosis (the normal has zero kurtosis) are more peaked at the center and have longer tails than the normal. When we include the effects of kurtosis on the variance of SD becomes:

$$\mathrm{Var}(\mathrm{s}) = \frac{n\sigma^2}{2}\left|1 + \frac{\gamma_2}{2}\right| \tag{C-3}$$

In practical terms this means the SD gives a very poor estimate when the data are contaminated with outliers. When dealing with small samples, the outliers are usually pruned by hand, but when the data sets are large an automatic procedure with well understood statistical properties is needed. MAD provides this. It is not possible to give a closed form solution for the variance of MAD either for normal or non-normal data. However, extensive simulation studies carried out in the 1970's verify that MAD is much more efficient over a wide variety of non-normal distributions. This completes the description of the MAD statistic used in this work.

The application of MAD to our problem is given by:

$$P_{MAD}(f) = \left|P(f) - \hat{P}_{median}(f)\right|. \tag{C-4}$$

where $\hat{P}_{median}$ is the sample median spetral estimate over the ensemble of transient or beat measurements. The MAD statistical estimate returns the beat numbers of the valve transient responses in a rank ordered list with the first entry corresponding to the CTM. MAD is applied to the resulting CTM ensembles, one for SLS and one for INT, to produce the UCTM representing the overall class response and spectra for the detailed analyses used in this report (see Figure X-1 for the procedure).

The MVDR spectral estimator originated from the work of Capon [11] and has also been labeled by various names such as the maximum likelihood method (MLM) and the minimum variance (MV) [7]. Note that the power spectrum estimation is equivalent to filtering a signal with a bank of narrow bandpass filters. In classical methods these bandpass filters are fixed, whereas in the MVDR method each filter is *data adaptive*, since it is designed to be optimum in the sense of rejecting as much out-of-band signal power as possible. The MVDR method solves the optimization problem at *each* spectral frequency bin creating an individual bandpass filter based on the spectral information

residing in the bin, that is, it solves the problem of finding a set of filter weights $\{w(n)\}$ at each spectral bin that minimizes the overall power except at the narrowband frequency. Formally, we search for the set of optimal weights satisfying

$$\min_{\underline{W}} \quad J = \underline{W}^T R_{zz} \underline{W} \qquad \ni \qquad \underline{V}^T(f_m)\underline{W} = 1, \tag{C-5}$$

where $J$ is the energy cost function, $z$ is the data, $R_{zz}$ is the data covariance matrix (NxN), $\underline{W}$ is the set of weights (N-vector) to be estimated and $\underline{V}(f)$ is the discrete vector of Fourier bins given by $\underline{V}^T(f_m) \equiv \left[1 \; e^{-jf_m} \cdots \; e^{-j(N-1)f_m}\right]$. The solution to this problem is easily determined using Lagrange multipliers [2,3] to yield the set of optimal weights as

$$\underline{W} = \frac{R_{zz}^{-1}\underline{V}(f_m)}{\underline{V}^T(f_m)R_{zz}^{-1}\underline{V}(f_m)} \tag{C-6}$$

$$\text{Output Power} = \underline{W}^T R_{zz} \underline{W} = \frac{1}{\underline{V}^T(f_m)R_{zz}^{-1}\underline{V}(f_m)} \tag{C-7}$$

Note that the weight in Eq. C-6 *changes* at each specified bin $(f_m)$ since it changes through the term $\underline{V}(f_m)$, thereby making the MVDR data adaptive. Thus, in practice the MVDR estimator essentially constrains the narrow bandpass filter to pass all frequencies in the bin at $f_m$ (gain constrained to unity) and minimizes any other energy not at that frequency. This method is *nonparametric* in the sense that it does not rely on any underlying parametric model in constrast to the maximum entropy method (MEM) that relies on the autoregressive (AR) or all-pole model. Thus, it performance is not as good as parametric methods in terms of high-resolution, but it is far superior to the classical fast Fourier transform or FFT-based techniques [1,2]. The MEM techniques rely on the AR-model and the primary problem is to decide on the "best" model order (number of poles) of that model to represent the data. For the anechoic data we found that the model order changed significantly between beats due to the low signal-to-noise ratio (SNR) available in the measurements and the fact that the data are non-stationary (time varying statistics); therefore, we abandoned the MEM and used the nonparametric, data adaptive, MVDR approach eliminating the model order estimation problem and utilizing the adaptive nature of the processor to approach the non-stationarity problem.

Before closing this discussion, it should be noted that the MVDR and MEM are intimately related by the following relation shown by Burg [1,2]:

$$\frac{1}{P_{\text{MVDR}}(f)} = \frac{1}{N}\sum_{k=1}^{N}\frac{1}{P_{\text{MEM}}(f,k)} \tag{C-8}$$

where $k$ is summed over the *maximum* model orders $N$ of the MEM technique. In essence this result shows that the MVDR processor essentially averages over all reasonable model orders to achieve its estimates. We actually employ this method to implement the MVDR processor in the subsequent estimates indicating the maximum model order selected for averaging. This implementation has the advantage that it is more numerically stable than the direct inversion of the covariance matrix in Eq. C-7 and provides some inherent smoothing by varying $N$.

We also used the multiple signal classification (MUSIC) algorithm to produce the sharp spectral peaks in the image spectra of Figures 11 and 18 of the body. MUSIC is a variant of the MVDR approach where $R_{zz}$ is replaced by a rank reduced version, that is,

$$R_{zz} = EDE', \tag{C-9}$$

is factored using a singular value decomposition [7] yielding the ordered eigenvector matrix, $E$, and the diagonal matrix of eigenvalues, $D$. Its rank, say $n$, is selected through various techniques [7] and $R_{zz}$ is replaced by:

$$\hat{R}_{zz}(n) = E_R(n) \times D_R(n) \times E_R^{'}(n), \tag{C-10}$$

where $\hat{R}_{zz}$ is the ($N$-$n$) by ($N$-$n$), rank reduced data covariance matrix, $E_R, D_R$ are the respective rank reduced eigenvector and eigenvalue matrices. MUSIC actually uses and unweighted diagonal matrix set to the rank reduced identity matrix of C-9 instead of the eigenvalue matrix. Thus, the final MUSIC spectral estimator is given by

$$\text{Output Power} = \frac{1}{\underline{V}^T(f_m)\hat{R}_{zz}^{-1}(n)\underline{V}(f_m)} \quad . \tag{C-11}$$

# *APPENDIX D:*

## *OPENING Sounds (Beats) for SLS and INT Heart Valves using the MVDR spectral estimator*

In this section we show the individual valve OPENING spectra and the CTM for each along with the corresponding Peak Frequency Histograms. Note that the precision of the measurements can be characterized by the spectral variations in the ensembles estimates (green on plots) to follow. The bounds have been calculated using the standard sample estimators and are included in the following Table. We first show the SLS spectra and then the INT group by their individual valve numbers (see Appendix B).

***Table D-1:*** *Opening/Closing Sound Spectral Variation: Valve Spectra Standard Deviations (S.D in dB.)*

| Valve Number | Opening Sound S.D. | Closing Sound S.D. |
|---|---|---|
| 1 | 1.2635 | 1.2892 |
| 2 | 1.2529 | 1.4616 |
| 3 | 1.2852 | 1.2662 |
| 4 | 1.3770 | 1.5027 |
| 5 | 1.3299 | 1.1809 |
| 6 | 1.3115 | 1.2473 |
| 7 | 1.4843 | 1.4478 |
| 8 | 1.3433 | 1.2043 |
| 9 | 1.3763 | 1.3704 |
| 10 | 1.2644 | 1.3816 |
| 11 | 1.3645 | 1.3369 |
| 12 | 1.4077 | 1.4541 |
| 13 | 1.2915 | 1.2740 |
| 14 | 1.3351 | 1.1742 |
| 15 | 1.2450 | 1.2912 |
| 16 | 1.3752 | 1.3974 |
| 17 | 1.6051 | 1.2492 |
| 18 | 1.4726 | 1.2402 |
| 19 | 1.3401 | 1.3493 |
| 20 | 1.2965 | 1.1930 |
| 21 | 1.3510 | 1.3188 |
| 22 | 1.3212 | 1.3605 |
| 23 | 1.3587 | 1.4397 |
| 24 | 1.2185 | 1.4198 |
| 25 | 1.4507 | 1.4749 |
| 26 | 1.3175 | 1.3921 |
| 27 | 1.4353 | 1.2904 |
| 28 | 1.5431 | 1.3569 |
| 29 | 1.3156 | 1.4829 |
| 30 | 1.4650 | 1.3633 |
| 31 | 1.3107 | 1.4845 |
| 32 | 1.3087 | 1.3969 |
| 33 | 1.2645 | 1.3873 |
| 34 | 1.3649 | 1.3483 |
| 35 | 1.4536 | 1.3354 |
| 36 | 1.3384 | 1.3019 |
| 37 | 1.4612 | 1.6022 |
| 38 | 1.3417 | 1.2309 |
| 39 | 1.5958 | 1.3320 |
| 40 | 1.3975 | 1.3080 |
| 41 | 1.2194 | 1.4845 |
| 42 | 1.3666 | 1.3715 |
| 43 | 1.5314 | 1.3656 |
| 44 | 1.4306 | 1.3823 |
| 45 | 1.3983 | 1.3323 |
| 46 | 1.3774 | 1.3882 |
| 47 | 1.3479 | 1.2074 |
| 48 | 1.4669 | 1.2937 |
| 49 | 1.3453 | 1.2621 |
| 50 | 1.3399 | 1.4512 |

# Heart Valve Numbers 2 to 15 SLS MVDR Max 50

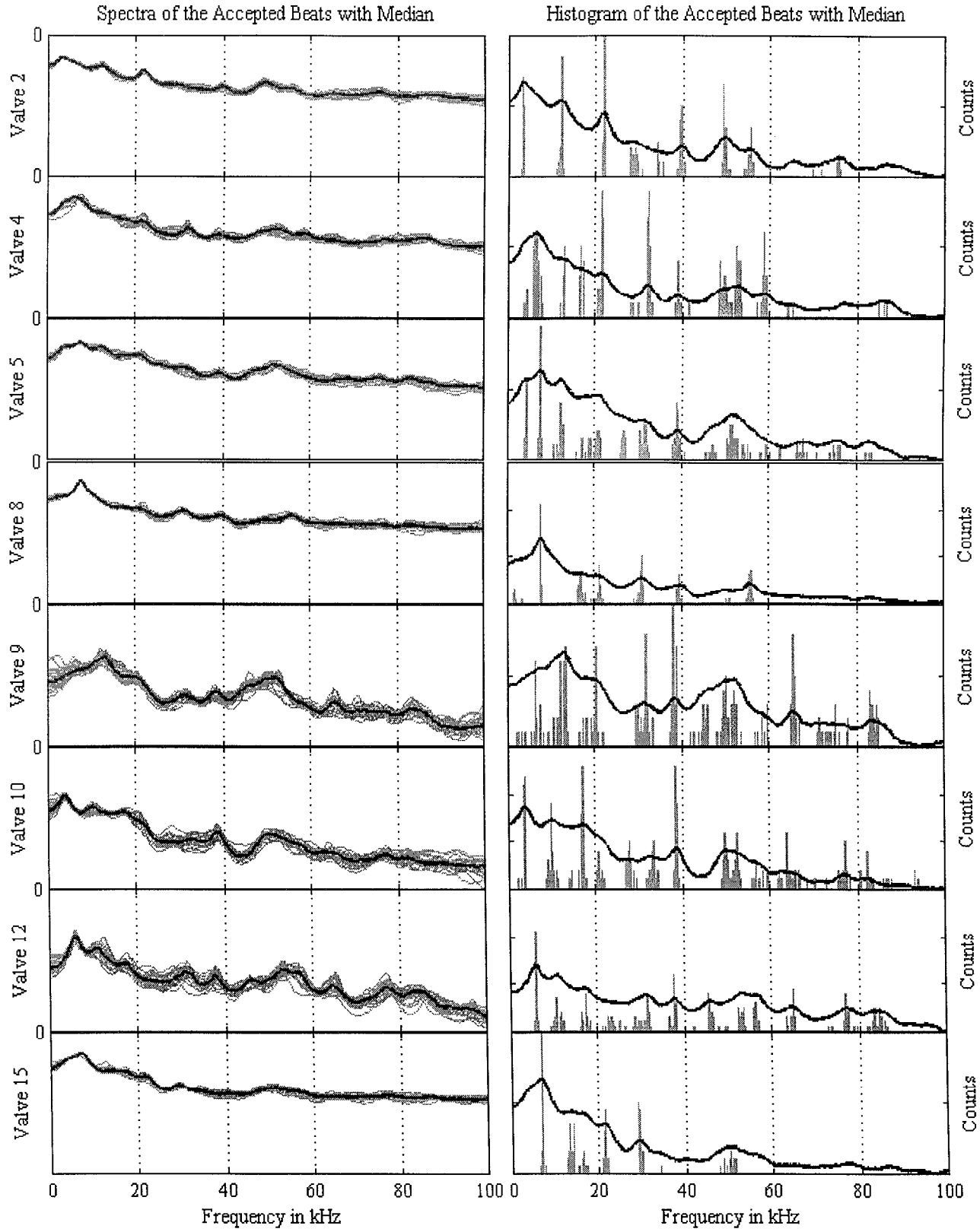

# Heart Valve Numbers 17 to 39 SLS MVDR Max 50

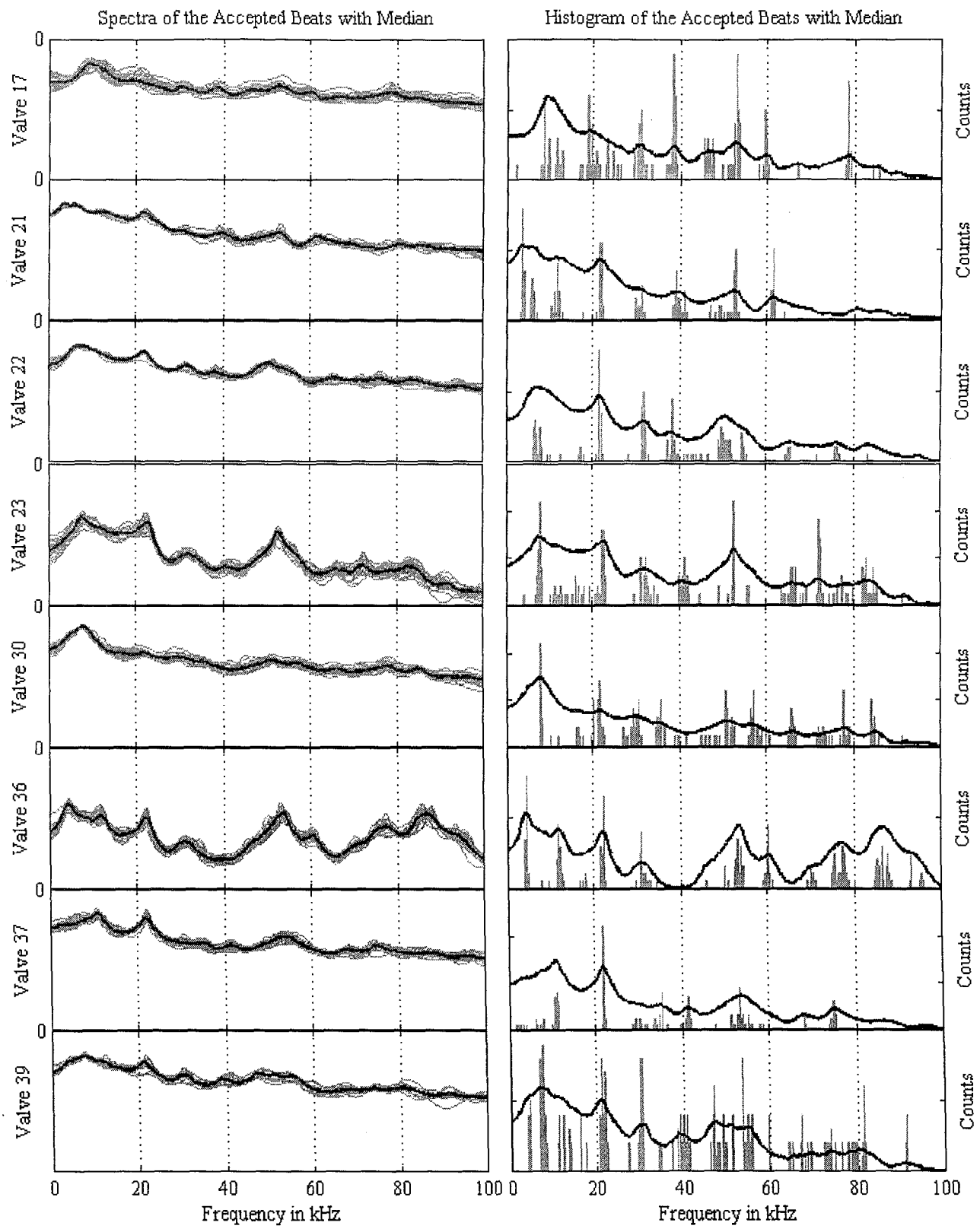

# Heart Valve Numbers 43 to 50 SLS MVDR Max 50

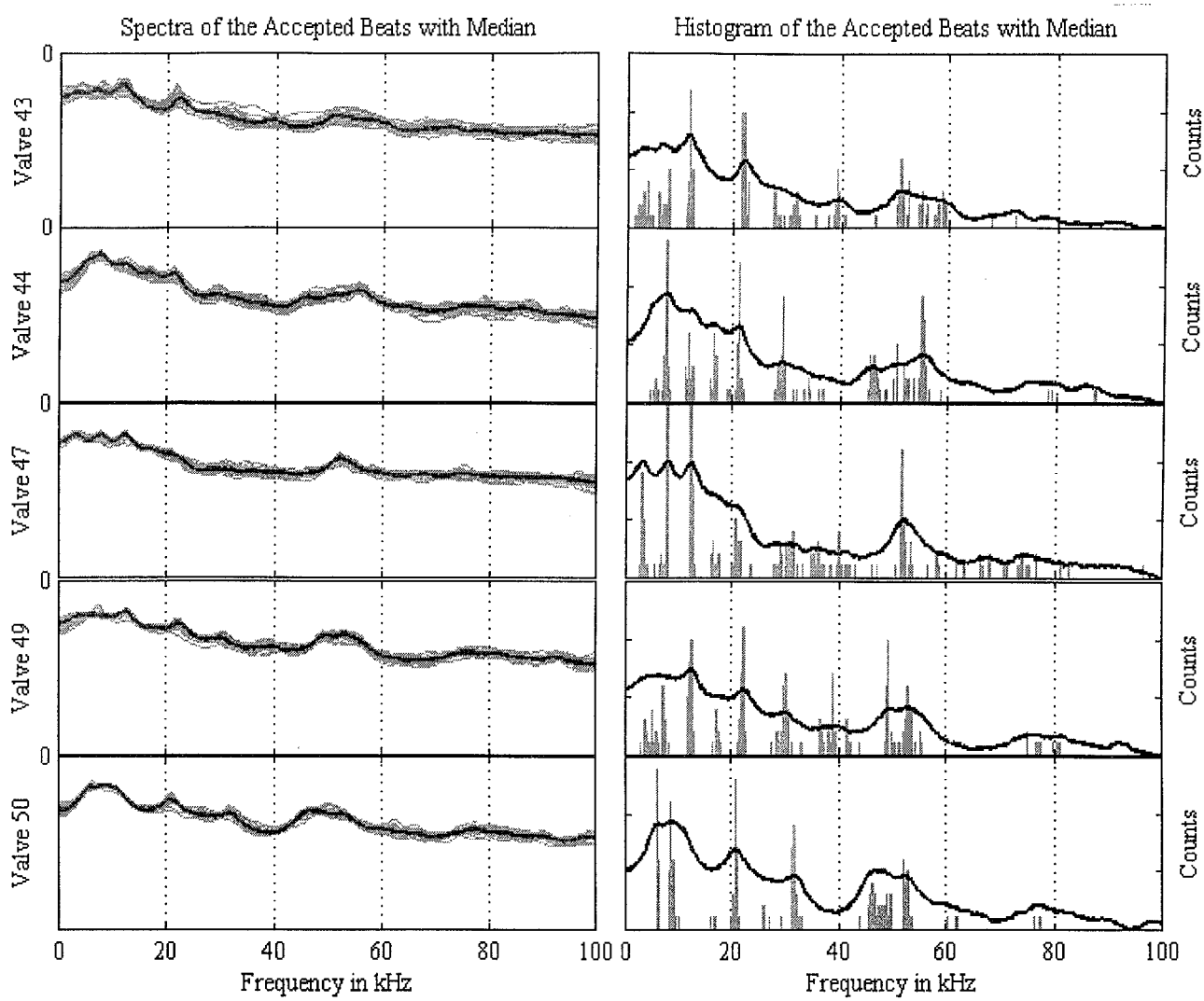

# Heart Valve Numbers 1 to 16 INTACT MVDR Max Order 50

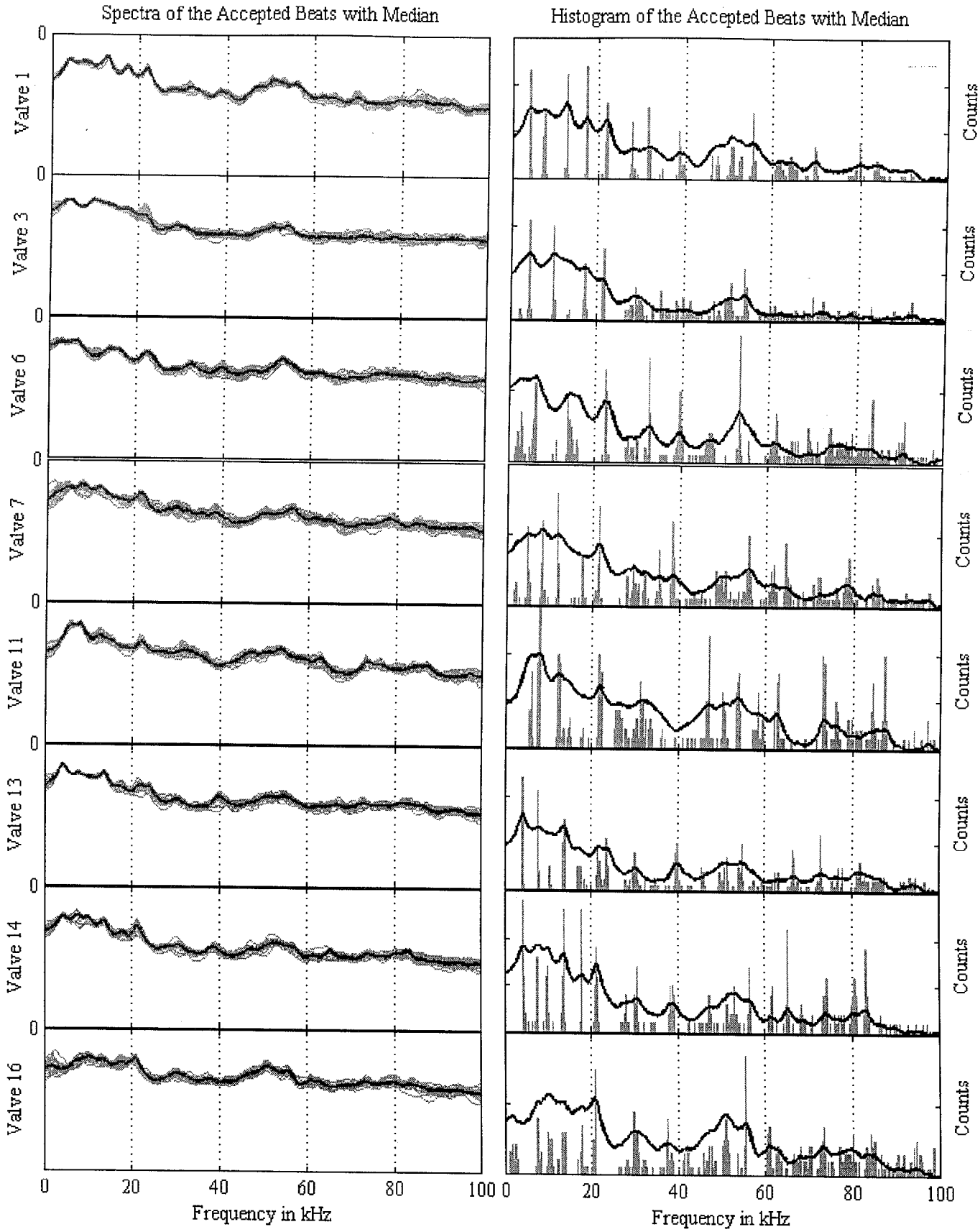

# Heart Valve Numbers 18 to 28 INTACT MVDR Max Order 50

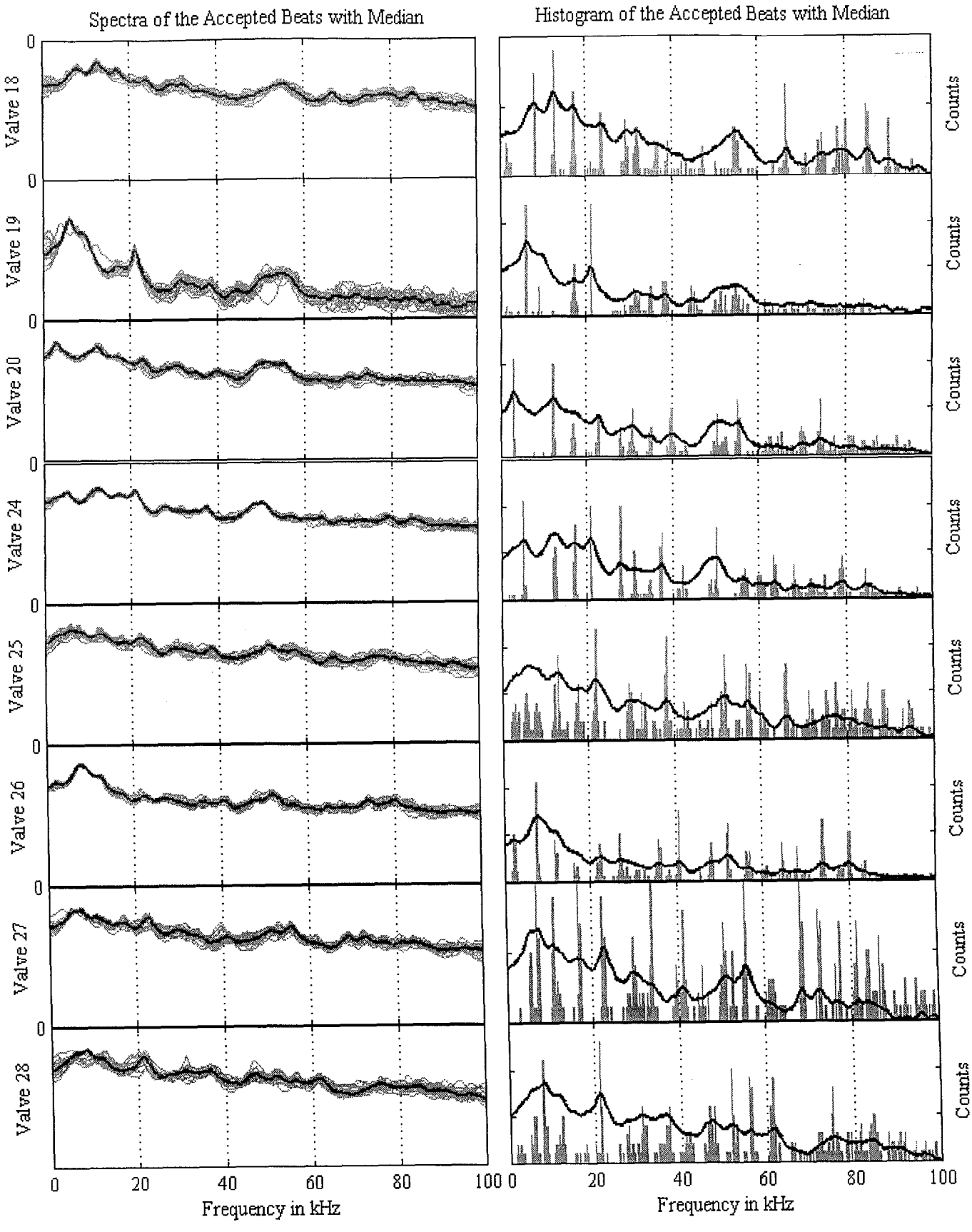

# Heart Valve Numbers 29 to 40 INTACT MVDR Max Order 50

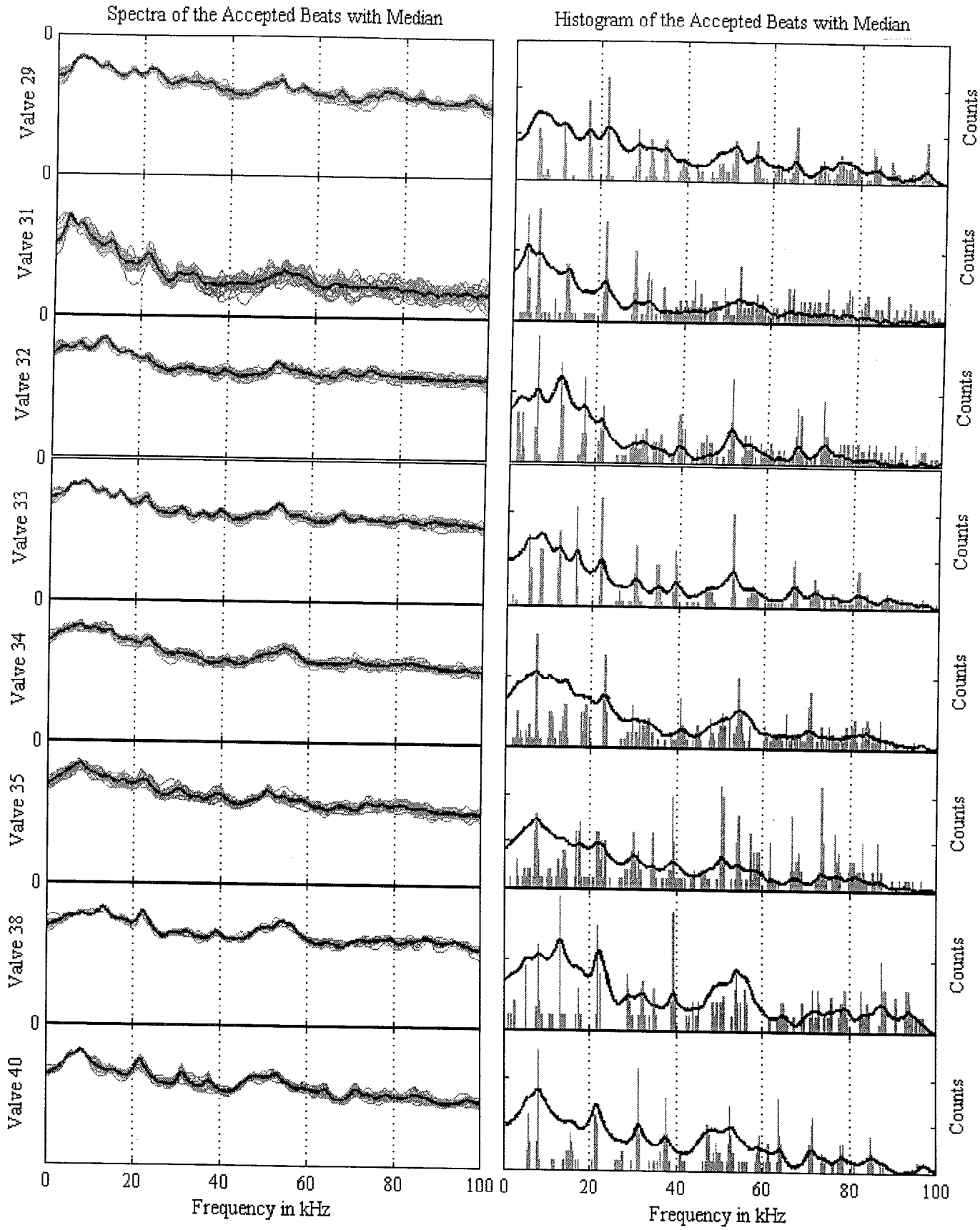

# Heart Valve Numbers 41 to 48 INTACT MVDR Max Order 50

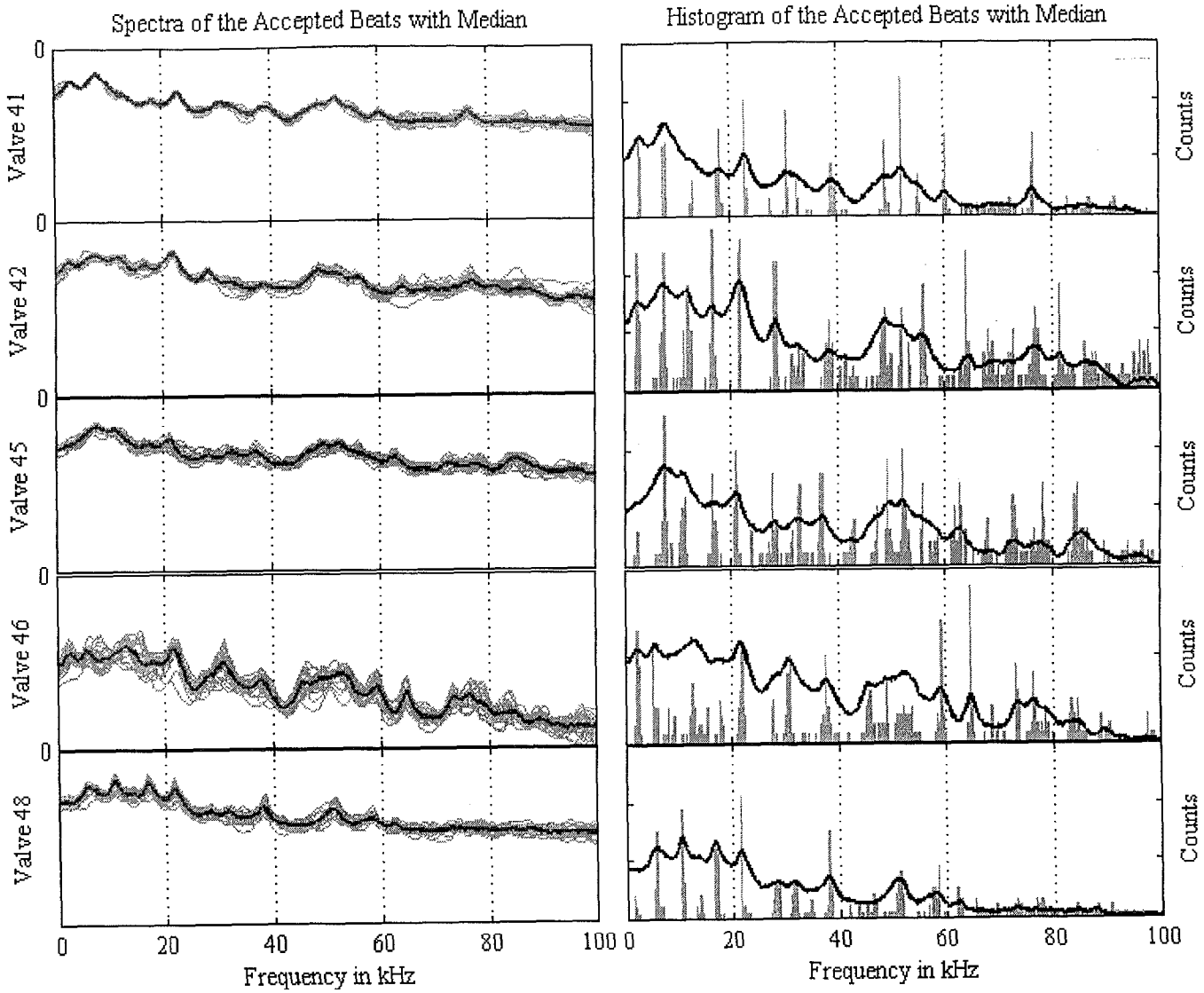

# *APPENDIX E:*

## *CLOSING Sounds (Beats) for SLS and INT Heart Valves using the MVDR spectral estimator*

In this section we show the individual valve CLOSING spectra and the CTM for each along with the corresponding Peak Frequency Histograms. Note that the precision of the measurements can be characterized by the spectral variations in the ensembles estimates (green on plots) to follow. The bounds have been calculated using the standard sample estimators and are included in the following Table. We first show the SLS spectra and then the INT group by their individual valve numbers (see Appendix B).

***Table E-1:*** *Opening/Closing Sound Spectral Variation: Valve Spectra Standard Deviations (S.D in dB.)*

| Valve Number | Opening Sound S.D. | Closing Sound S.D. |
|---|---|---|
| 1 | 1.2635 | 1.2892 |
| 2 | 1.2529 | 1.4616 |
| 3 | 1.2852 | 1.2662 |
| 4 | 1.3770 | 1.5027 |
| 5 | 1.3299 | 1.1809 |
| 6 | 1.3115 | 1.2473 |
| 7 | 1.4843 | 1.4478 |
| 8 | 1.3433 | 1.2043 |
| 9 | 1.3763 | 1.3704 |
| 10 | 1.2644 | 1.3816 |
| 11 | 1.3645 | 1.3369 |
| 12 | 1.4077 | 1.4541 |
| 13 | 1.2915 | 1.2740 |
| 14 | 1.3351 | 1.1742 |
| 15 | 1.2450 | 1.2912 |
| 16 | 1.3752 | 1.3974 |
| 17 | 1.6051 | 1.2492 |
| 18 | 1.4726 | 1.2402 |
| 19 | 1.3401 | 1.3493 |
| 20 | 1.2965 | 1.1930 |
| 21 | 1.3510 | 1.3188 |
| 22 | 1.3212 | 1.3605 |
| 23 | 1.3587 | 1.4397 |
| 24 | 1.2185 | 1.4198 |
| 25 | 1.4507 | 1.4749 |
| 26 | 1.3175 | 1.3921 |
| 27 | 1.4353 | 1.2904 |
| 28 | 1.5431 | 1.3569 |
| 29 | 1.3156 | 1.4829 |
| 30 | 1.4650 | 1.3633 |
| 31 | 1.3107 | 1.4845 |
| 32 | 1.3087 | 1.3969 |
| 33 | 1.2645 | 1.3873 |
| 34 | 1.3649 | 1.3483 |
| 35 | 1.4536 | 1.3354 |
| 36 | 1.3384 | 1.3019 |
| 37 | 1.4612 | 1.6022 |
| 38 | 1.3417 | 1.2309 |
| 39 | 1.5958 | 1.3320 |
| 40 | 1.3975 | 1.3080 |
| 41 | 1.2194 | 1.4845 |
| 42 | 1.3666 | 1.3715 |
| 43 | 1.5314 | 1.3656 |
| 44 | 1.4306 | 1.3823 |
| 45 | 1.3983 | 1.3323 |
| 46 | 1.3774 | 1.3882 |
| 47 | 1.3479 | 1.2074 |
| 48 | 1.4669 | 1.2937 |
| 49 | 1.3453 | 1.2621 |
| 50 | 1.3399 | 1.4512 |

# Closing Sounds
# Heart Valve Numbers 2 to 15 SLS MVDR Max Order 50

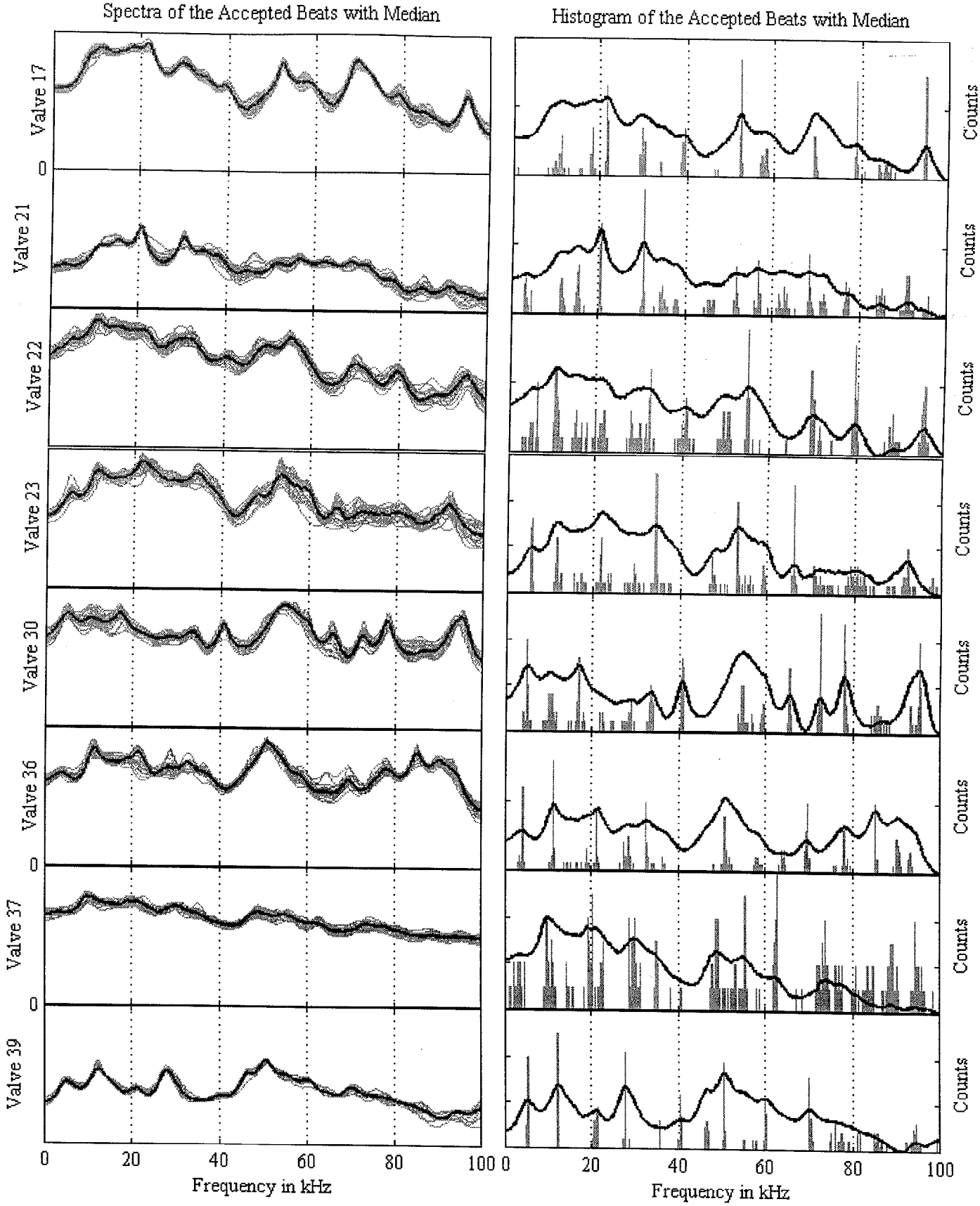

# Closing Sounds
# Heart Valve Numbers 17 to 39 SLS MVDR Max Order 50

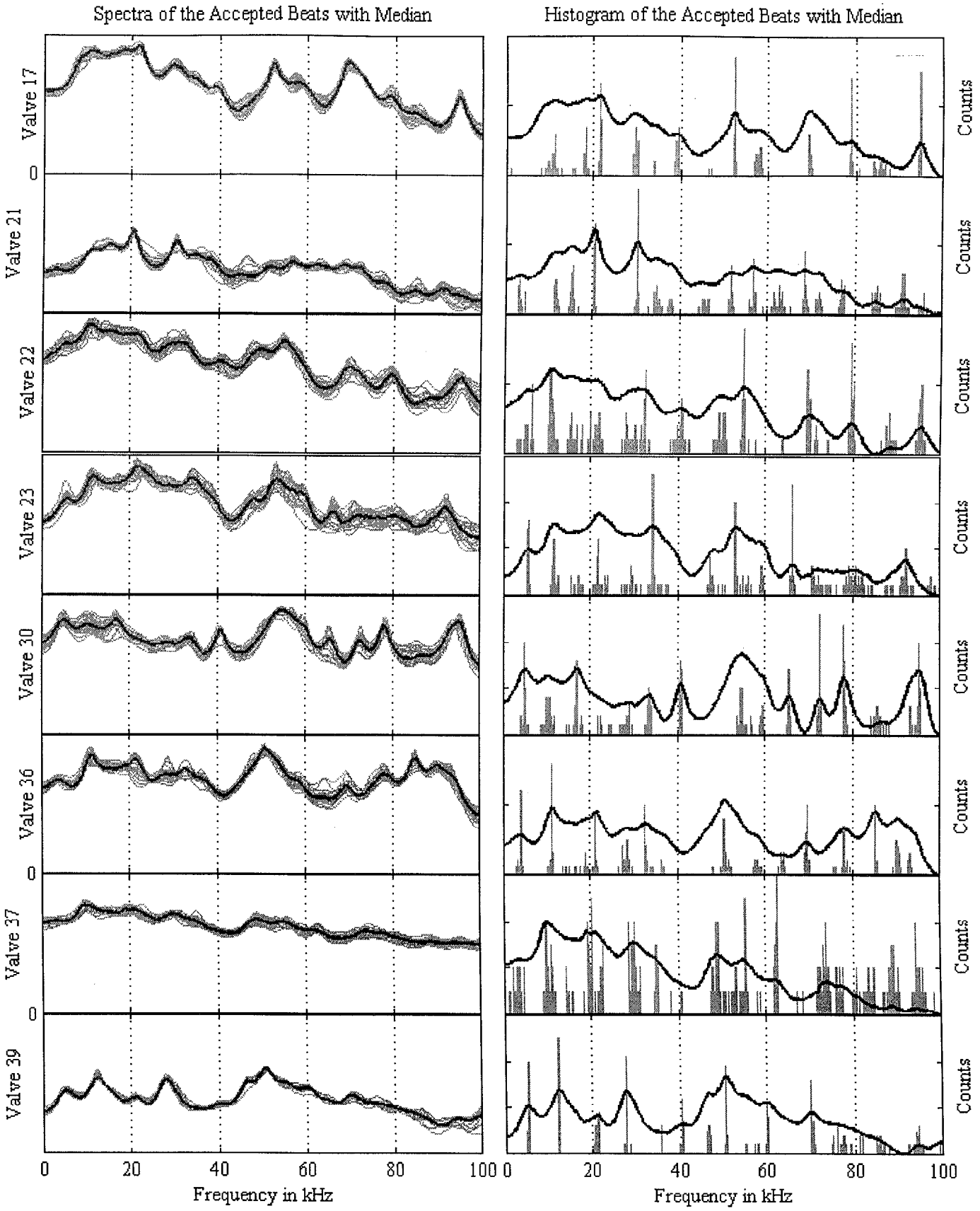

Closing Sounds

# Heart Valve Numbers 43 to 50 SLS MVDR Max Order 50

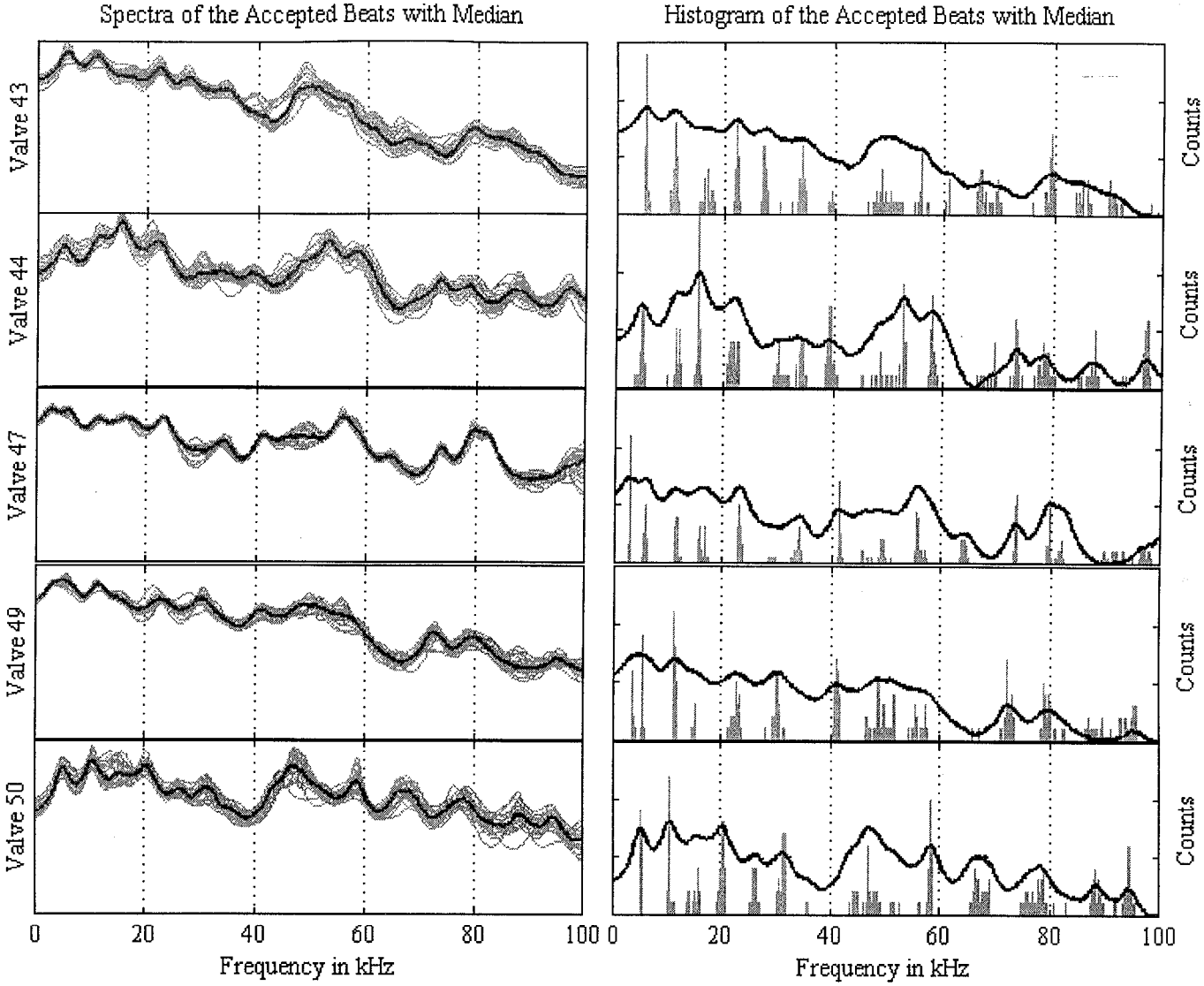

# Closing Sounds
# Heart Valve Numbers 1 to 16 Intact MVDR Max Order 50

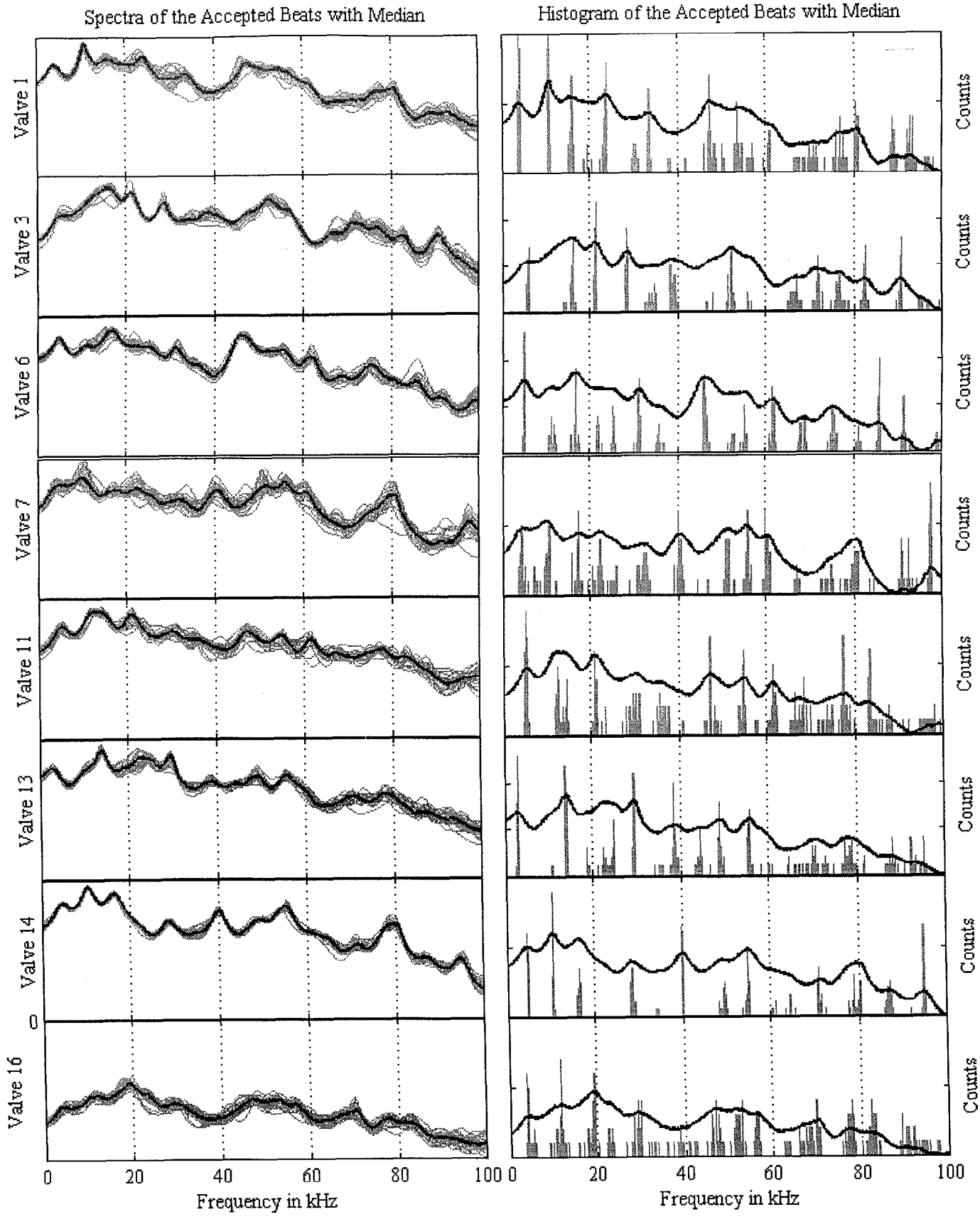

# Closing Sounds

## Heart Valve Numbers 18 to 28 Intact MVDR Max Order 50

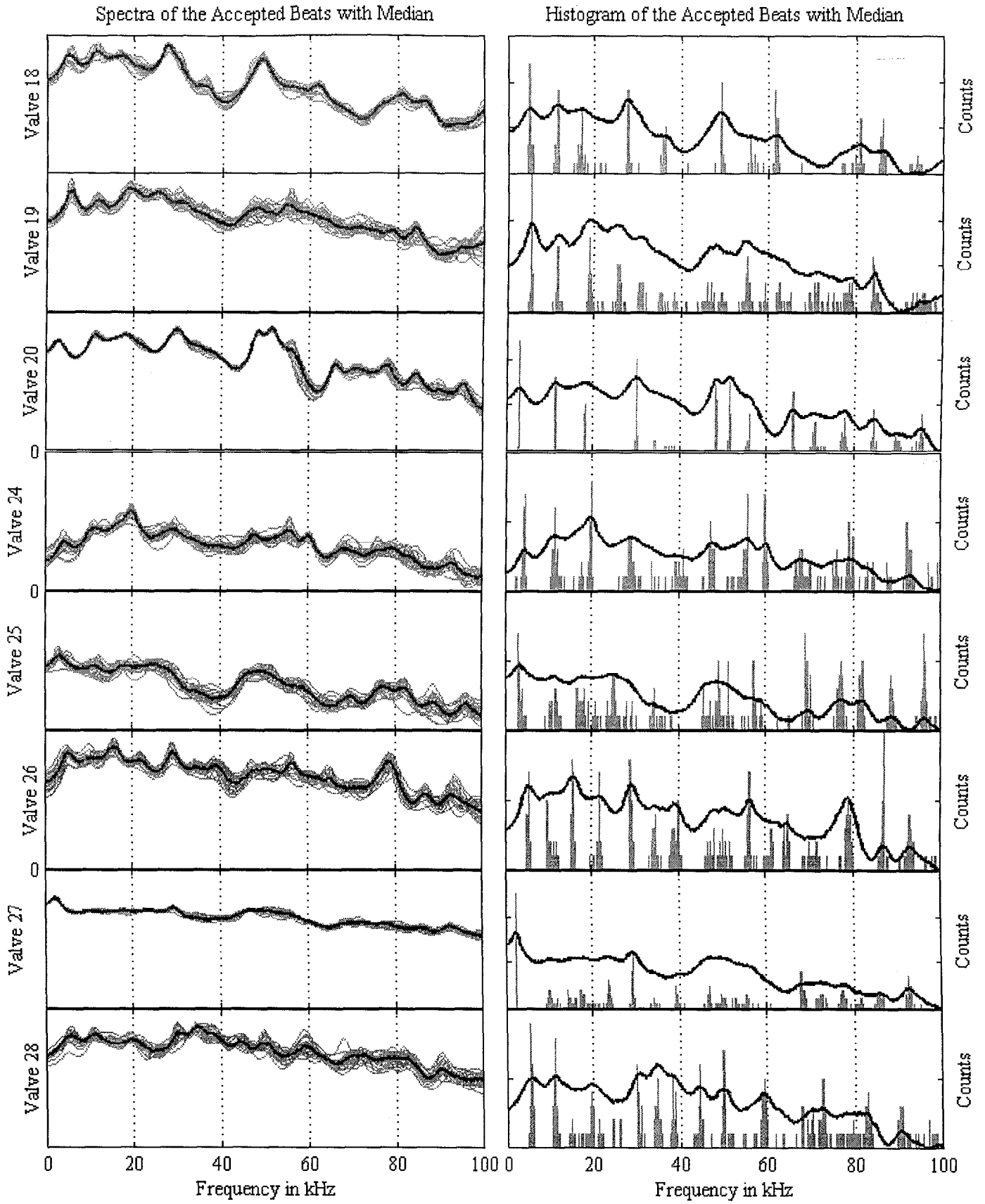

# Closing Sounds
# Heart Valve Numbers 29 to 40 Intact MVDR Max Order 50

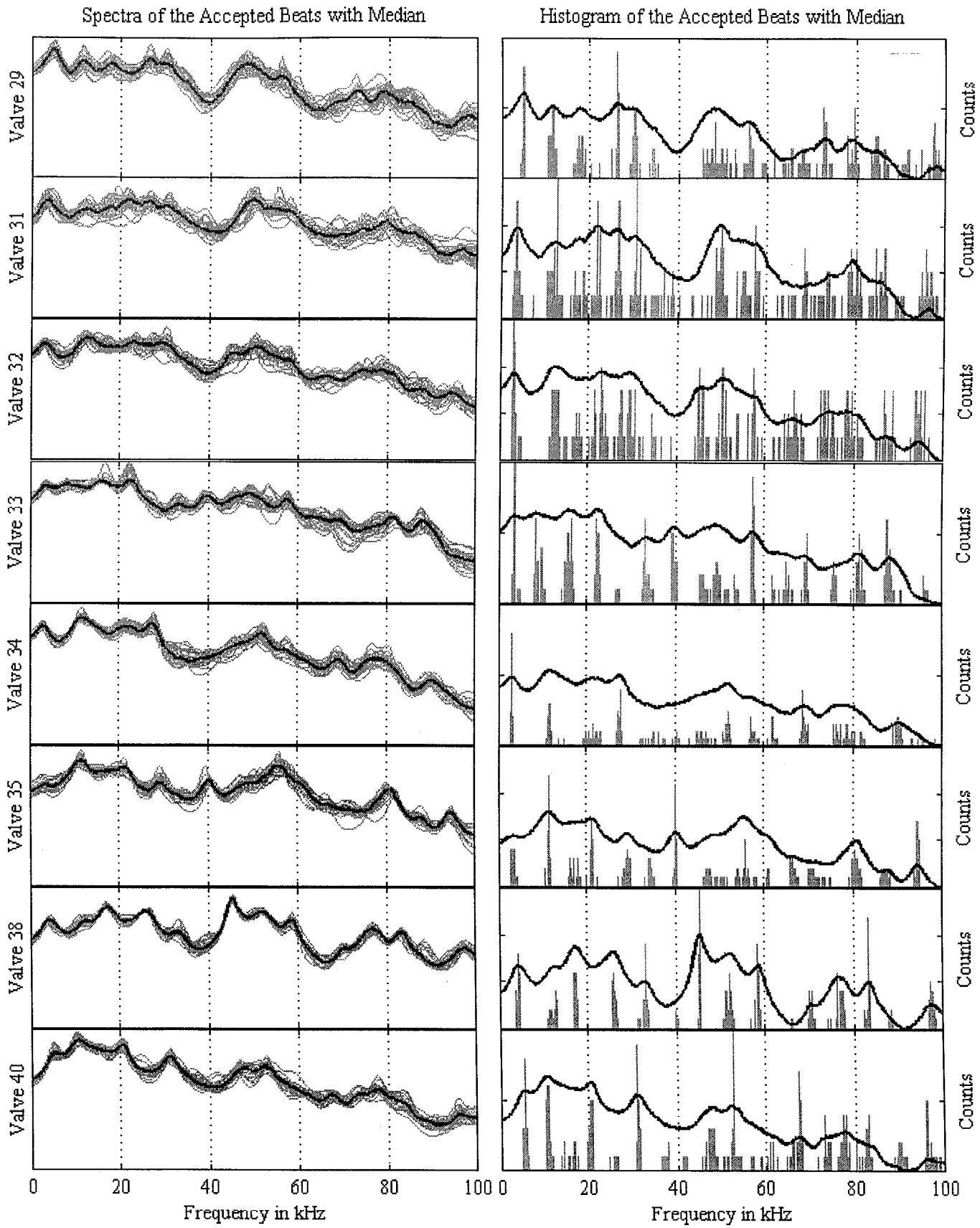

# Closing Sounds
# Heart Valve Numbers 41 to 48 Intact MVDR Max Order 50

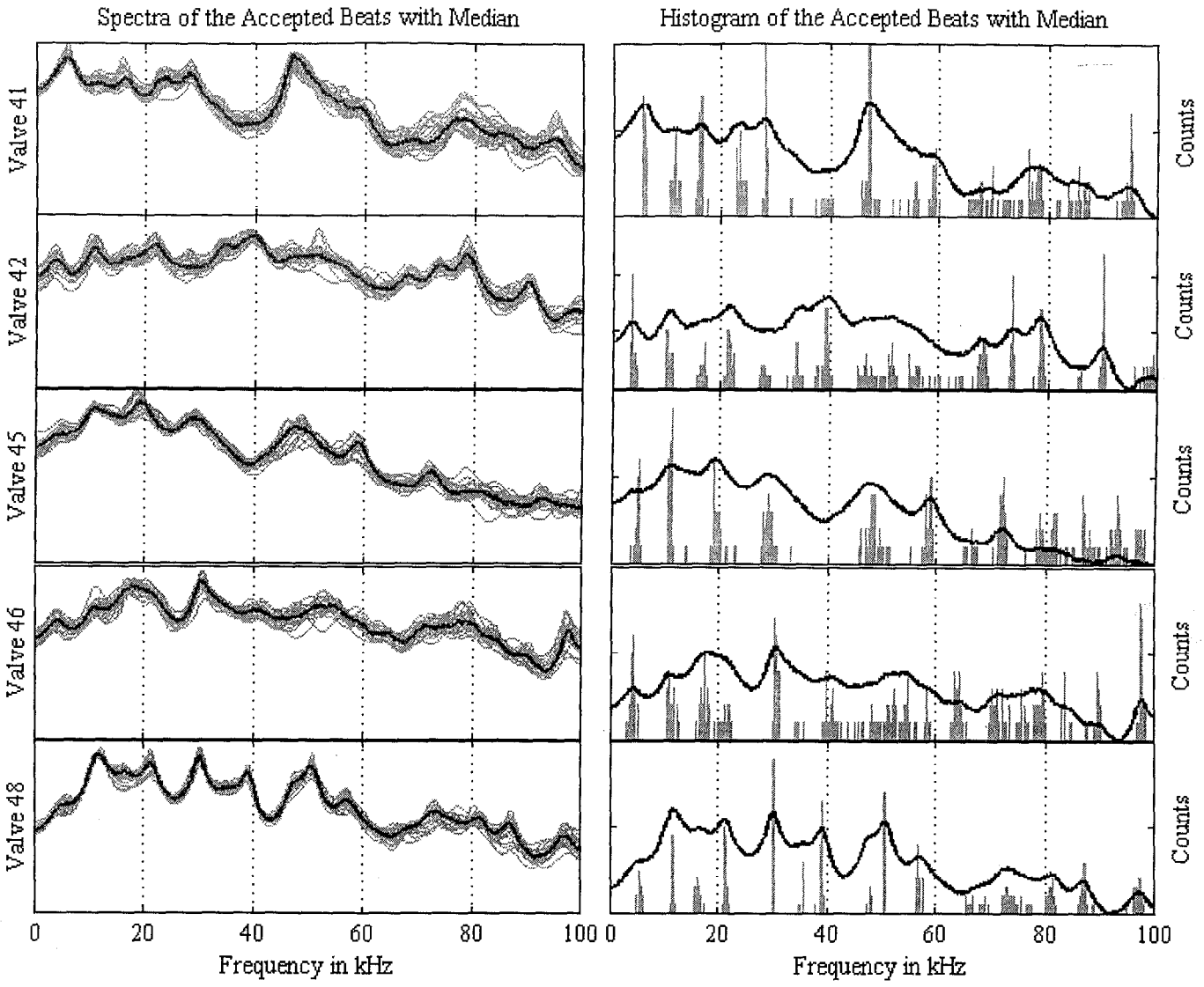

# *APPENDIX F:*

# *Noise/Correlation Cancelling Processor for OPENING and CLOSING Valve Sounds*

In this Appendix we discuss the basic theory of noise/correlation cancelling processor designs applied to the sounds emanating from prosthetic heart valves under test. The noise/correlation canceller evolved directly from the work of Widrow [11] using the so-called least mean-squared (LMS) algorithm. The basic structure is shown in Figure F-1 below where we see that the canceller consists of a *measurement* channel and a *reference* channel on input and an *error* channel on output. The basic idea is that the canceller uses the reference channel, which is correlated to the measurement, to design a filter which provides an optimal (in LMS sense) set of weights producing an *estimate* that is now "highly correlated" to the measurement and removed (subtracted) to generate the "uncorrelated" error output.

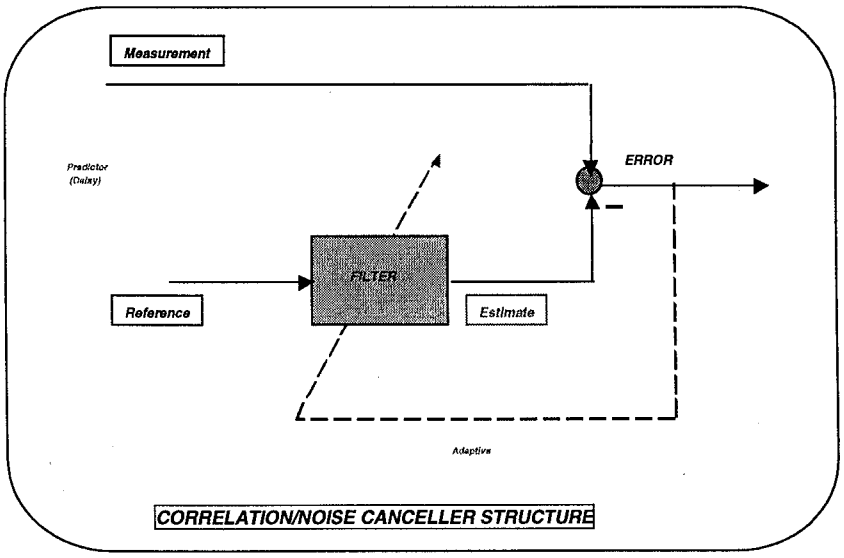


***Figure F-1.*** *Basic Noise/Correlation Canceller Structure.*

The optimal solution to this problem is available for stationary (time invariant moments) data in the form of the so-called Wiener filter; however, for non-stationary (time-varying moments) data an adaptive form (dashed blue line) of the algorithm is available in the form of the LMS gradient adjustment algorithm [2,11]. In fact, if we define our terms as shown in Figure E-2 below, then we see that the optimal Wiener solution is given by:

$$H_{\text{opt}}(t) = R_{rr}^{-1} R_{yr} \,. \tag{F-1}$$

If the reference channel is actually noise correlated to the measurement, then the canceller removes the correlated noise from the measurement and produces a direct estimate of the signal. The key in this case is that the reference channel must <u>not</u> have any signal at all or it will also remove it along with the correlated noise thereby decreasing some of the possible signal enhancement that could be achieved with a "signal free" reference. The resulting relations for this case are given by

$$\begin{aligned} e(t) &= y(t) - \hat{n}(t) = \left[s(t) + n(t)\right] - \hat{n}(t) \approx s(t) \\ \hat{n}(t) &= H_{opt}(t) * r(t) \end{aligned} \tag{F-2}$$

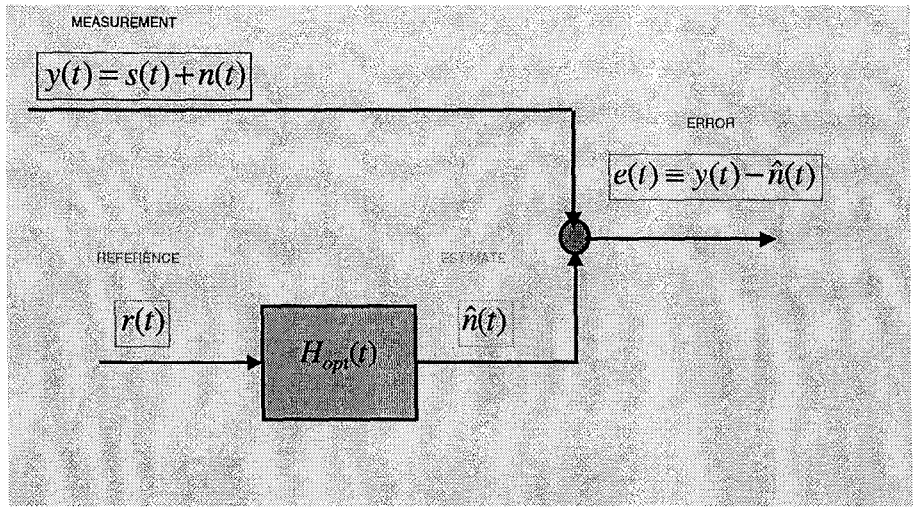


:

***Figure F-2.*** *Basic Noise/Correlation Canceller Definitions.*

The adaptive form of the canceller is identical in structure as in Figure F-2, but the weights take the form of:

$$\underline{H}(t+1) = \underline{H}(t) + \Delta_t \underline{X}^T (N-t)e(t) \qquad \text{(F-3)}$$

where $\Delta_t$ is the gradient step-size and $\underline{X}$ is the N-dimensional data vector with $e$ and $\underline{H}$ defined as before. This method is useful for slowly (quasi-stationary) time-varying data.

For our problem, this approach is ideal, since we can locate data prior to the onset of the opening or closing transients which we term "pre-noise." The pre-noise can be use to enhance our signal in a low SNR situation. We show a typical canceller output for an INT valve opening CTM spectrum below in Figure F-3. Note that removing the noise has a dramatic effect on the canceller output spectrum. Since we know the noise spectrum is exponentially decaying with broad energy bands centered around 20 and 55 kHz, we expect the removal of noise energy in these regions and an overall enhancement of resonances. The raw data spectrum is shown in blue (dashes) while the cancelled spectrum is shown in red. The processor enhances the spectral levels in the lower frequency band and clearly enhances the spectral peaks. This is especially noticeable around *15 kHz* with noise peaks and valleys eliminated in the higher frequency bands.

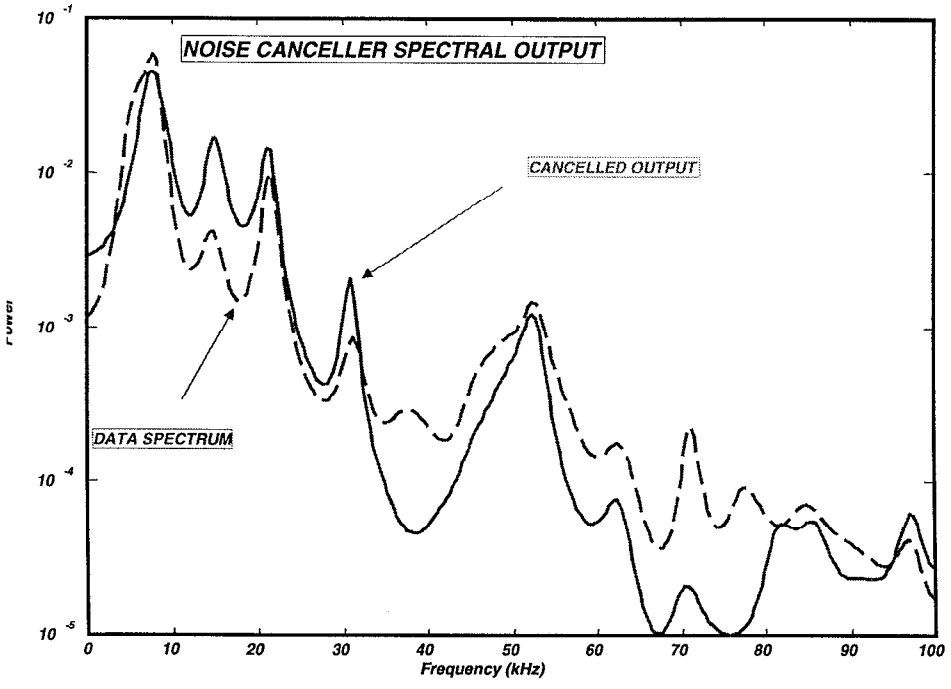


*Figure F-3. Cancelled INT Valve Opening Spectrum for CTM Sound Estimates.*

From the pure correlation cancelling idea, the canceller can be viewed as an optimal "separator" or "decomposer" in which it decomposes the data signal into its correlated and uncorrelated parts. We use the canceller to solve both of these problems and help us in the analysis of our data sets. Next we show the results of applying the canceller to the sets of CTM opening and closing sounds.

It is quite clear from the canceller output spectra of Figure F-4 when compared to the uncancelled ensemble CTM spectra of Figure 10 that the spectra have been enhanced. The resonances are more easily distinguished (visually) especially for the SLS CTM spectra shown in Figure F-4c at the SLS values at *16.8, 31.1*, and *39.1, kHz*. The INT bands are shown in Figure 4a at frequencies of *51.9* and *55 kHz* are also enhanced significantly with the spectra above *60 kHz* whitened (flattened) further. We used these cancelled CTM ensembles to estimate the cancelled UCTM for SLS and INT classes. These UCTM were then analyzed in detail for comparison of class responses (see Figure 15).

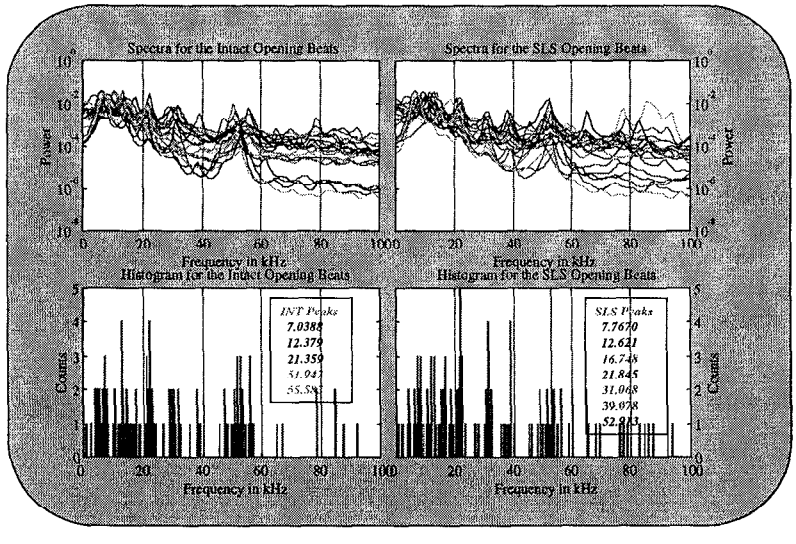


***Figure F-4.*** *Noise Cancelling Spectra for INT and SLS Valve Opening Sounds: (a) INT CTM Ensemble. (b) INT CTM Ensemble Peak Frequency Histogram. (c) SLS CTM Ensemble. (d) SLS CTM Ensemble Peak Frequency Histogram.*

# *APPENDIX G: SPECTROGRAMS*

In this appendix we discuss the application of instanteous spectral techniques to estimate the corresponding power spectrum as a function of time, that is, the time-frequency spectrogram. The approach we take is to use *recursive-in-time* parametric processors which enable us to estimate a pole-zero or autoregressive moving average (ARMA) model at each time sample [2,13]. With these parameters available at each point in time, we are able to generate a corresponding power spectrum and analyze jointly just how the behaves during excitation in the anechoic tank. Other approaches to time-frequency estimation are well-documented with the major approaches being probabilistic using the Wigner-Ville distributions [14] or more recently the wavelet tranform [15]. Here we will limit our investigation to the parametric ARMA spectral estimator, since we know we are dealing with a physical system that can be represented by a set of resonances (poles-zeros) which determine its spectral response and have physical meaning. Next we briefly review the approach and the recursive algorithm employed.

*Parametric Time-Frequency Spectrogram Estimation*

In this sub-section we develop the recursive-in-time approach to instantaneous spectral estimation enabling us to produce the desired spectrogram (amplitude vs. time vs. frequency). Suppose we parametrically model the enhanced measurement data by an instantaneous time-frequency representation specified by an autoregressive moving average (ARMA) model. This model takes the general difference equation form, $ARMA(N_a, N_c)$ given by

$$A(q^{-1},t_n)x(t_n) = C(q^{-1},t_n)\varepsilon(t_n), \tag{G-1}$$

for the enhanced measurement, $x(t_n)$, contaminated with zero-mean, white gaussian noise, $\varepsilon \sim N(0,\sigma_\varepsilon^2)$, with the corresponding instantaneous polynomials at the $t_n$ instant defined by

$$\begin{aligned} A(q^{-1},t_n) &= 1 + a_1(t_n)q^{-1} + \ldots + a_{N_a}(t_n)q^{-N_a}, \\ C(q^{-1},t_n) &= c_o + c_1(t_n)q^{-1} + \ldots + c_{N_c}(t_n)q^{-N_c}. \end{aligned} \tag{G-2}$$

Here the *backward shift* or delay operator is defined by, $q^{-i}x(t_n) \equiv x(t_{n-i})$, and therefore, we can write Eq. G-2 simply as

$$x(t_n) = -\sum_{k=1}^{N_a} a_k(t_n)x(t_{n-k}) + \sum_{k=0}^{N_c} c_k(t_n)\varepsilon(t_{n-k}). \tag{G-3}$$

If we take the DFT of the difference equation, then we obtain the *instantaneous transfer function* (ignoring stochastic aspect)

$$H(e^{j2\pi f},t_n)=\frac{X(e^{j2\pi f},t_n)}{\mathrm{E}(e^{j2\pi f},t_n)}=\frac{C(e^{j2\pi f},t_n)}{A(e^{j2\pi f},t_n)}, \tag{G-4}$$

or more appropriately the corresponding *instantaneous power spectrum* given by

$$S(f,t_n)\equiv\left|H(e^{j2\pi f},t_n)\right|^2=\frac{\left|C(e^{j2\pi f},t_n)\right|^2}{\left|A(e^{j2\pi f},t_n)\right|}. \tag{G-5}$$

So we see that if we use the parametric $ARMA(N_a,N_c)$ representation of the enhanced measurement signal and transform it to the spectral domain, then we can obtain the instantaneous spectral estimate.

There are a wealth of ARMA algorithms available in the literature [13], but since we are primarily interested in estimating the spectrum at each time instant, we confine our choices to those that are *recursive-in-time* enabling us to achieve our goal with minimal loss of temporal resolution evolving from window-based methods such as the short-time Fourier transform. Recursive-in-time algorithms (real data) all take on the following generic form:

$$\hat{\underline{\alpha}}(t_{n+1})=\hat{\underline{\alpha}}(t_n)+\underline{G}(t_n)e(t_n) \qquad \text{[parameter update]}$$

$$e(t_n)=x(t_n)-\hat{x}(t_n)=x(t_n)-\underline{\varphi}^T(t_n)\hat{\underline{\alpha}}(t_n) \qquad \text{[prediction error]}$$

(G-6)

$$\underline{\varphi}(t_n)\equiv\left[x(t_{n-1})\ \ \mathrm{L}\ \ x(t_{n-N_a-1})\,|\,\hat{e}(t_n)\ \ \mathrm{L}\ \ \hat{e}(t_{n-N_c})\right]$$

$$\hat{\underline{\alpha}}(t_n)\equiv\left[-\hat{a}_1(t_{n-1})\ \ \mathrm{L}\ \ -\hat{a}_{N_a}(t_{n-N_a-1})\,|\,\hat{c}_o(t_n)\ \ \mathrm{L}\ \ \hat{c}_{N_c}(t_{n-N_c})\right]^T,$$

with $\underline{G}(t_n)$ the so-called *gain* or weighting vector and the ^ symbol defining the "best" (minimum error variance) estimate at the specified time. There are also many variations and forms of this basic recursion [13], but here we limit our application to the recursive

prediction error method (RPEM) based on a local Gauss-Newton optimization method (see [2,13] for details).

We applied this algorithm to the UCTM opening and closing heart valve sounds for both SLS and INT valves and the results are shown below in Figures G-1 thru G-4. In G-1 we see the instantaneous spectrum of the closing SLS UCTM sound. From the figure it is clear that the valve is rich in spectral contents and that the resonances settle down after a short period of time.

We see the spectrogram of the INT opening UCTM sound. The spectrogram image shown in Figure G-1 indicates high frequency resonances up to *0.5 ms*. The pole-zero parameters converge to steady state (i.e., no significant spectral change) values after *0.75 ms*. In steady state, we see the dominant low frequency resonances *at 6, 10, 16, 18, 22* and a set of fixed high frequency resonances at: *28, 40, 55, 62 kHz*. The SLS UCTM opening sounds shown in Figure G-2 indicate a different response at the lower frequency bands. The UCTM in this case occurs after *5 ms*. During the transient a set of resonant frequency stablize rapidly and after approximately *1 ms* the entire spectrum converges to resonances at: *4, 9, 15, 18, 31, 39, 53, 65 kHz* and higher.

The closing UCTM sounds exhibit a more erratic behavior probably due to the stronger vibrations creating much louder sounds. During the initial transient phase, the spectrogram shown in Figure G-3 don not stablilze for the INT valve until approximately *0.75 ms* and at *0.6 ms* with resonances at: *5, 11, 19, 25, 35, 40, 48, 52, 55 kHz* for the SLS UCTM response shown in Figure G-4. The pole-zero parameters stabilize after *1.25 ms* in both cases and to steady state after *2 ms*. The set of resonances after that time are at:

We summarize these results to conclude that the non-stationary nature of the UCTM valve spectral responses are readily apparent in the closing sounds and less obvious in the openings. It appears that the opening sounds converge more rapidly and remain steady for the majority of the response time.

This work was performed under the auspices of the Department of Energy by the Lawrence Livermore National Laboratory under contract W-7405-Eng-48.

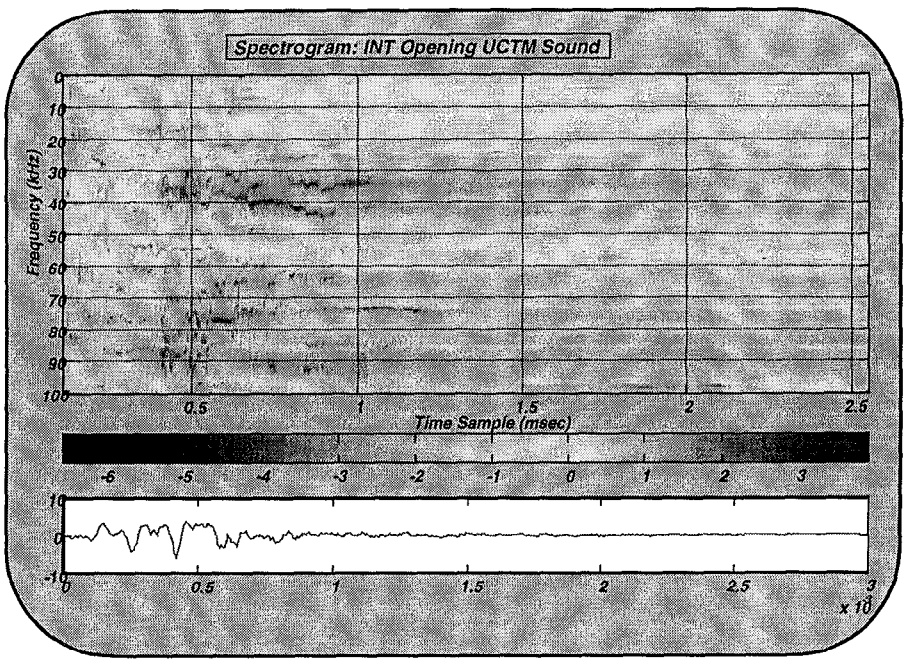


***Figure G-1.*** *Spectrogram of INT UCTM Opening Sound.*

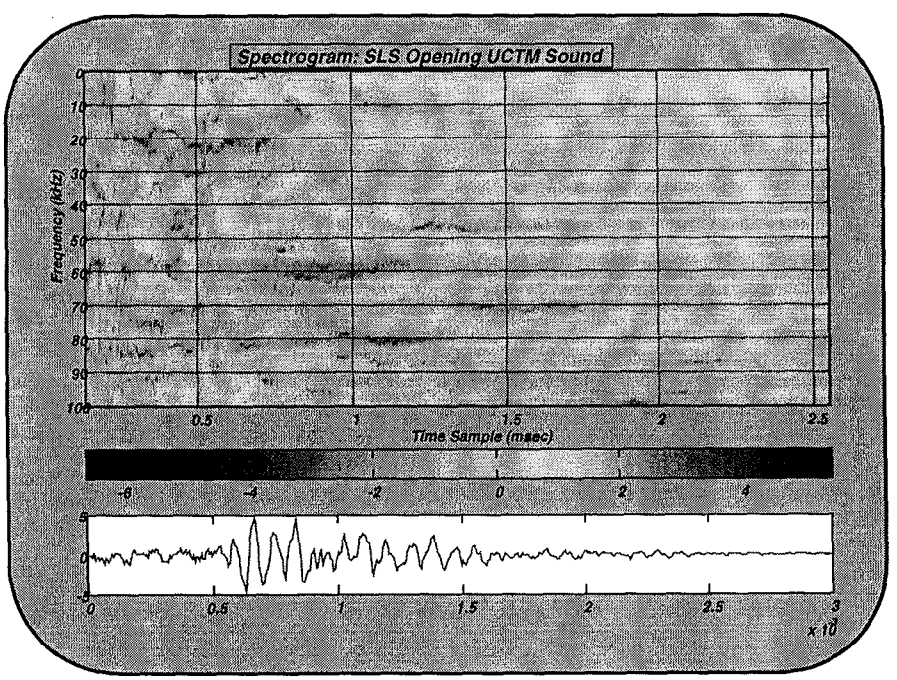


***Figure G-2.*** *Spectrogram of SLS UCTM Opening Sound.*

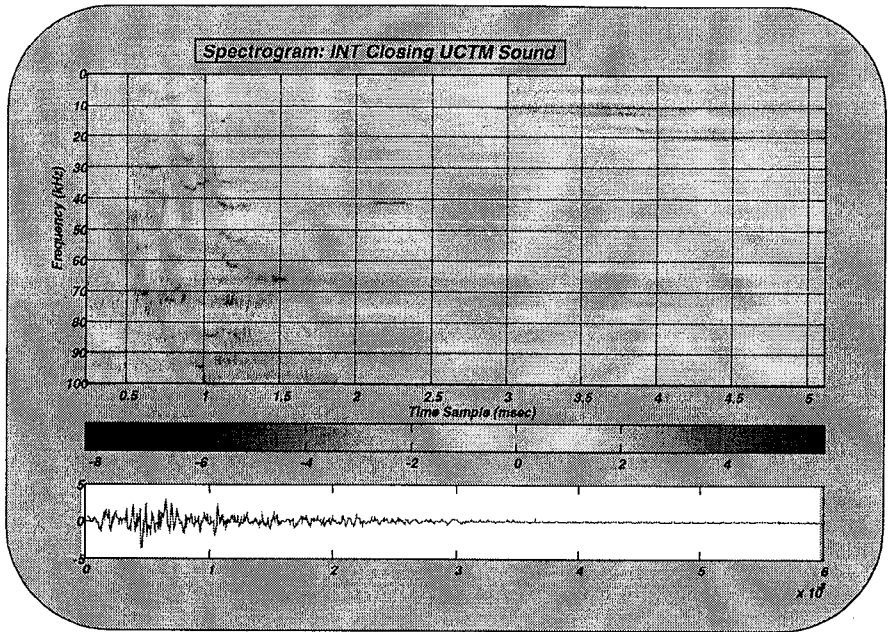


***Figure G-3.*** *Spectrogram of INT UCTM Closing Sound.*

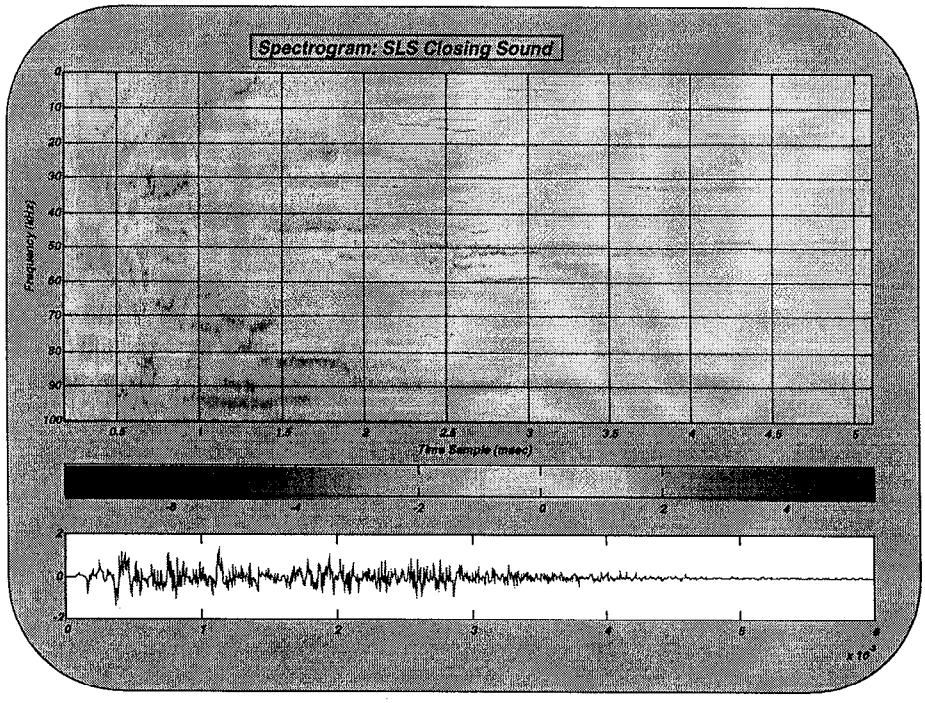


***Figure G-4.*** *Spectrogram of SLS UCTM Closing Sound.*

# *APPENDIX H: GLOSSARY*

| | |
|---|---|
| AIC | Akaike Information Criterion |
| B&K | Bruel & Kjaer microphone vendor. |
| BPHVSP | Bowling-Pfizer Heart Valve Supervisory Panel. |
| BSCC | Bjork-Shiley Concave-Convexo. |
| COR | correlated. |
| CTM | closest-to-median. |
| GB | gigabyte. |
| INT | intact valve. |
| Jazz | Iomega Jazz storage device. |
| kHz | kilohertz. |
| LLNL | Lawrence Livermore National Laboratory. |
| LMS | Least Mean Square, a mathematical procedure. |
| MAICE | Minimum Akaike Information Criterion Estimate, a procedure for model selection. |
| MAD | Median Absolute Deviation, a statistical procedure. |
| MEM | Maximum Entropy Method, a mathematical procedure. |
| MUSIC | Multiple Signal Classification Response, a mathematical procedure. |
| MVDR | Minimum Variance Distortionless Response, a mathematical procedure. |
| RMS | Root Mean Square. |
| SAI | Science Associates Inc. |
| SLS | Single Leg Separation Valve. |
| SNR | Single to Noise RatioSPAWARS The U.S. Navy's Space and Naval Warfare Systems Center. |
| TransDec | The U. S. Navy's Transducer Evaluation Facility. |
| UNCOR | uncorrelated. |
| UCTM | universal closest-to-median. |
| WFO | Work For Others, a type of contract. |